

REPORT DOCUMENTATION PAGE			Form Approved OMB No. 0704-0188	
Public reporting burden for this collection of information is estimated to average 1 hour per response, including the time for reviewing instructions, searching existing data sources, gathering and maintaining the data needed, and completing and reviewing the collection of information. Send comments regarding this burden estimate or any other aspect of this collection of information, including suggestions for reducing this burden to Washington Headquarters Services, Directorate for Information Operations and Reports, 1215 Jefferson Davis Highway, Suite 1204, Arlington, VA 22202-4302, and to the Office of Management and Budget, Paperwork Reduction Project (0704-0188), Washington, DC 20503.				
1. AGENCY USE ONLY (Leave blank)		2. REPORT DATE 30-March-2001		3. REPORT TYPE AND DATES COVERED Final Report
4. TITLE AND SUBTITLE Plasma Influence on Characteristics of Aerodynamic Friction and Separation Flow Location			5. FUNDING NUMBERS ISTC Registration No: 1780	
6. AUTHOR(S) Dr. Serguei Leonov				
7. PERFORMING ORGANIZATION NAME(S) AND ADDRESS(ES) Moscow Technical Company-Institute of High Temperature RAS MTC-IVTAN, Izhorskaya str., 13/19 Moscow 127412 Russia			8. PERFORMING ORGANIZATION REPORT NUMBER N/A	
9. SPONSORING/MONITORING AGENCY NAME(S) AND ADDRESS(ES) EOARD PSC 802 BOX 14 FPO 09499-0200			10. SPONSORING/MONITORING AGENCY REPORT NUMBER ISTC 00-7004	
11. SUPPLEMENTARY NOTES				
12a. DISTRIBUTION/AVAILABILITY STATEMENT Approved for public release; distribution is unlimited.			12b. DISTRIBUTION CODE A	
13. ABSTRACT (Maximum 200 words) This report results from a contract tasking Moscow Technical Company-Institute of High Temperature RAS as follows: The contractor will study the application of plasma technology for flow control. In particular, he will study the change in aerodynamic friction and the flow separation point using various electric discharges near a model's surface. He will analyze experimental data obtained previously at his lab (and elsewhere) in order to define better-oriented experiment. The investigation will then be made on a simple model namely a plate. Three types of surface discharges will be tested in this work, a) HF multi-streamer discharge; b) micro-hollow cathode discharge and c) glide surface discharge. It is thought that the most interesting for the aerodynamic application will be HF micro-streamer pulse repetitive discharge. Therefore more emphasis will be made on the latter. The main emphasis of the comparison will focus on the energetic effectiveness of the plasma influence.				
14. SUBJECT TERMS EOARD, Aviation Technology, Aerodynamics			15. NUMBER OF PAGES 111	
			16. PRICE CODE N/A	
17. SECURITY CLASSIFICATION OF REPORT UNCLASSIFIED	18. SECURITY CLASSIFICATION OF THIS PAGE UNCLASSIFIED	19. SECURITY CLASSIFICATION OF ABSTRACT UNCLASSIFIED	20. LIMITATION OF ABSTRACT UL	

NSN 7540-01-280-5500

Standard Form 298 (Rev. 2-89)
Prescribed by ANSI Std. Z39-18
298-102



Partner Project

EOARD-IVTAN-ISTC

No. 1780P

Approval date April 1, 2000

Institute of High Temperature

Russian Academy of Science (IVTAN)

Izhorskaya street, 13/19, of. 231

Moscow, 127412, Russia

Influence of Surface Plasma on Characteristics of Viscous Friction and Separation Zones Location.

Final Report

Delivery 4.

Written by:

Dr. S. Leonov

Prof. V. Bityurin

Prof. A. Yuriev

Dr. A. Bocharov

Dr. V. Gromov

Dr. E. Gubanov

Dr. Yu. Kolesnichenko

Mr. A. Mityagin

Mr. A. Okunev

Mr. K Savelkin

Dr. N. Savishenko

Dr. V. Sukhov

MOSCOW- 2001

Contents

1. Introduction.
2. Background.
 - 2.1. Brief Review of Experimental and Theoretical Works.
3. Surface Plasma Influence on Viscous Friction and Separation Parameters.
Transonic and subsonic test.
 - 3.1. Experimental arrangement and parameters of the test.
 - 3.1.1. Transonic Wind Tunnel ST-1.
 - 3.1.2. Measurement System and Synchronization.
 - 3.1.3. Plasma Generator of Surface Type.
 - 3.2. Experimental Results.
 - 3.2.1. Description of the Runs.
 - 3.2.2. Balances Measurements.
 - 3.2.3. Visualization of the Interaction.
 - 3.2.4. Measurements of Pressure Redistribution.
 - 3.2.5. Plasma Influence on Turbulence.
 - 3.3. Mathematical Simulation.
 - 3.4. Interim Conclusion.
4. Surface Plasma Influence on Separation Zone Parameters. Short Time Wind Tunnel Test.
 - 4.1. Description of Experimental Conditions.
 - 4.1.1. Short time wind tunnel PWT-10.
 - 4.1.2. Parameters of airflow.
 - 4.1.3. Plasma Generator of Surface Type.
 - 4.1.4. Measurement System and Synchronization.
 - 4.1.4.1. Pressure measurements.
 - 4.1.4.2. Spectroscopic measurements.
 - 4.1.4.3. Synchronization.

4.2. Experimental Data.

4.2.1. Two Modes of Plasma Spacing.

4.2.2. Discharge Influence on Pressure Distribution.

4.2.3. Temperature in a Separation Zone.

4.2.4. Discharge Influence on Turbulence.

4.3. Mathematical Simulation.

4.4. Interim Conclusion.

5. Short Discussion. Conclusion.

6. References.

7. Acknowledgements.

8. Applications.

1. Introduction.

The aim of this experimental work is to continue a study of the fundamental plasma technology in a plasma -airflow interaction area, in particular, to change an aerodynamic friction and separation zones location by means of surface plasma formation on simple models in airflow. A main objective of the latest works in a field of Advanced Flow Control (AFC) is to increase efficiency of vehicles and to safe or disturb stability and controllability at atmospheric flight by means of plasma objects applications. The plasma formation can effect on aircraft's elements by change of their aerodynamic characteristics. Well known that the drag of bodies in airflow consists of three main parts: the pressure drag, the base drag and the friction. In some important cases viscous friction is the most part. From the other side the phenomena of flow separation limit the lift of wings at non-zero angle of attack. An instability of separation line position leads to problems in flight control. A shock induced flow separation is an important problem for bodies of a complex shape. We suggest that plasma technology could solve some problems in this field.

Up to present time some experimental and theoretical works have been fulfilled in frames of the study of plasma influence on airflow. One can see large differences for the plasma-airflow-body interaction when the different kinds of discharge have been used for the plasma excitation. In this project, on-board surface plasma generator of a multi-electrode configuration has been used as an agent of modeling. At the same time there were few works on L/D and separation zone. Each experiment was made under the unique conditions and with models of different shapes. This Report describes results of the model experiment on an airflow modification near surface as well as separation processes control by means of plasma influence at the simple aerodynamic configurations.

Traditional methods of viscous friction reduction are based on a directed mechanical influence on airflow near body surface; actually, it is the control of laminar and turbulent boundary layer. Such a control can be realized by means of two ways: change of velocity vector of an external airflow or/and properties and temperature of the surface. The plasma technique can be useful in two ways by changing of thermo-physical properties of the working media (density, the first and the second viscosity coefficients) and by the flow field modification through the controllable energy release. From the other hand the modification of the friction can result implicitly in a total drag reduction through the boundary layer

separation and the laminar-to-turbulence transition phenomena. Thus, the general problem becomes rather complicated and non-linear.

Plasma influence on near-surface layers can lead to contradictory effects. Each aerodynamic situation requires a specific approach to be effected by plasma positively. The experimental observations give the important information on details of the interaction. It is expected that the energy addition into the up-coming flow provided by an electrical discharge could result in: (1) - stabilization of the boundary layer because of increasing of the heat transfer rate to the 'cold' wall from the 'heated-up' airflow; (2) – decreasing of separated flow zones effects on the flow parameters distribution along the body surface; (3) – suppressing the laminar-to-turbulent transition by the increasing of the specific energy of the air flow.

The solution of the problem described above is most important in the case of high-speed subsonic and transonic airflows for vehicles with vast surface. So, our experiments have been provided in airflow at Mach number from 0.4 up to 0.99 and static pressure from 100Torr to 650Torr, which are typical for airplane flights.

The first Phase of this work has been fulfilled in the frame of EOARD-MTC contract No. F61775-99-WE106. So, some data in this Report were reflected in previous documents last year.

The results of model experiments and the analytical data are discussed in the following sections. The experiments have been made in short time wind tunnel PWT-10 of IVTAN (Mach number 0.9-1.1) as well as in transonic wind tunnel ST-1 (Mach number 0.5-1.05). Another side of the research was comparison of the experimental results with mathematical simulation data and adjustment of the CFD codes in accordance with experimental picture.

Nine experimental sessions took place in frames of this Contract: July, 5-7; September, 27-28; October, 02; October, 04-05; October, 25-30; November, 02-03; November, 12-13; December, 18-20 in 2000 year and February, 2-4 in 2001 year. The experimental results are presented in this Report.

Chapter 2.

Scope and Background. Brief Review.

At the present time there are a number of theoretical and experimental works, which show that energy release to airflow near/fore streamlined bodies can reduce a total drag of these bodies. In a case of blunted body the drag reduction can be provided with a rather high effectiveness even higher than 100% [1-5]. In general case a drag force at zero lift is represented as a sum of three components: shape (pressure/wave) drag, the friction drag and the base drag. At the most cases the attention was fixed on pressure and wave share of a total drag. At the same time the drag, which could be associated with the friction, can have a significant part. For modern long-distance airplanes at Mach numbers $\dot{M} = 0.7-0.9$ the friction drag value can be estimated in 60% of the total drag value approximately. Herewith only few papers are devoted to the friction problem solution with newly proposed plasma technology [6,7]. There are a couple of papers discussing the pure plasma effects on the surface and near surface phenomena [9,10]. It should be noted, however, that a so-called MHD boundary layer control when both electrical and magnetic fields are used to modify flowfield and, consequently, to control the surface friction and turbulence development in boundary layers is known for a long time already.

As it was shown by recent investigations an energetic method of boundary layer control (volume energy release to gas near surface by means of electrical discharge) leads to non-trivial response. Wall steps and cavities are offered as a constructive element in supersonic combustors. Such an element can provide an artificial separation zone for the flame front stabilization and the fuel-air mixture initiation of the burning. Recently a plasma assisted combustion technology is discussed for purpose of a high-speed combustor development [11].

Besides of a traditional thermal approach some investigators propose mechanisms of a laminar and turbulent boundary layer modification through a change of the second viscosity of the gas [12,13]. In this case an extra vibrational excitation of the gas can play an important role in the viscous drag reduction.

At volume type of energy input in boundary layer the gas is “hot” not only near a point of heating but in downstream region due to airflow (independently on velocity of outer flow). Below the point (line) of energy input there is a heated boundary layer and relatively “cold” wall. At least, heat transfer has direction to the wall. In this case BL is stabilized due to more

full profile of it. A gas temperature in BL is changed slower along streamlines due to recombination processes. Correspondingly a local Reynolds number changes slower also.

The most peculiarity of hypersonic BL is a similar to supersonic and subsonic BL with energy release in more or less degree. Main difference is that a heating of BL is provided by means of outer sources (dissipation of electromagnetic energy in discharge, for instance) but not only by dissipation of mechanic power. A power of external source can be controlled outside in accordance with defined task.

At high level of input energy and thin BL (high power density) a gas density in BL could occur so low, that mode of flow passes continuous to transitional or free-molecular one. So, the Knudsen number in this case will be large. For example, at altitude 20-30km and gas temperature 3000-10000K Knudsen number will be in range $Kn=0.02-0.1$. Plasma influence in such places is just unpredictable. So local measurements are preferable. Taking into account above, the best place for a plasma formation (heat release) is the area with maximal mechanical energy loses, namely: area of critical point and line of reconnection after flow separation, fore part of plates and profiles and areas of shock waves interaction with BL. A laminar-turbulent transition removes below. In case of flow separation due to interaction of BL with SW on a profile, plasma formation prevented a separation process.

Generally, the volume type of energy input into the BL effects on external non-viscous flow. A character of influence depends on specific mechanism of interaction between discharge and gas flow. Two different modes: “streamlining” and “flowing through” can be released. Really both mechanisms take place in a different proportion. In first case the influence on external flow is higher than in second one. Speed of flow is important at description of specific mechanism of interaction. At location of such discharge in a special geometrical configuration there is possible to provide a frictionless flow around a body. In the second case an energy release or plasma formation more influents on a boundary layer itself, in particular, leads to increase of a kinetic energy of gas.

The friction drag is a result of a velocity shift inside a boundary layer close directly to the FV surface. Friction coefficient value, as known, depends on a set of factors, the basic ones of them are Reynolds number (Re), Mach number (M), Prandtl number (Pr), Schmidt number (Sc) which determine the processes of energy dissipation, heat exchange, diffusion, as well as wall temperature value, turbulence level value and surface roughness level value, FV geometry etc. An influence of each a factor mentioned has its own physical nature. The Reynolds number characterizing a ratio between inertial and viscous properties of a boundary

layer determines a flow mode in it. In case of a laminar mode the friction drag coefficient can be ten times less than the one in case of a turbulent mode. At the same time Reynolds number increase results in friction coefficient reduction at any flow mode, until the surface roughness influence begins exhibiting in case of a turbulent mode. When Mach number, being a parameter of a similarity on a compression, increases, the friction coefficient decreases as a result of a boundary layer thickness increase caused by its heating due to dissipation processes. [14]

There is a strong correlation between the factors, influencing the aerodynamic drag components that can be seen from the brief enumeration of these factors. Therefore an attempt of changing of one component results in changing of others and this change can have both identical and opposite signs. For example, friction coefficient reduction in front of the base shear results in base rarefaction increase and, as a consequence, in base drag increase.

The existing ways of friction drag reduction are based on a directed influence upon airflow near the surface and in fact are the ways of control laminar and turbulent boundary layers. Under the flow laminar mode the friction drag is ten times less than the one under the turbulent mode. Therefore preservation of a gas flow laminar mode in a boundary layer permitting in separate cases make the drag friction 90% less underlies a way called "laminarization of a boundary layer". As is well known, the laminarization can be reached by means of a surface shape selection, by the suction of small gas portions through the permeable skin, by utilization of elastic-damping coverings and influence of magnetohydrodynamic effect on transition from a laminar flow mode to a turbulent one.

The pressure profile along the external boundary of a boundary layer considerably depends upon the shape of a streamlined surface. Essential influence of a longitudinal gradient of pressure upon the transition had been detected experimentally in 40th already, underlay the elaboration of laminarized profiles. Thus for planes wings for Reynolds numbers $5 \times 10^6 - 4 \times 10^7$ creation of a laminar segment in a boundary layer for the space of (along the) 50-70% of a chord and friction drag reduction more than three times were a success only due to the choice of geometric shape and ensuring of surface smoothness. However it is possible to keep up a laminar flow over major parts of a surface by artificial way only, for example, by the suction of small air portions from a boundary layer through the very thin slots in the FV covering. Systems ensuring a suction, have passed testing of principle under operational conditions at the experimental planes F-94 and X-21 (USA) and HP-113 (England) in 60-th already.

Moreover steady reduction by 40-60% (taking into account an output required for the boundary layer suction) of the planes aerodynamic drag was obtained. Suction is also an effective method for different boundary layer instability suppression. Thus in [19] suction influence on Taylor-Goertler instability accelerating the growth of Tollmien-Schlichting waves and, consequently, accelerating the laminar-turbulent transition process is investigated theoretically. It is shown that the suction results in flow stabilization as well as in case of Tollmien-Schlichting waves. For the flow stabilization in a boundary layer one can use suction through a porous surface, uniform for a surface part or for the whole surface and suction concentrated in one or in several surface points, defined by the flow character as well. The combination of a periodic injection-suction [20] is also applied. The essential friction reduction can be also achieved by damping of velocity fluctuation in a boundary layer with the use of elastic damping covering of the skin that promotes laminar mode preservation. The deformation of a surface should be enough for the wall to carry out the work under fluid i.e. to return energy to a boundary layer. In case of wall deformation realized in anti-phase to the unstable Tollmien-Schlichting wave the successful damping of this wave is possible.

Thus in [21] the outcomes of theoretical research of damping capability of already developed waves with the help of vibrator with specially selected parameters are presented. It is also shown in [21] that such devices allow to suppress disturbances in a laminar boundary layer and to delay its transition into turbulent mode. The fact that at high velocities a gas becomes conductive, makes possible using electrical and magnetic fields generated on FV board for boundary layer parameters control. Thus, for example, magnetic field can laminarize a boundary layer [22] but acceptable efficiency of such influence can be reached only if the gas in a boundary layer is highly conductive.

The friction drag reduction in case of a flow turbulent mode can be achieved, as a rule, with the help of gas injection either through the skin slots or through a porous surface or by using ablative injection. The injection can be either perpendicular to a body surface or tangential, and the last one is more effective [23]. However significant drag reduction can be reached and by means of injection through a porous wall as well, and injection effect can be strengthened by using the other kind of gas. [24]

The other possible way of friction drag reduction is the application of fine-ribbed (-edged) surfaces with the edges directed along the flow. The outcomes of experimental researches [25, 26] have shown, that with appropriate edges geometry drag of a plane plate in a subsonic flow ($V = 5-100$ m/s) can be reduced by 8-10%.

Considering this or another way of friction drag reduction it should be kept in mind that a laminar boundary layer is more predisposed to a separation than a turbulent one. Therefore an influence on a boundary layer in order to reduce friction drag raises the possibility of its separation that can result in the appearance of non-counted modes. If these modes result in more negative consequences than the friction increase it is necessary to take measures for separation preventing. Such measures can be a change of the body surface shape or boundary layer turbulization by application of obstacles or mechanical vortex generators with a various design and surface arrangement [27]. The opposite case is possible as well - for example, boundary layer turbulization in order to separation shift at "thick" low-streamlined bodies (an orb) and at "thin" bodies (wing profiles). In the first case, providing base drag reduction with friction drag increase due to turbulization we obtain reduction of total drag. In the second - the friction drag increase value exceeds the base component reduction value what results in the total drag growth. The theoretical principles of all these methods are presented in [22] and the examples of their practical realization can be found in [27, 29].

It should be noted that methods of friction drag reduction considered are based on either removal of high-entropy gas layers at the wall (suction), or additional mechanical energy transfer to these layers (mobile walls, tangential ejection, mixing intensification with upper layers of a boundary layer etc.).

Other well-known ways of friction drag reduction use wall heating or wall cooling, as the wall temperature change influences a lot both the drag value itself under this or that flow mode and laminar-turbulent transition, i.e. the critical Reynolds number value. It is known that heat supply from a wall to a boundary layer decreases velocity gradient increasing the layer thickness that results in reduction of friction stress. The physical explanation is that the relative wall temperature increases with Mach number at the thermal insulating surface grows. As a result the boundary layer thickness increases, the velocity profiles completeness decreases, and the laminar boundary layer becomes less steady. As it can be seen the well-known methods are based for the particular body on the influence on a boundary layer using as a rule the wall condition change.

The ways of lift increase at the boundary layer control are based, as a rule, on separation prevention and delaying for a particular body or on a controlled separation generation. These methods include well-known mechanical methods (dashboards, trimmers, rollers, slats, rotated cylinders installed at a wing leading edge, trimmer with a free streamline) or gas-dynamic (injection, suction etc.) methods mentioned above.

Recently in search of new economic and simply realized methods of boundary layer control the possibility of control by means of gas property and gas state changes in a boundary layer itself and in an external non-viscous flow is considered. This direction is connected to the development of power methods of streamlining control based on energy supply to a flow streamlined body. Though the theoretical and experimental researches carried out within the framework of this direction are mainly devoted to the wave drag reduction, the results of some of them demonstrate the possibility of influence on a boundary layer as well.

In [32] volumetric energy supply in rectangular area of laminar and turbulent boundary layers on a plate at number $Re = 3$ was considered. In ref. [33] influence of energy supply to a turbulent boundary layer also was investigated but in contrast to the mentioned above conditions of constant wall temperature the condition of thermal insulating wall was used.

In a Kogan's works [6,7] the possibility of laminar boundary layer stabilization by means of plate heating at a leading edge was studied. It is shown that the heating increases stability of a laminar boundary layer. The result is interesting. Usually such effect because of known reasons results in wall cooling. Electro-gasdynamic influence on the development of the small disturbances in a boundary layer at the plate and in the thin profile was considered. Here the unipolarly charged ionic jet spread along a surface is considered. The system of electrodes used for an ionic jet in glow discharge generation was simulated by two semi-infinite gauze electrodes (not causing a flow disturbances) installed in sections x_1 and x_2 of a profile perpendicular to a running flow and by one electrode inside a profile in its tip. It was shown that at the electro-gasdynamic streamlining Reynolds number of a boundary layer transition could increase up to 13% for a plane plate and up to 8-11% for a thin profile.

All samples above show that a lot of different factors defines a behavior and conditions of a boundary layer. Namely, these are three main groups:

- parameters and conditions of outer non-viscous, in relation to boundary layer, airflow;
- parameters of a gas and flow inside boundary layer;
- parameters and conditions of wall itself.

A value of friction tension depends on Mach number of non-viscous flow and longitudinal gradient of velocity strongly. From the other side a degree of initial turbulence essential influents on a boundary layer instability development. It effects on laminar-turbulent transition point, i.e. on a critical value on Reynolds number.

Roughness of a streamlined body wall exerts a similar influence as a degree of initial turbulence. At turbulent mode the roughness of a wall defines a friction tension. Besides, a

curvature of the wall (influence of centrifugal forces), permeability of surface (blowing out, sucking of a gas through the wall, erosion of wall substance...), flexibility, relative temperature of the wall, catalytic ability of a wall surface influent on a friction drag and a separation point. Two last factors are rather important for a high temperature, chemical active layers. Recombination will do on a different way in depends on relation between a wall temperature and stagnation temperature of flow. It directly influents on a value of thermal load on a wall and on viscous tension. A catalytic ability of the surface also effects on processes inside of boundary layer.

Besides of factors in outer airflow and conditions on a wall, role of gas properties inside of boundary layer is important as well as thermal and chemical processes. They are viscosity, heat transfer, diffusion, character and intensity of direct and inverse chemical reactions, rate of them and relative rates of relaxation processes.

At mathematical simulation of boundary layer problem on continuation there was defined that initial data on left edge effect on BL development below in flow. At the same time they (initial condition) depend on formation processes of BL. An essential difference exists in initial state of turbulent BL in case of development at reconnection after laminar separation or in case of laminar-turbulent transition. The similar difference might be at formation of BL in critical point of blunted bodies in supersonic airflow in dependence on condition in points of reconnection on bodies with nose needles. A further development of BL depends on type of transition or initial conditions. At any cases (on profiled bodies and plane plate) viscous tension has a maximal value in places of BL occurring. It shows that namely in such places loses of mechanical energy are maximal. So a parameter, which present ratio a thickness of energy loses via thickness of impulse loses, has a significant importance. Seems that namely on this reason a gas blowing out near fore part is the most effective. Moreover, heating of simple plate near fore edge decreases a friction drag and leads to stabilization of laminar boundary layer (in contradiction with general conception).

An observation of BL and recognition of the gas parameters inside of BL are difficult due to low thickness and small gradients of gas density. New informative methods are complex technically, as a rule [36,37]. More conventional methods give limited information and have to be used together one with others [38].

Charter 5.

Short Discussion. Conclusion.

This Report analyses and discusses results of the last experimental works on influence of discharge surface plasma formation on characteristics of viscous friction and separation processes under high-speed airflow. Very often plasma generation occurs on a non-homogeneous manner. It provides an energy release to airflow as well as change of gas-kinetic and electro-magnetic properties of the medium. The work is providing in frames of Advance Flow/Flight Control (AFFC) concept.

The analysis is based on a suggestion of a viscous friction reduction and change of transition line position. New experimental results on plasma influence on a boundary layer near a plain plate and a profiled plate are presented. The experiment was conducted in transonic wind tunnel at Mach number $M=0.5-1.1$. In dependence with Mach number a Reynolds number (on length 1m) was in range $1-1.5 \times 10^7$. During the test a balance measurements of friction drag and optical observations (natural, shadow and Schlieren) were fulfilled. Shadow photos show a structure of airflow and a separation line location. The most prospective configuration was a plasma generation near fore edge of the plate (i.e. in an area of maximal energy losses of airflow). Large plasma influence has been observed. Effective configurations for a plasma generation are proposed. New experimental data on plasma generation near the body's surface and influence on a position and volume of separation zones are presented. The experiment has been conducted under the condition of transonic airflow.

The condition of boundary layer determining value of friction stresses depends on a great number of factors. All of them could be broken in three groups: factors of the inviscid flow external to the boundary layer; factors, determined by conditions on the round-flown surface and properties of the wall itself; properties of gas in the boundary layer itself and by aerothermochemical processes developing inside it. The third group of factors when it is not subject to external action is determined by the factors of the first two groups, i.e. is dependent on them, and there is no sense to allocate them to a separate group. However the situation changes when there is an external action against the boundary layer not dependent on the wall conditions and those in the external inviscid flow. Direct energy supply right into the boundary layer via electrical discharge, laser or microwave radiation, etc. could be an example of such external action.

Condition of the boundary layer downstream, as it was noted earlier, in many respects is determined by conditions of its formation. It is stipulated by the fact that losses of mechanical energy in those places, as the practice shows, are maximal. Their value may come out different depending on flow mode (laminar or turbulent), as well as on whether the boundary layer is formed in a flow or the one earlier turn off the surface is being attached. Desire to take into account influence of as many of the factors referred to above as possible during experimental research of influence of electrical discharge upon value of friction drag has determined selection of transonic flow modes ($\dot{I}=0,4 - 1,05$).

Discussion of optical and weight experiment results. Flat plate. $\dot{I}=0,9-0,99$. Photographs received with a Schlieren shadow device allow to note the following features. There is a lambda shock formed in the front part of the plate. The first (oblique) lambda shock appears approximately at the nose of the model, while the main shock is localized in the plate area, moving up and down the flow as measured against the middle of the plate. It is necessary to note, that the reason for bifurcation of the first oblique lambda shock in the upper part is its weakening by disturbance waves radiating from a part of the fixed plate, on which the electrodes are placed. For the same reason, as well as because of weakening of the first oblique lambda shock, it is possible to observe some “diffuseness” of the main shock wave. These photos match cases of flow without discharge and with discharge. Switching on discharge does not influence the first oblique lambda shock form, resulting, nevertheless, in essential change of the main shock wave. On shadow photos it is possible to see separation and noticeable bias down the flow of the main shock in the middle part of the model's width, where the electrical discharge energy was supplied to the boundary layer. It is possible to put in the basis of explanation of those phenomena the following considerations. The place of discharge is a source of the boundary layer laminarization because of gas viscosity increase in the boundary layer. Due to that intensive intermixing of heated in discharge and cold layers of external flow gas occurs later. A boundary “plasma” thermal layer is formed, which cross-sectional sizes are much greater than thickness of the boundary layer itself in case of discharge absence. It results in laminar-turbulent transition point moving down the flow and increasing the effective Mach number of the flow in supersonic area. Hence, the straight shock relocates downstream.

The same features are exhibited in the case of supplying energy behind an obstacle in the form of triangular barrier set before the movable plate. It is necessary to pay attention here to absence of disturbance waves produced in the previous cases by plate/electrode and

electrode/electrode joints, since they are in a stagnant zone behind the obstacle. As a result the first oblique lambda shock, following the powerful centered wave of rarefaction going out of the side top, has, as it is seen in the picture, a precisely contoured shape. It is also necessary to note, that energy supply to the stagnant area is characterized by larger power insertion, than in the previous cases. Therefore heat up of large masses of gas at the wall results in “spreading” the shock in the boundary layer at a greater distance from the wall.

$\dot{I}_{\text{э}}=0,8 - 0,9$. On the shadow photos one can also see a lambda shock, which position completely meets known legitimacies of transonic flows - when Mach number is decreasing, extent and intensity of shock waves go down too, and they move to the front edge. It is confirmed by comparison of flow patterns to strain gauge readings record. These photos show that the main shock wave at discharge burning moves from the movable plate to the area located between electrodes, while the slope angle of the first oblique lambda shock increases.

$\dot{I}_{\text{э}}=0,5-0,7$. Processed shadow photos allow to make a cautious conclusion about a probable laminarization of the boundary layer, i.e. tightening of laminar - turbulent transition. The obstacle on the movable plate stabilizes discharge because of a stagnant zone formation.

Contoured plate. $\dot{I}_{\text{э}}= 0,8$. During the runs shadow photos do not show visible differences in pressure distribution for cases with and without discharge, which provides grounds to believe that the apparent reduction of drag at excited discharge is stipulated by reduction frictional force. This reduction of frictional force is determined by the boundary layer thickness increase due to its heating by electrical discharge.

$\dot{I}_{\text{э}}=0,4-0,56$. Weight tests show, that discharge results in drag reduction of approximately 30-90%. The shadowgraphs show noticeable difference between cases with switched on and switched off discharges in the boundary layers. With discharge switched on one can observe a thick enough homogeneous heated up boundary layer. The reason of dropping drag should be searched for in heating of the boundary layer. It allows making a conclusion that in the latter case the boundary layer was laminar before the discharge, while switching on discharge has not changed flow mode in it, considerably lowering viscous drag.

Transonic flow. At large supercritical Mach numbers a lambda shaped shock wave is formed on the top of the model. The first oblique lambda shock starts approximately from the model's nose, while the main shock is located approximately in the middle of the movable plate. The flow boost to supersonic velocity in the top of the flow becomes possible due to formation of a small locked separation area near the front sharp edge being a corollary of flow stall because

of a small positive angle of attack. This angle of attack (equal to zero prior to the run) is being established after the duct (WT)'s reaching the working mode due to strong lifting force, defined by the model's asymmetry. Switching on the discharge, as one can see on the photo, barely influences the first oblique lambda shock's shape, while the main shock wave moves downstream noticeably. The explanation to this phenomenon can be given according to the following arguments.

It is known that after passing of the first oblique lambda shock, depending on its intensity the boundary layer may remain laminar, become turbulent or tear off the plate's surface with a subsequent affixion (separation zone formation). In the first case the subsonic part of the boundary layer is much greater in thickness than in the case of the turbulent boundary layer (compare velocity profiles). Therefore shock wave strength in the boundary area in the first case is lower, than in the second one. On the other hand, thickness of the turbulent boundary layer along the plate grows faster, than thickness of the laminar layer. Therefore deceleration degree of the external supersonic flow before the main shock in the second case will be greater. These two circumstances (larger intensity of the main shock and smaller local Mach numbers before it) result in placement of the main shock wave in the second case closer to the front edge.

Applying those reasons to our case, it is possible to explain displacement to the stern part of the main shock wave under plasma excitation, if the following suppositions are made. With Mach number close to one, intensity of the first oblique lambda shock is sufficient for the boundary layer attached behind the front separation area to become turbulent. This case is matched with shock wave structure on the photo of switched off discharge. Application of electrical discharge energy laminates the turbulent boundary layer formed after affixing, by warming it up (increments its mechanical energy and reduces Reynolds's number). The latter in view of the above-mentioned arguments provides an explanation of the reasons for displacement of the main shock wave to the stern part of the model.

Subsonic profile flow around. According to weight tests results, at Mach numbers smaller than critical the discharge excitation at the plate before the front edge of the model's contoured movable part results in considerable drag reduction. This reduction of general drag is a consequence of reduction of both friction and profile drag. The reasons of friction drag decrease are described above. As for profile drag decrease, it could be explained if the discharge "flow around" model were accepted. Provided that the discharge, excited at the

wall, organized directly behind the front separation zone, which in this case becomes open, together with it forms an extended stagnant area in front of the lower pressure profile. Pressure decrease at the frontal part of the profile results in profile drag decrease. Pressure distribution measurements agreed with such a motivation.

The condition of a separation as well as the shape and volume of separated zones are important for the objectives of external aerodynamics and internal flows both. The model experiment demonstrates possibility of plasma control of gas parameters (pressure, temperature) and geometric parameters (dimensions, vorticity) in such a zone. Comparison with data of mathematical simulation allows predicting possible after-effects at different level of energy deposition.

Conclusions.

1. The study has demonstrated the fact of considerable influence of surface plasma formations on characteristics of flow around developed surface models. The rule of the most response on an external influence when applying in the area of maximal mechanical energy losses is confirmed. The mechanisms of plasma influence are resolved. The dependence of plasma effects on power release is obtained.
2. The work has demonstrated the change of a transonic flow structure with plasma formations created in the flow closed to the model surface. The energy supply to the boundary layer in transonic modes may cause the reformation of shock wave structure resulting in either increasing or decreasing of the friction drag depending on particular flow conditions. The displacement of a normal shock wave above the surface has been observed in a result of plasma influence. Under conditions of the subsonic flow around a contoured plate the total drag reduction in several times is observed while a surface discharge creating.
3. The potentiality of a properly organized electrical discharge to prolonging laminar-turbulent transition and to reducing friction drag as well has been demonstrated for both laminar and turbulent boundary layer cases. The turbulence spectrum in airflow has trend to low frequency disturbances suppression. At the same time the discharge plasma can add own low scale disturbances to flowing gas.
4. The comparison of experimental data and calculation results based on laminar boundary layer and turbulence development models has shown that the obtained experimental data is sufficient for the calculation code validation calculation in cases of surface energy input.

5. For maintenance of stable discharge excitation the electrodes should be placed behind shelves or in cavities, if the surface design allows. On flat surfaces it is necessary to apply discharges with high propagation velocity such a high frequency or pulse streamer/filament discharge. The design of a plasma generator and the definition of operation modes depend on specific flow conditions (no universal decisions).
6. Two modes of discharge spacing near fixed separated zone (back step type) are described: (1) current localized between the “hot” and grounded electrodes, and (2) current from “hot” electrodes to back wall of the test section. Plasma excitation in separation zone (mode 2) causes the pressure redistribution. The longitudinal pressure gradient in separation zone is decrease significantly. Translational temperature in a separation zone is achieved the value 1500K. At the same conditions the vibrational temperature can be in a range of 5000K. A mathematical simulation shows results qualitatively closed to the experimental ones. The pressure and temperature behaviour in the separated zone are in accordance with experimental data and correspond to the significant modification of separated flow structure. Moreover, the simulation predicts a separation-less mode at higher energy release. This effect observed at the first in the present study needs more experimental and analytical efforts to evaluate its practical importance.

6. References

1. Workshop on Weakly Ionized Gases. USAF Academy, Colorado, 9-13 June 1997; Second Workshop on Weakly Ionized Gases. Proceedings. Norfolk, 24-25 April 1998, Third Workshop on Weakly Ionized Gases. Proceedings. Norfolk, 1-3 November 1999.
2. V.Bityurin, A.Klimov, S.Leonov "Assessment of a Concept of Advanced Flow/Flight Control for Hypersonic Flights in Atmosphere." Suggested to be presented to 3rd Workshop on WIG. November 1-5, 1999 / Norfolk, Virginia, AIAA 99-4820.
3. T. Cain, D. Boyd "Electrodynamics and the effect of an electric discharge on cone/cylinder drag at Mach 5", 37th AIAA Aerospace Sciences Meeting and Exhibit, January 11-14, 1999/Reno, NV, AIAA 99-0602.
4. S. Leonov, V. Nebolsin, V. Shilov "Effectiveness of plasma jet Effect on Bodies in an Airflow", Proceedings of Workshop "Perspectives of MHD and Plasma Technologies in Aerospace Applications", Moscow, IVTAN, 1999, pp. 58-65.
5. G.G.Chernyi, The impact of electromagnetic energy addition to air near the flying body on its aerodynamic characteristics. 2-nd WIG Workshop, proceeding, Norfolk, VA, April 24-25, 1998. Levin V. A., Afonina N. E., Gromov V. G., Influence of Energy Input by Electric Discharge Supersonic flows around bodies. 2nd WIG Workshop, Proceedings, Norfolk, VA, April 24-25, 1998.
6. Kazakov A., Kogan M., Kuriachi A., Influence on the friction of local heat addition to the turbulent boundary layer. Mech. Of Fluids and Gases, N1, 1997. Kurjachi A. P., Boundary layer transition by means of electrodynamics method. Prikl. Math. I Mech., vol.49, issue 1,1985.
7. A.V. Kazakov, A.P. Kuryachii, Electrogasdynamic influence on the development of the small disturbances in a boundary layer in the thin profile Izv. ÀN USSR, Mekhanika zhidkosti i gaza, 1, 1986
8. S. Leonov, V. Bityurin, V. Gromov, N. Savischenko, A. Yuriev "Influence of Surface Electrical Discharge on Friction of Plate in Subsonic and Transonic Airflow". 39th AIAA Aerospace Sciences Meeting & Exhibit, 8-11 January 2001 / Reno, NV, AIAA 2001-0640.

9. Yu. Shcherbakov, N. Ivanov, N. Baryshev et al. Drag Reduction by AC Streamer Corona Discharges along Wing-like Profile Plate, 31-th AIAA Plasmadynamics and Lasers Conference, Denver, 2000, AIAA-2000-2670.
10. Guillermo Artano et al. "Flow Control with Electrohydrodynamic Actuators" 39th AIAA Aerospace Sciences Meeting & Exhibit, 8-11 January 2001 / Reno, NV, AIAA-2001-0351
11. . Klimov A., Byturin V., Brovkin V., Vinogradov V., Van Wie D.M. "Plasma Assisted Combustion", 39th AIAA Aerospace Sciences Meeting & Exhibit, 8-11 January 2001 / Reno, NV, AIAA 2001.
12. E. Kogan, I. Zavershinsky, Drag force coefficient in presence of heterogeneous relaxation. Proceedings of the 2nd Workshop on MHD-PA in aerospace applications. Moscow, IVTAN, 2000, p.180.
13. N. Molevich, V. Nenashev. Bulk viscosity in non-equilibrium media. Proceedings of the 1st Workshop on MHD-PA in aerospace applications. Moscow, IVTAN, 1999, p.124.
14. D. Kyukheman, Aerodynamic Planes Designing. M.: Mashinostroyeniye, 1983, p.555.
15. P. Chzhen, Separation flow Moscow: Mir, 1973 v.3, p.14.
16. A.S.Yuriev, V. Yu. Borzov, I.V.Rybka, Dependence of high-speed elements on local heat sources in approaching flow, 2nd WIG Workshop, Proceedings, Norfolk, VA, April 24-25, 1998;
17. V.M. Nizovtsev, N.P. Savishyenko, A.S. Yuriev, Method of the definition of the heat emission coefficient on a model surface in a gas flow with use of laser radiation, 10th Vsesoyuznaya teplofizicheskaya shkola "Fizika relaksiruyushikh sistem", Tambov, 1990.(rus.)
18. Goshek, High-speed Aerodynamics, S.: "Inostrannaya literatura", 1954
19. J. M. Floryan, W. S. Saric, Effects of Suction on the Gortler Instability of Boundary Layers, Aerospace Technics, vol. 2, No. 7, July, 1984, p.p.134-139.
20. V.M. Gilev, V.V. Kozlov, Influence of a periodic injection-suction on a process of transition in a boundary layer. Preprint 1-85. Novosibirsk: ITMP SO AN USSR, 1985
21. O.A. Efremov, O.S. Ryzhov, E.D. Teren'tyev, About damping unstable oscillations in a boundary layer, Izv. ÀN USSR, Mekhanika zhidkosti i gaza, 1987, p.p. 20-26.(rus)
22. NASA, Rep. 1358, 1958.
23. Technical information // News of foreign science and engineering. Air and rocket engineering / ÎNTI TsAGI , 3, 1984, page 1-32.
24. A. Smith, Progress in Hypersonic Turbulent Boundary Layer Control, AIAA-2000-2322.

25. G.V. Yenyutin, Yu.A. Lashkov, N.V. Samoylova, Experimental research of influence longitudinal edging on plane plate friction drag, *Izv. ÀN USSR, Mekhanika zhidkosti i gaza*, 2, 1987
26. Walsh M. J., Lindemann A. M., Optimization and application of riblets for turbulent drag reduction | 22nd AIAA Aerospace Sciences Meeting. January 9-12, 1984, Reno, Nevada/
27. P. K. Chang., Control of Flow Separation. M.: MIR, 1979.
28. G. Schlichting, The theory of a boundary layer, M.: Nauka, 1974
29. P. K. Chang, Separation of Flow, M.: MIR, 1973, vol. 1-3.
30. A.P. Mel'nikov, I.A. Sychyov, N.F. Fillipov, *Gashydrodynamics*, L. p. 470, 1968
31. Levin V. A., Afonina N. E., Gromov V. G., Influence of Energy Input by Electric Discharge Supersonic flows around bodies. 2nd WIG Workshop, Proceedings, Norfokk, VA, April 24-25, 1998.
32. V.N. Nizovtsev, G.N. Moskalets, Influence of the local heat- and mass supply area arrangement on pressure and friction profiles (distribution) on the plate surface in supersonic viscous gas flow, In issue "Methods of researches of the aerothermodynamic characteristics of the hypersonic flight vehicles", Thes. Of the reports, shkola-seminar TsAGI "Mekhanika zhidkosti i gaza", Feb. 25 - March 1, 1992 p.p.140-141
33. Larin O., Numerical Investigation of the flow in supersonic laminar boundary layer with external heat addition, *Inst. Of Mech. Moscow Univ.*, Report 4351,1994.; Larin O., The turbulent supersonic flow in boundary layer with external heat addition. *Inst. Of Mech. Moscow Univ.* Report 4436, 1995.
34. P. Baronets, A. Kolesnikov, S. Kubarev... Superequilibrium heating of surface in subsonic jet of dissociated air. *Izvestiya RAS, MZhG (rus)* 3, 1991, p.144-149.
35. Yu. Rayzer Physics of gas discharge. Moscow: Science. 1987. pp 479.
36. P. Wu, R. Miles, MHz Rate Visualization of Separation Shock Wave Structure, AIAA-2000-0647.
37. A. Yalin, W. Lempert and others, Planar imaging in a Mach 8 flow using sodium laser-induced fluorescence. AIAA-96-2270.
38. J. Naughton, M. Sheplak, Modern Skin Friction Measurement Techniques: Description, Use, and What to do With the Data. AIAA-2000-2521.

7. Acknowledgment.

This Report is based upon work supported by the European Office of Aerospace Research and Development, Air Force Office of Scientific Research, Air Force Research Laboratory, under the EOARD-ISTC-IVTAN Project No. 1780P. The work has been monitored by Dr. S. Walker.

The authors would also like to acknowledge an accurate and well-disposed assistance of Dr. Ch. Raffoul personally.

8. Applications.

(A) "The Contractor, Dr. Sergey Leonov, hereby declares that, to the best of its knowledge and belief, the technical data delivered herewith under ISTC Project No. 1780P is complete, accurate, and complies with all requirements of the contract."

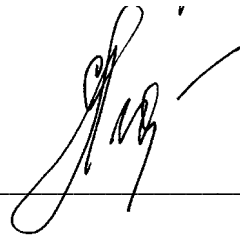
(B) "I, the Contractor, Dr. Sergey Leonov, certify that there were no subject inventions to declare as defined in FAR 52.227-13, during the performance of this contract."

(C) "Any opinions, findings and conclusions or recommendations expressed in this Report are those of the authors and do not necessarily reflect the views of any other persons and organizations."

DATE: _____April,02, 2001_____

Name and Title of Authorized Official:

Dr. Sergey Leonov, Project Manager



Chapter 3.

Surface Plasma Influence on Viscous Friction and Separation Parameters. Transonic and subsonic tests.

3.1. Experimental arrangement and parameters of the test.

Experimental installation consists of the following parts:

- transonic wind tunnel ST-1 with a control panel;
- aerodynamic model with a build-in balance;
- plasma generator and power supply;
- visualization system;
- data acquisition system;
- measuring devices and synchronization system.

3.1.1. Transonic Wind Tunnel ST-1.

Transonic wind tunnel ST-1 concerns to the type of ejector open-ended short-term operation tubes. It consists of a fore-chamber (1), nozzle (2), operating (test) section (3), Mach number regulator (4), ejector (5), diffuser (6), receiver (7) and high-pressure line with an adjusting valve (8) and setting valve (9) (Fig. 3.1.1).

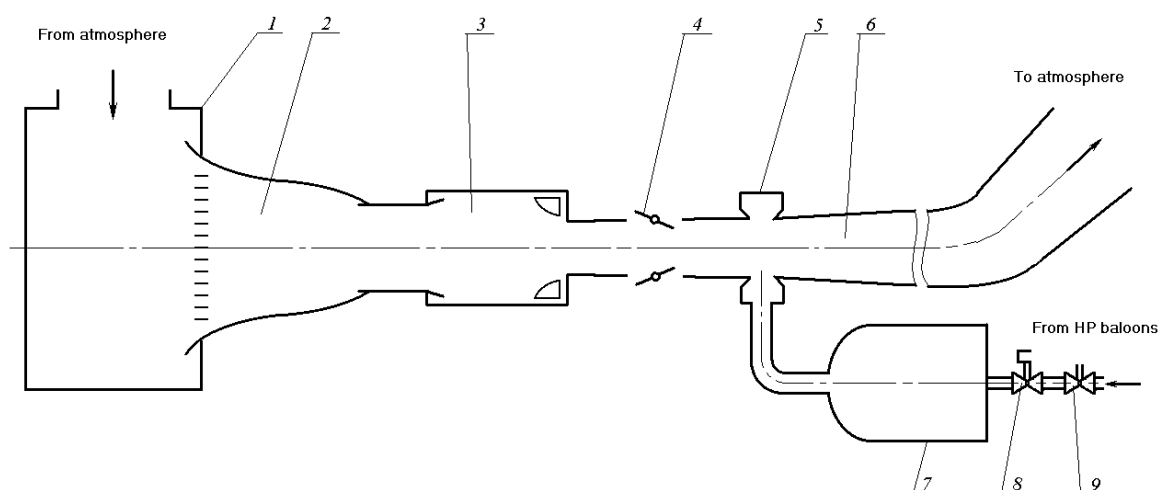


Fig.3.1.1.1. Principal layout of WT ST-1.

The fore-chamber communicates with the atmosphere and provides an air supply to the nozzle. The flow velocity in it is so small that the deceleration conditions existence is possible

to be assumed.

In the nozzle the flow is accelerated. The highest outlet velocity value can reach the sound velocity value. The further velocity increase takes place due to flow extension.

The operating section is closed and has a rectangular cross-section of 300x250 mm. The under test model is set on the special holder in the operating section. For the optical (direct) observation and model monitoring there are several windows closed by protective glasses in lateral walls of an operation section.

The flow Mach number regulation is made with the help of the shutters (4) set in tunnel walls behind the operating section. At the closed shutters the air flows through the operating section and therefore flow velocity in it will be maximum. At the shutters opening the flow velocity in the operating section decreases proportionally to the shutters turning angle value as the air will be partially sucked through the opened shutters, passing the operating section.

The ST-1 tunnel allows obtaining the transonic flow with Mach number that can vary continuously from 0.4 up to 1.17 for a small model.

The high-pressure air is supplied from the receiver to the ejector with the help of which the pressure difference necessary for the obtaining of the accounted velocity value in the operating section is created. Through the ejector loop circuit high-speed air in-flowed to the diffuser and carrying away the operating section air creates a flow in it. Then this flow is ejected in the atmosphere through the diffuser. The flow deceleration takes place in the diffuser in such a way that the energy losses were maximal.

The ejector operation stability is provided for the receiver dampening pressure fluctuations arising during the air throttling by the regulating valve.

The ST-1 tunnel switch-in and cut-off are realized with the help of shutoff and regulating valves which are operated by the remote control unit as well as the Mach number regulator shutters.

The airflow Mach number in the operating section is determined under the aerodynamic functions tables by stagnation pressure to static pressure ratio. The static pressure measurement is realized with the sensor whose sensing element represents the thin-walled metal chamber with bonded resistance strain gauges.

For the monitoring of the model streamlining by the airflow in the tunnel operating section a Schlieren device is applied — a device IAB-451 assembled by the mirror-meniscus optical scheme.

Model.

The scheme of the model is presented in the Fig.3.1.1.2.

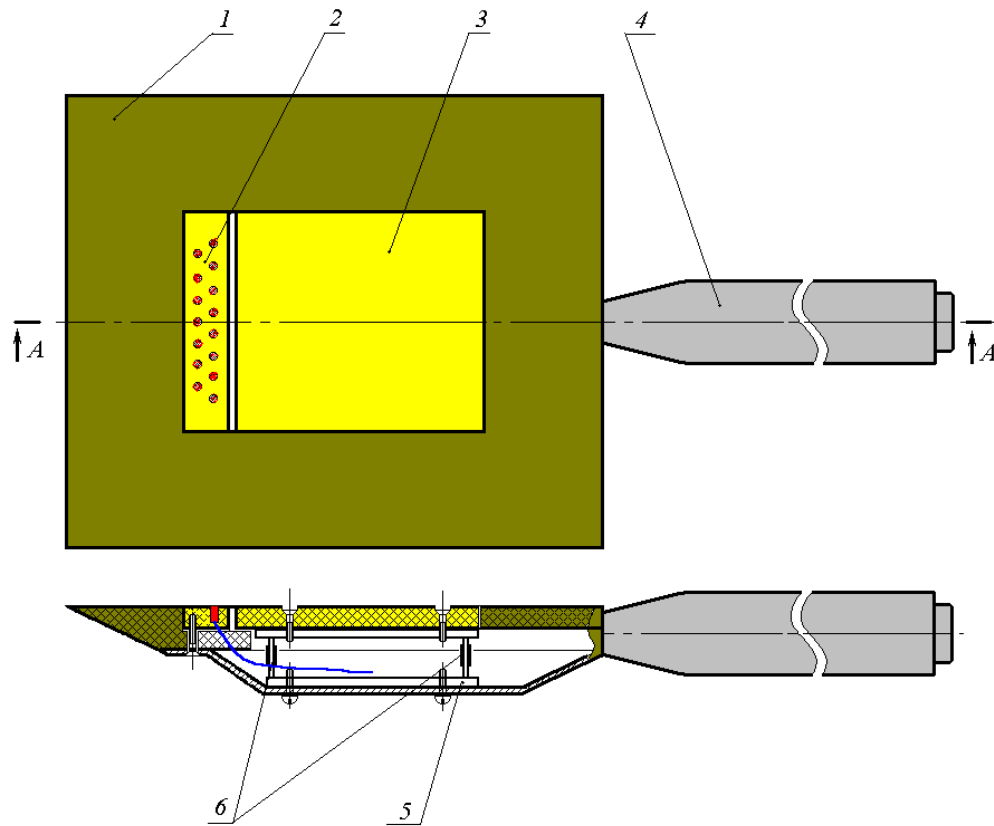


Fig.3.1.1.2. Principal scheme of the model for ST-1 runs.

For the research of the friction reduction on a surface with the help of the surface plasma a special model has been designed. It consists of the following basic elements:

1. · Aerodynamic body, installed from one window up to second one;
2. · Immovable (small) plate with 17 electrodes;
3. · Movable (large) plate without electrodes in this series;
4. · Holder with the strut;
5. · Strain gauge balance;
6. · Tenso resistive strain gauge bridge elements.

The basic element of the model is the body (1) that plays a role of a structure carrier. The model body is right-angled with a sharpen leading edge and fastens on the model holder.

The body consists of two parts. The base part represents a metal duct with housing for the balance. The top part represents a dielectric wedged nose plate 1,5cm width with a slot for the installation of large and small plates with electrodes. Its upper plane is aligned to the up-

running flow direction. The screws connect body top and bottom parts.

Holder (4) represents a hollow steel cylinder with a nose as a truncated cone. The model body is fastened directly to the cone forward part. The balance wires are laid inside the holder. The model is set in the tunnel pylon with the help of the holder.

The large plate has no electrodes in this series of experiments. It is attached to the dual-component strain balance (5) that is inside the body. The balance is intended for the large plate aerodynamic drag measurement. The balance represents a steel frame that is a sensing element. The frame fastens to the back wall of the model body bottom part. The large plate fastens to the frame top part by the screws. For the force measurements four tenso resistance strain gauges (6) are located at the balance frame. The resistance strain gauges are assembled in a semi-bridge circuit. The signal from them is amplified with the help of the low-frequency 8-channel amplifier.

Fig.3.1.1.3. Geometry of the model for a ST-1 experiment. The electrodes on a large plate can be used for the next step of the work.

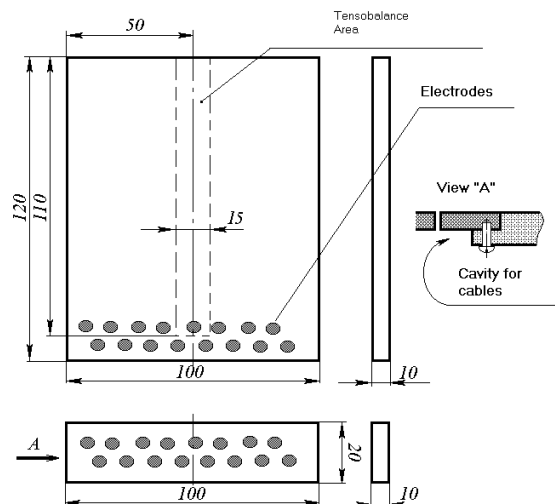
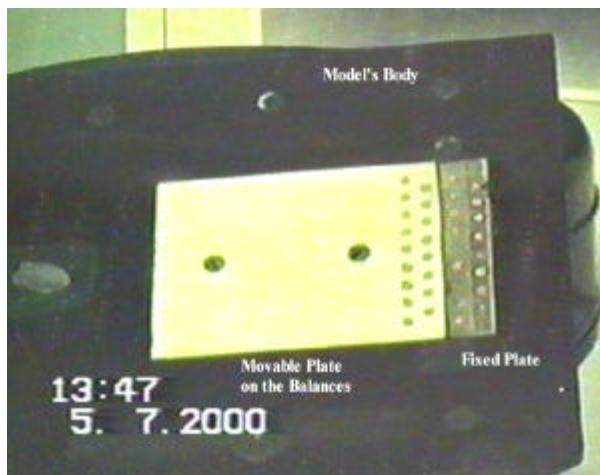


Fig. 3.1.1.4. Photos of the equipped model for ST-1 runs.

Large and small plates (2 and 3) are right-angled. At the small plate there are the electrodes for the electric discharge realization. The feeding wires from the electrodes are removed in a base part of the model body. The small plate with electrodes is fixed at the body by the thermosetting adhesive. Photo of assembled model for test in ST-1 is shown in Fig.3.1.1.4. Electrodes have been made from a cooper alloy. The wires have a good double Teflon insulation.

Several different configurations of discharge plate and a measuring plate in respect of airflow have been tested. They are differed by the shape of a measuring plate, presence of an

artificial obstacle and electrodes position. The most prospective configuration might be a plasma generation near fore edge of the plate (i.e. near an area of maximal energy losses of airflow). Figure 3.1.5 shows these cases.

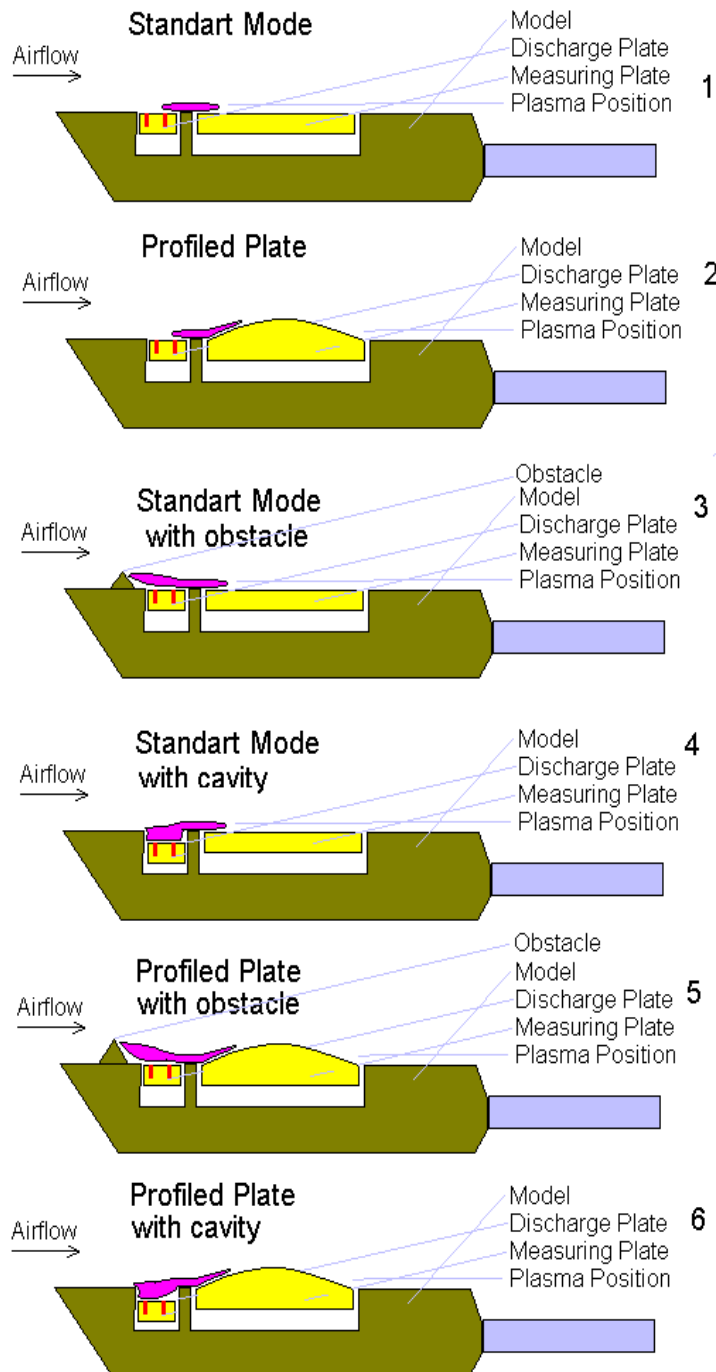


Fig.3.1.1.5. Different layouts of the test.

At the first case, when a plane plate is used and electric discharge is excited in a free stream (no separation) near the surface, plasma area is a thin layer. An appropriate photo is presented in Fig.3.3.3 (see below).

The second case gives almost the same plasma configuration but at profiled plate.

Artificial obstacle (cases 3 and 5) has been applied to generate a separation zone. In a separation area the discharge plasma looks much brighter and powerful (see the next section). The photo of such a case is presented in Fig.3.1.3.4. The problem is that the obstacle changes a structure of external airflow. In a case of cavity (figs.4

and 6) such an influence is less. Nevertheless conditions for a plasma excitation inside of such a cavity is much easier than in a free stream.

3.1.2. Measurement System and Synchronization.

Measuring-registering instrumentation complex of ST-1. Short description.

At the experimental research of the plain and profiled plate aerodynamic drag reduction with the help of energy supply the measuring-registering instrumentation complex has been used. This complex consists of the following elements:

- · Pressure transducers in the ST-1 tunnel operating section (3);
- Pressure transducers for a pressure distribution measurements on a model surface
- · Strain gauge balance (4);
- · 8-channel amplifier 8 АИ× (5);
- · Mirror-galvanometer oscillograph NO43.1 (6);
- · Shadow Schlieren device IAB-451 (7-10).

After a modernization the oscilloscope “Tektronix TDS-210” electronic pressure commutator ESP-32 and computer “Toshiba-420” have been included for the digital recording of balances signal and a pressure distribution.

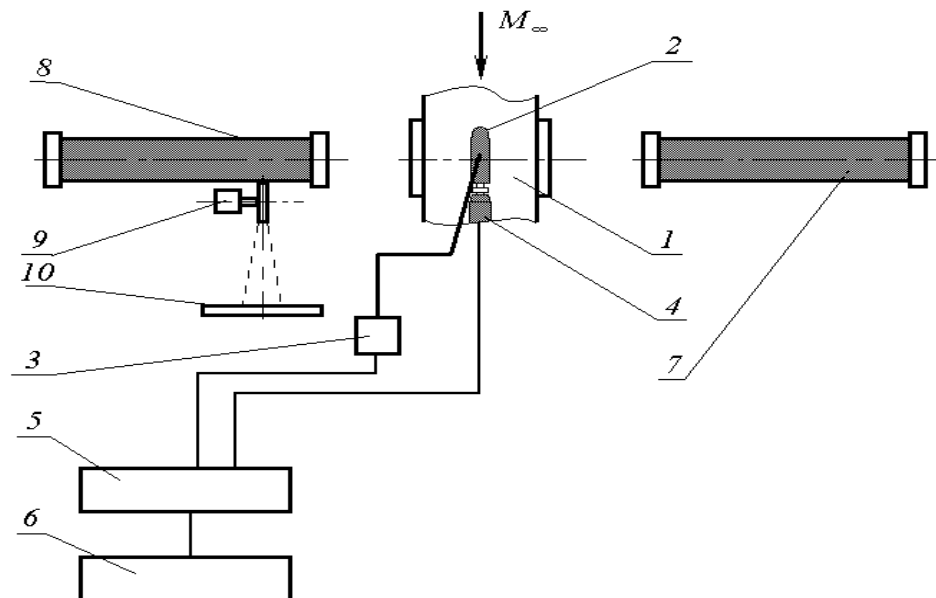


Fig.3.1.2.1. Layout of measuring system of ST-1.

The pressure transducers in ST-1 tunnel test section (3) are applied for the test section Mach number definition (1). The transducer signal is amplified by the low-frequency 8-channel amplifier 8 АИ× (5). Then the signal from the amplifier is transmitted to the mirror-galvanometer oscillograph (6), which in turn records the pressure variation diagram on a

photo-tape. For the aerodynamic drag measurements strain gauge balance (4) is used, the signal from which is also transmitted to the 8-ANCh amplifier and then to the mirror-galvanometer oscillograph and is recorded as the temporary diagram. Before the experiment realization the pressure transducer and strain balance calibration is carried out for the calibration coefficients K_p and K_q are to be determined.

For the model streamlining monitoring the device IAB-451 is used, which consists of a collimator (7) and an observation tube (8). At the experiment realization either the streamlining monitoring is occurred by the help of a screen (10) or the image is recorded by photo or video camera (9). An appropriate layout is presented in Fig.3.1.2.1.

In the out of a wind tunnel the gauge of absolute pressure “Honeywell™” is established, reference of base pressure is deduced in a point of measurements of this gauge, and thus, the checking of reference of the base pressure gauge is made.

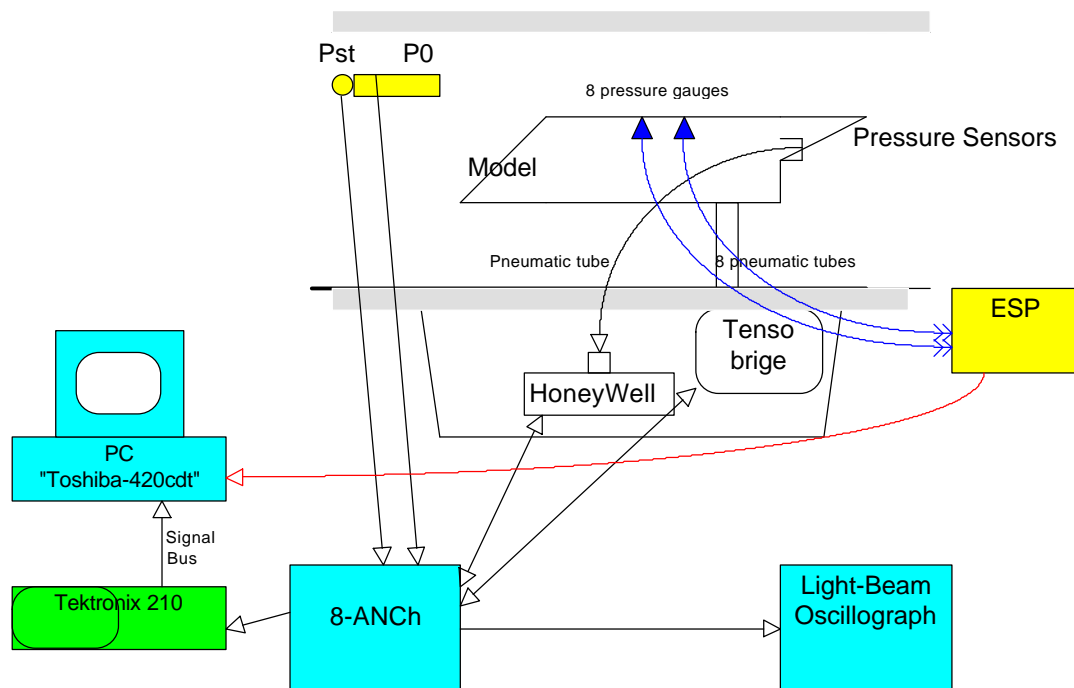


Fig.3.1.2.2. Principal layout of data acquisition system.

An appropriate scheme of data acquisition is presented in Fig.3.1.2.2. Flow control gauges P_0 and P_{st} of the “Honeywell” differential type are used for calculations of the aerodynamic characteristics of a flow (Mach number, high-speed pressure). Their reference pressure is observed and calculated on calibration curves according to the indications of the gauge of absolute pressure “Honeywell™”. Instead of light-beam oscilloscope the digital oscilloscope “Tektronix TDS-210” has been used to record the balances data. After this the results are recorded by PC “Toshiba” by means of PCMCi port.

During processing the acquired information, all measured values were transformed to absolute physical ones. The characteristics of a flow and aerodynamic factor C_d and C_f were calculated.

An observation of BL and recognition of the gas parameters inside of BL are difficult due to low thickness and small gradients of gas density. New informative methods are complex technically, as a rule. More conventional methods give limited information and have to be used together one with others.

Diagnostic part of the installation includes the following:

- Schlieren-system, allowing visualizing the flow under investigation with separation of the needed phase of a process;
- Pressure sensors, with the possibility to select a necessary phase of a process;
- Tenso-balances;
- Video-tape recorder;
- Thermo-tabs and thermocouples.

All these allow researching the processes of interaction of surface plasmas with AD bodies in subsonic and transonic flow.

Schlieren system has been modernized especially for this experiment. A time resolution of it is about 1ms. It can be synchronized with defined phase of plasma excitation process. Real spatial resolution is about 1mm. The Schlieren system has been connected with a video camera.

Temperature of the surface of the model has been evaluated by using the painted thermo-tabs with a different threshold of reaction (100-150-200C).

Synchronization.

A time diagram of the processes at the standard run of ST-1 is shown in Fig.3.1.2.3.

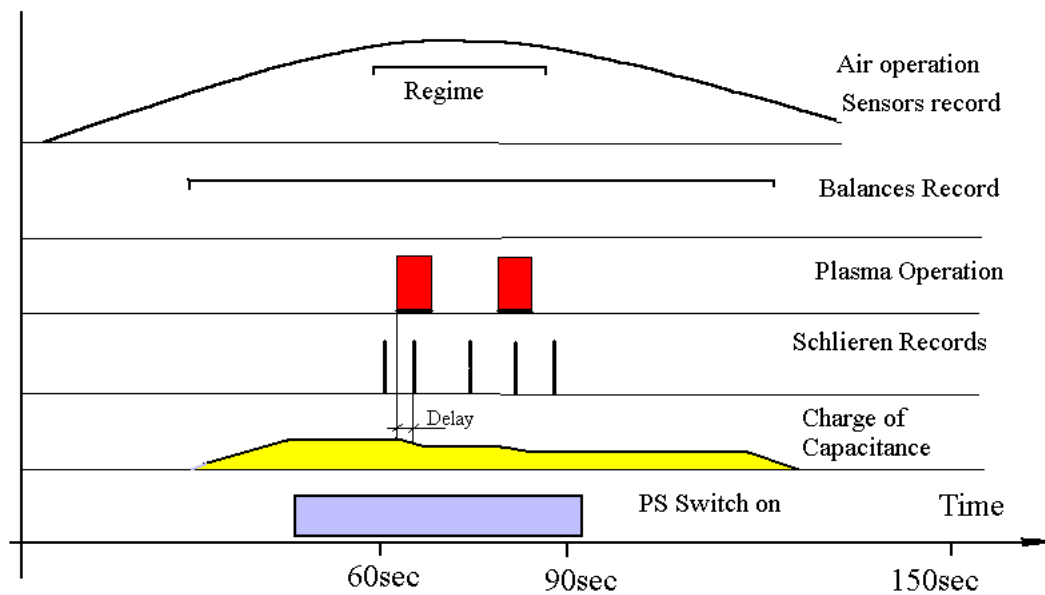


Fig.3.1.2.3. Time Diagram of ST-1 operation.

A process starts from opening of an air gauges for an ejector operation. When Mach number achieves a defined value, permission for systems operation is given. At this time the capacitance is charged and the PS is switched on without 5kV input. After signal “Regime” 5kV is switched on and plasma is burned during a defined time (1-2sec, as a rule). Photo-camera makes the record before, during and after each plasma excitation with a defined delay. The run duration usually is about 2.5 minutes.

3.1.3. Plasma Generator of Surface Type.

A quasi-continuous multi-electrode surface discharge is used for a plasma excitation at the experiment. Electric energy input to the plasma volume 2-15kW at area of plate's surface 10cm². An original power supply with individual excitation of each electrode has been used. The PS provides DC power with voltage 5kV from large electrical capacity and high current pulses with a frequency from 10Hz up to 5kHz. These pulses go on high voltage transformers, individually for each electrode. Thus all electrodes have an independent excitation of the electric discharge. Ballast resistors manage two functions: limit a discharge current and redistribute the discharge current on all electrodes homogeneously. A principal scheme of the PS connection with the surface plasma generator is presented in Fig.3.1.3.1.

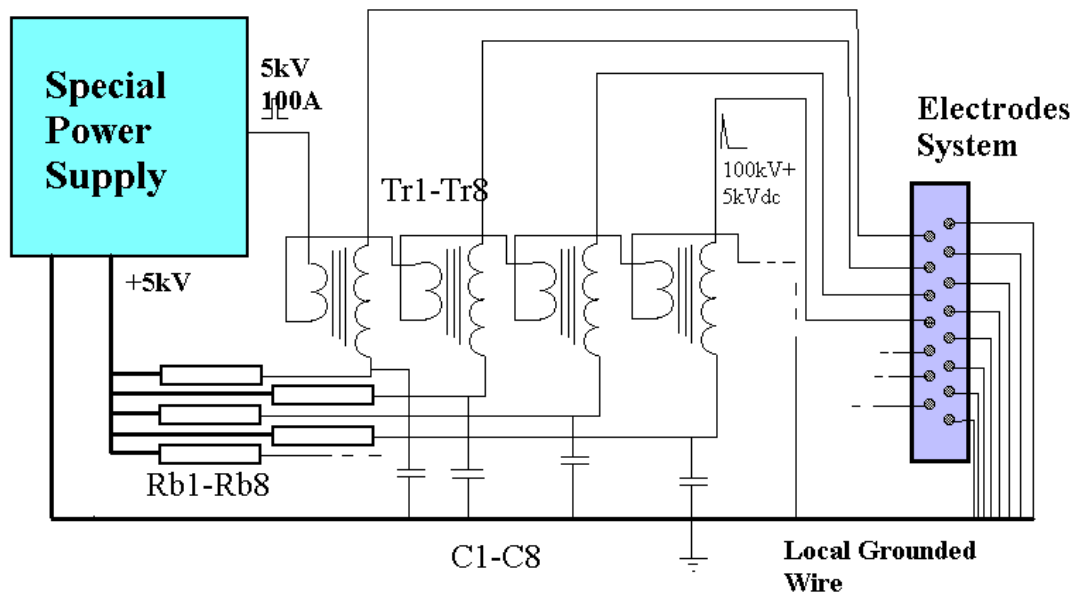


Fig.3.1.3.1. Principal scheme of Power Supply connection.

At such a kind of discharge supply it is possible to measure an input power by means of measuring of voltage on the discharge gap. The input power can be calculated in accordance with a simple formula:

$$W_{pl} = N \times U_{pl} \times (U_{ps} - U_{pl}) / R_b;$$

where W_{pl} - input power to a plasma volume, U_{pl} -voltage on a plasma gap; U_{ps} -voltage of power supply; N -number of ballast resistors; R_b -resistivity of ballast. The dependence of

input power on voltage of plasma gap is presented in Fig.3.1.3.2 for a ballast resistor $R_b=10\text{k}\Omega$. Well seen that the maximal input power is achieved at gap voltage in a half of input voltage. Two values of ballast resistor have been used at the experiment: $10\text{k}\Omega$ and $2\text{k}\Omega$. So at the first case a maximal input power could be about 4kW , at the second case- about 22kW .

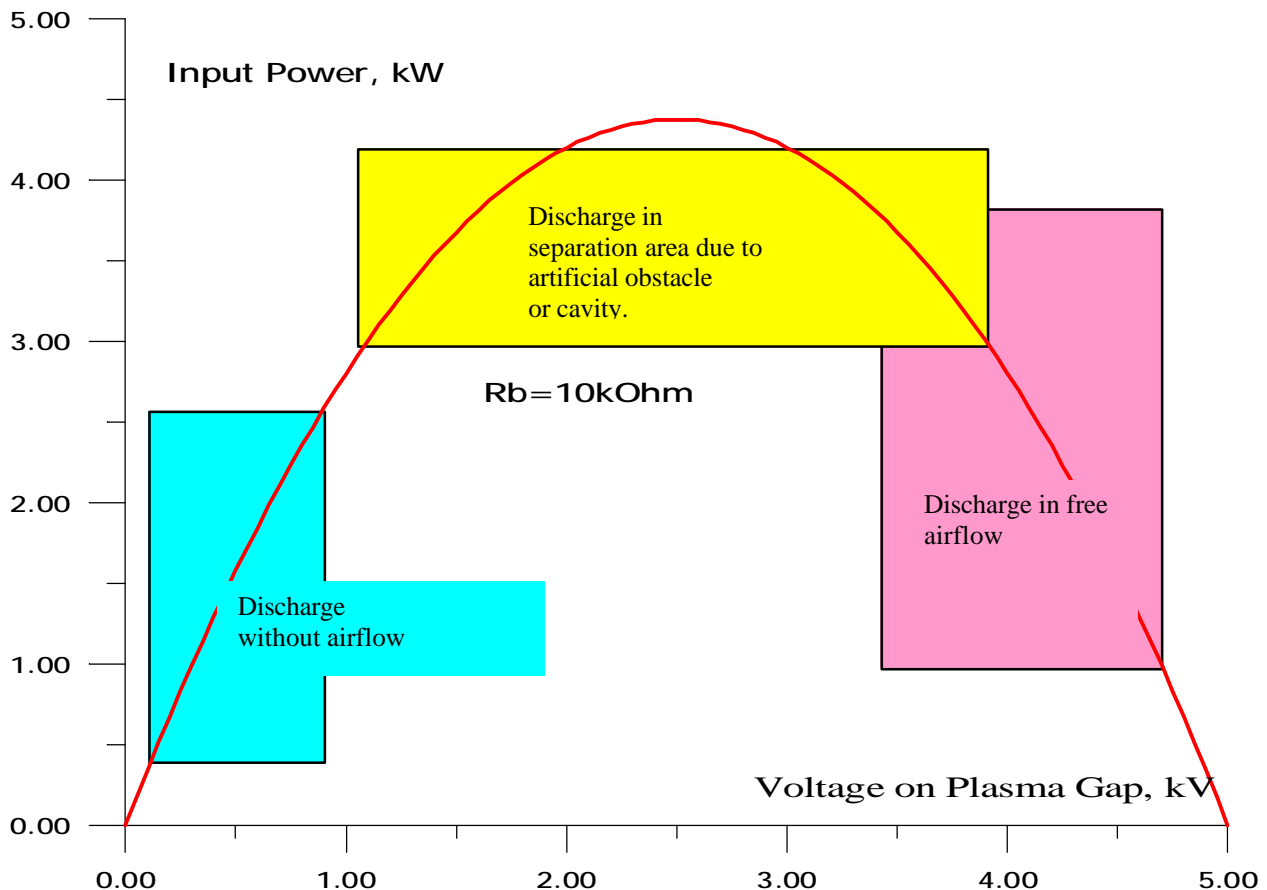


Fig.3.1.3.2. Volt-Power characteristic of the discharge and areas of the discharge existing at different conditions. $P_{st}=400-760\text{Torr}$.

It has to be noted that different conditions of the plasma excitation and burning leads to a different level of input power. Such areas are presented in Fig.3.1.3.2 roughly. At atmospheric condition without airflow the discharge is quickly transformed to arc-like configuration on a one or few electrodes. This form is stable and, as a rule, leads to an electrode damage. Voltage on the electrodes is not exceeded level 1kV . The discharge structure in airflow was non-homogeneous in free stream and relatively homogeneous at using the artificial separation

initiator. These forms are relatively stable. Gap voltage in high-speed airflow is about 3-4.5kV and 2-3kV at discharge location in a circulation zone. In a free stream a large level of wide-spectrum vibrations are appeared on a voltage record. To avoid a large level of EM noise we were forced to disconnect of power supply from grounded parts of the WT. So only well-insulated instruments could be apply for the measurements. Duration of the discharge operation was 0.5-5sec.

Several different schemes have been tested to provide a stable plasma generation on all electrodes simultaneously at relatively high pressure. Finally, the power supply with an individual discharge excitation on each electrode has been chosen. It can be characterized by the following parameters:

Frequency of high voltage pulses	up to 5kHz;
Initial voltage	5kV;
Breakdown voltage	not less than 50kV;
Current on each electrode	0.2-2A;
Pulse duration	0.01-5s;
Numbers of active electrodes pairs	7;
Electrode diameter	4mm;
Material of active dielectric plate	boron-nitride, Nylon-6, boron-silicate;
Operation modes	pulse-periodic, quasi-continuous.

Following photos present main operation modes of multi-electrode surface discharge.

Discharge Appearance.

The photo in Fig.3.1.3.3 presents the discharge image on B-N plate at transonic airflow. Exposition is 20ms; $I_{pl}=1.5-2A$, $U_{pl}=4.5kV$; $R_b=2k\Omega$. The plasma of the discharge is penetrating in X direction for several cm. One can see three images of the discharge on photo. Two last images are result of reflection from glass windows. Switches on were about 2sec of duration.

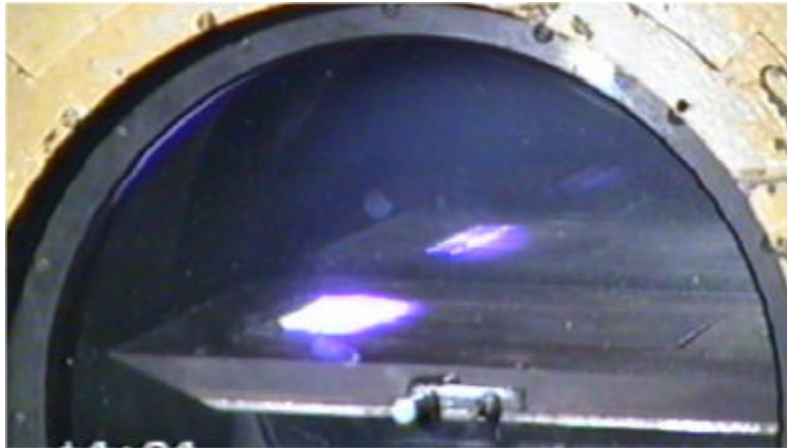


Fig.3.1.3.3. Photos of the discharge in transonic airflow. $P_{st} \approx 500 \text{ Torr}$.

Transversal-longitudinal mode of transonic discharge.

$M=0.8$

$I_d=1.5-2A$, $V_d=4.5kV$;

$R_b=2k\Omega$.

The photo in Fig.3.1.3.4 presents the discharge on B-N plate at subsonic airflow in a presence of circulation zone after an artificial obstacle. Exposition was 20ms.

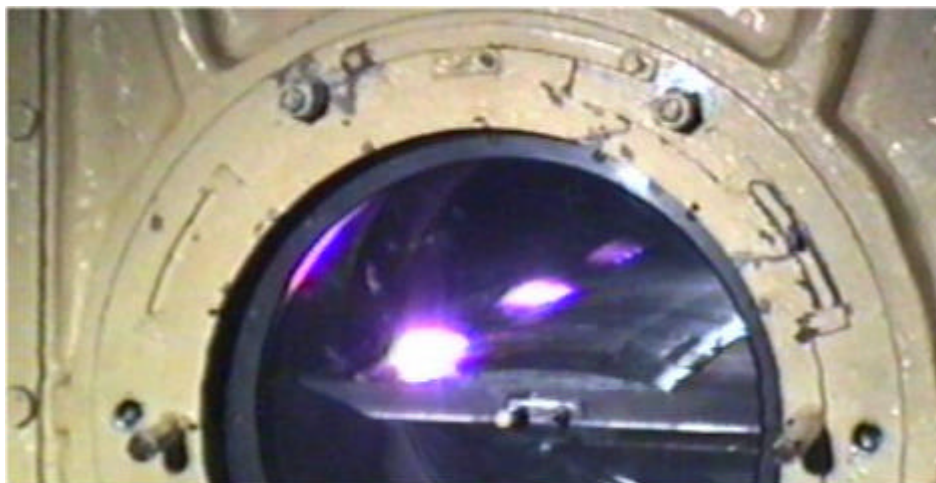


Fig.3.1.3.4. Photo of discharge at presence of separation zones. Profiled Plate.

$I_d=5A$, $V_d=3kV$,

$R_b=2k\Omega$.

Switches on were about 1sec of duration. One can see three images of the discharge. Two last images are result of reflection from glass windows. A circulation zone increases the input power. Each portion of gas blows through the discharge area during a more time.

The photo in Fig.3.1.3.5 presents the discharge on B-N plate at subsonic airflow in a presence of separation zone inside of the cavity. Exposition was 20ms.

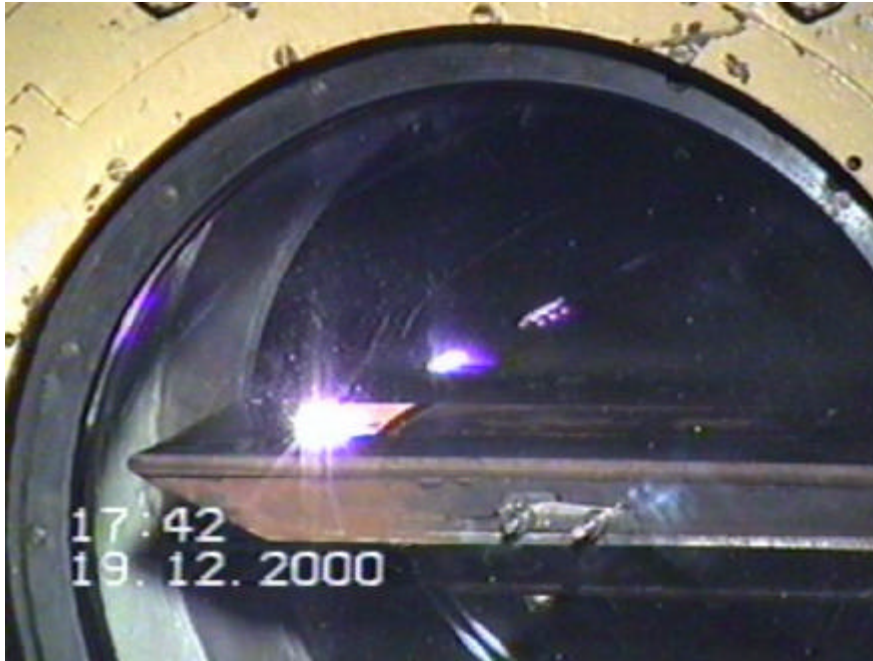


Fig.3.1.3.5. Discharge appearance in a cavity.

$P_{st}=500\text{Torr}$
 $I_d=7\text{A}$, $V_d=2.5\text{kV}$,
 $R_b=2\text{k}\Omega$.

Switches on were about 1sec of duration. One can see three images of the discharge. Two last images are result of reflection from glass windows.

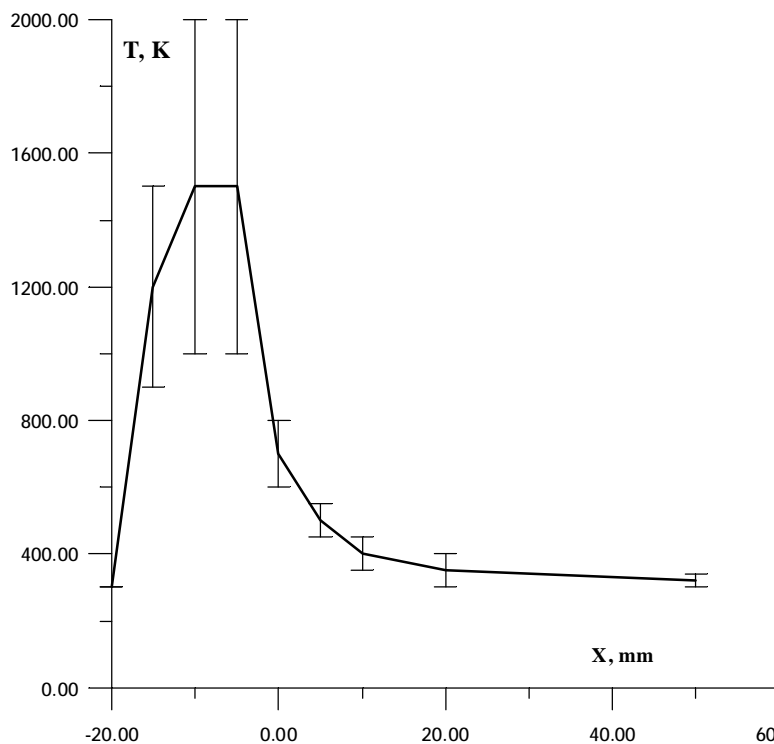


Fig.3.1.3.6. Evaluation of a surface temperature at discharge excitation. $T=2\text{sec}$.

The maximal surface temperature of the model has been evaluated by means of painted thermotabs with a different threshold of reaction (100-150-200-400°C). The edge of a movable plate had a traces and small nidus of erosion. It allows estimating the high temperature. The results can be summarized by a chart, which is presented in figure on a left side. The curve has been obtained for a transonic operation mode at input power 10-15kW. Co-ordinate $X=0$ is a fore-edge of the movable plate.

Chapter 4.

Surface Plasma Influence on Separation Zone Parameters.

Short Time Wind Tunnel Test.

Second part of the Report is devoted to description of the results of a model experiment on plasma influence on parameters of stabilized separation zone downstream of a wall step.

4.1. Description of Experimental Conditions.

Experimental installation was a short time blow-down wind tunnel PWT-10. It can be characterized by the following main parameters.

- | | |
|-------------------------------|---|
| • Operation mode | transonic at $M \approx 1.1 \div 1.2$ in a section of the step. |
| • Test section | rectangular, $20 \times 100 \text{ mm}$. |
| • Static pressure | $P_{st} = 50 \div 300 \text{ Torr}$ during steady stage time. |
| • Total pressure | up to $P_o = 800 \text{ Torr}$. |
| • Total Temperature | ambient. |
| • Reynolds number | up to 10^6 (for 0.1 m). |
| • Steady stage operation time | $0.2 \div 0.6 \text{ sec}$. |
| • Type of discharge | surface, multi-electrode, DC+Pulse High Voltage. |
| • Number of electrodes | 8 pairs. |
| • Input electric power | typical value $W = 5 \div 8 \text{ kW}$, max up to 15 kW . |

Three main parts of experimental installation is describing: gas-dynamic installation PWT-10 (pulse wind tunnel, cross-section of main nozzle 10 cm^2); electric circuit for a discharge excitation and measuring system.

4.1.1. Short time wind tunnel PWT-10.

General layout of the experimental gas-dynamic installation PWT-10 is presented in Fig.4.1.1.1. It has been modified especially for this test.

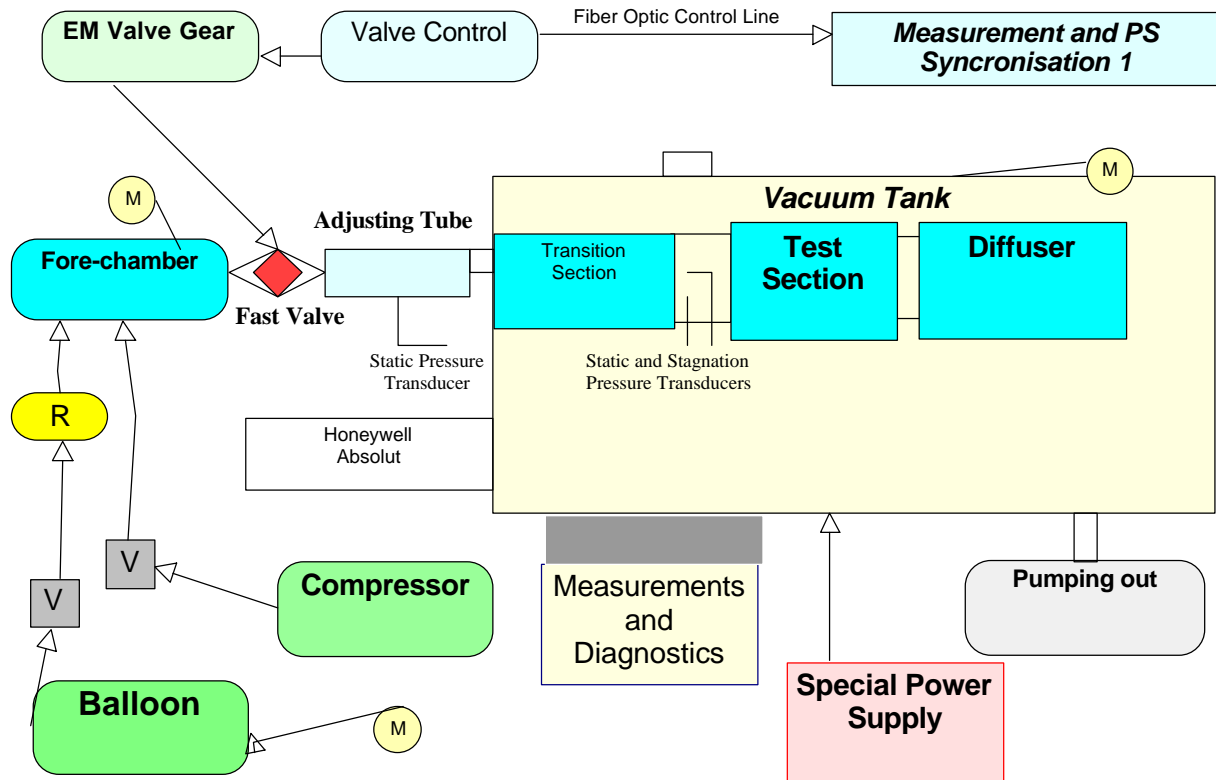


Fig. 4.1.1.1. Gas-Dynamic Installation PWT-10.

Installation PWT-10 contains following components, which operate at following parameters.

- Fore-chamber has volume about 0.1m^3 and working pressure 1-5atm. It is connected with fast valve by stainless steel tube with inner diameter 50mm and with suppliers of pressured air.
- Two parallel lines can provide a pressured air: balloon's line and compressor's one. Compressor gives maximal pressure up to 5atm. Balloon contains pressured air at pressure up to 150atm. Reductor "R" is used on this line. In the most cases 1atm of the pressure in the fore-chamber is enough for the operation at Mach number $M=1.1$ and static pressure about 100Torr (See below).

- Key component of a setup is a fast valve with diameter 50mm and electromagnetic control. This valve is used at non-standard configuration. A response time of the valve is not more than 10ms.
- Adjusting tube is needed to provide a more-less homogeneous distribution of gas velocity on a cross-section. Measurements have shown that non-homogeneity of airflow parameters is quite low.
- Transition section transforms a circular cross-section to a rectangular one at the condition of constant square.
- Test section has a rectangular cross-section with dimensions 20*100mm. Vertical (long) walls have circular windows, which were made from a quartz glass. TS has length about 250mm. TS has a wall step of 15mm of depth.
- A subsonic diffuser is applied between TS and vacuum chamber.
- Vacuum chamber has volume about 0.63m^3 .

Photo of the experimental TS from a lateral view direction is presented in Figs.4.1.1.2. Aerodynamic step is made in the test section to provide an area with flow circulation. Long wall has a large optic window from quartz glass. Simple subsonic diffuser is installed between TS and atmosphere. TS with transition section and diffuser have length about 700mm. This assembled section is installed inside of vacuum tank.

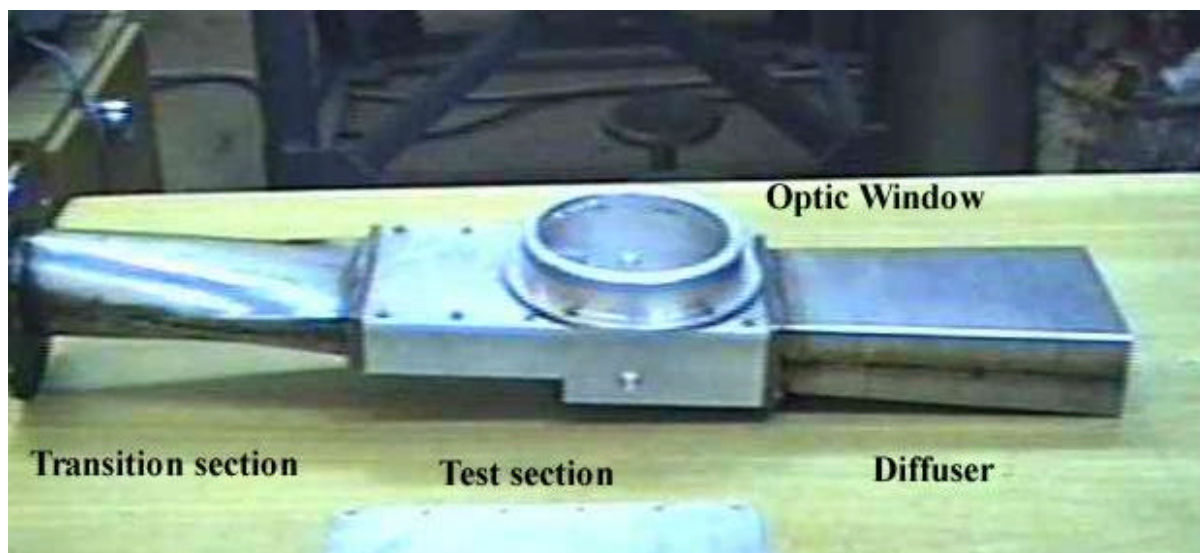


Fig.4.1.1.2. Photo of test section in conjunction with transition section and diffuser.

Set-up PWT-10 is equipped by the following devices for a measurements and diagnostics:

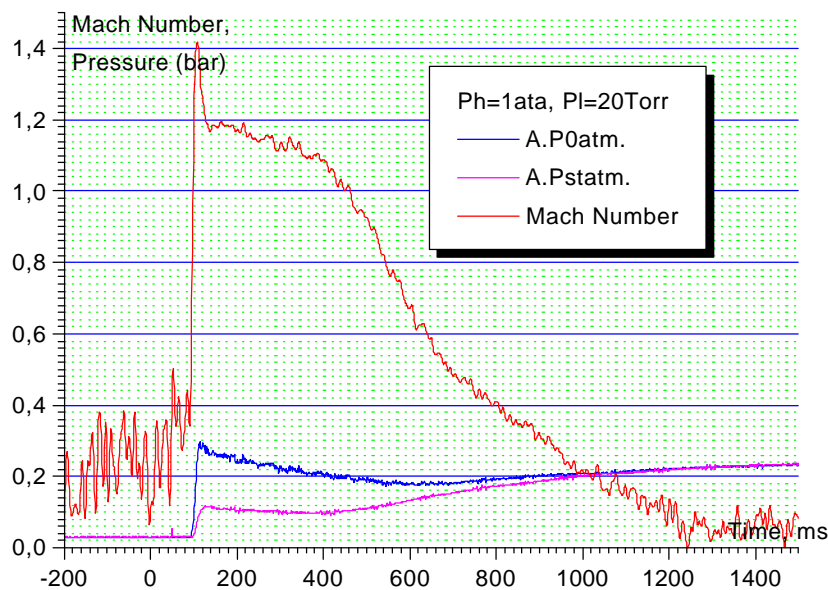
- Pressure sensors “Honeywell™” for measurements of airflow parameters in a test section. Response time of them is less than 1ms. A static pressure is measured in a several points along a test section near the wall. A sensor of stagnation pressure connected with Pitot pipe, which can remove across a cross section.
- Electronic pressure scanner ESP-32 for 32 channels.
- Photo camera and videotape recorder.
- Spectrograph with CCD-camera.
- Electrical current and voltage sensors.

4.1.2. Parameters of airflow.

Certification of main experimental operation modes of PWT-10 has been done. It includes a measurement of main parameters of the airflow in dependence on the initial conditions. Following graphs in Figs.4.1.2.1÷3 present several basic operation modes of PWT-10. Here P_h is the pressure in the fore-chamber (FC), P_l is the pressure in the chamber of low pressure (LPC), P_{st} is a static pressure in a test section, P_o is a stagnation pressure in a test section. M is the Mach number of the airflow. Parameters of initial airflow are considered for the central cross-section of TS (coordinate X appropriate to a wall step).

When a Mach number is calculated there can be a large error without airflow. So, values of Mach number before the valve is started is zero.

Fig.4.1.2.1. Airflow parameters in PWT-10. Operation mode at $P_h=1\text{ata}$.



Well seen that airflow parameters are quite constant during the first 0.4sec. Static pressure is about 70Torr. The diffuser operates well and the influence of initial low pressure on airflow parameters is relatively weak. At $P_h=1\text{ata}$ the transonic mode is realized up to $P_l<150\text{Torr}$. At increasing of P_l a steady stage operation time is decreased.

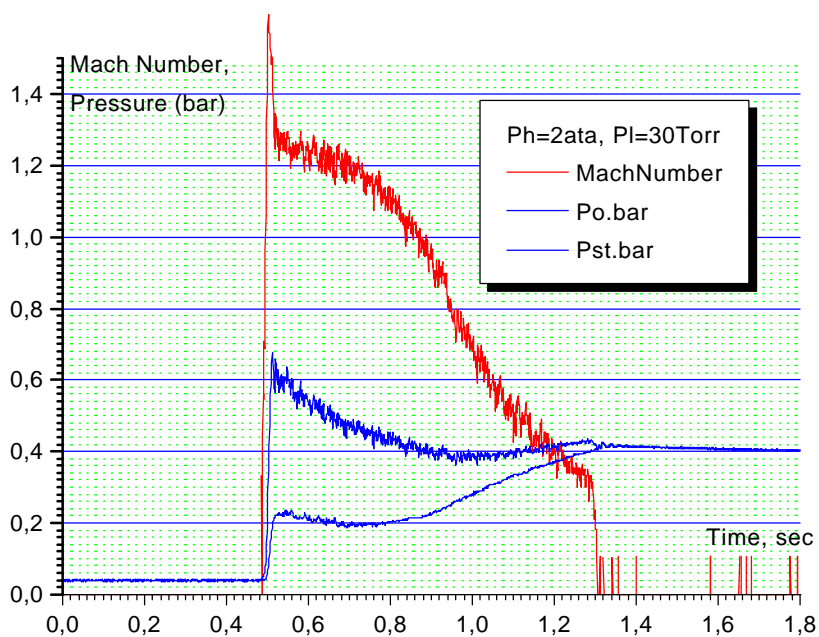


Fig.4.1.2.2. Airflow parameters in PWT-10. Operation mode at Ph=2ata.

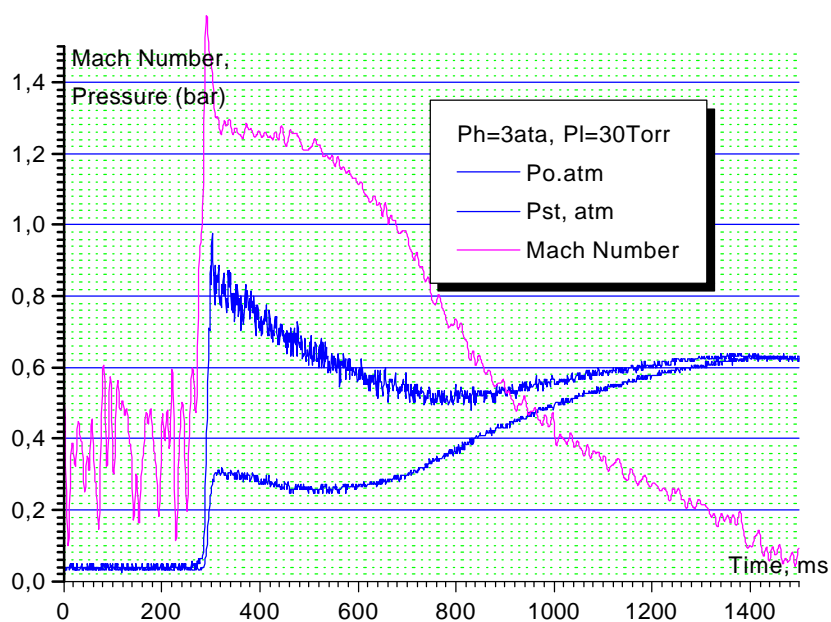


Fig.4.1.2.3. Airflow parameters in PWT-10. Operation mode at Ph=3ata.

The main parameters of airflow are quite stable. A static pressure inside of a separation zone is much less than in a free stream. The next chart in Fig.4.1.2.4 presents a record of static pressure in a separation area in comparison with a static pressure in free stream. Well seen than time period of a separation zone existence is less that supersonic area time. At $Ph=1ata$ this time is about 150-200ms. Such a time is quite enough for measurements.

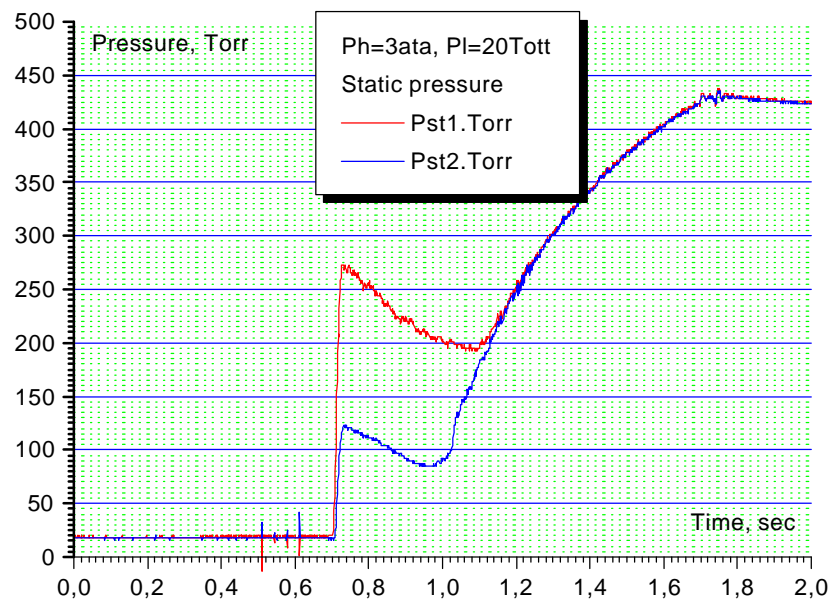


Fig.4.1.2.4. Static pressure inside of a separation zone.

A full picture of the airflow structure can be seen in 4.3 section.

4.1.3. Plasma Generator of Surface Type.

General description of surface type plasma generator has been given in section 3.1. This section is devoted to some important peculiarities of such a generator. Samples of volt-ampere characteristics are shown in Figures from 4.1.3.1 up to 4.1.3.4. Without airflow a gap voltage is depends on a pressure and occurs much less that at airflow: in a range of 100-300V.

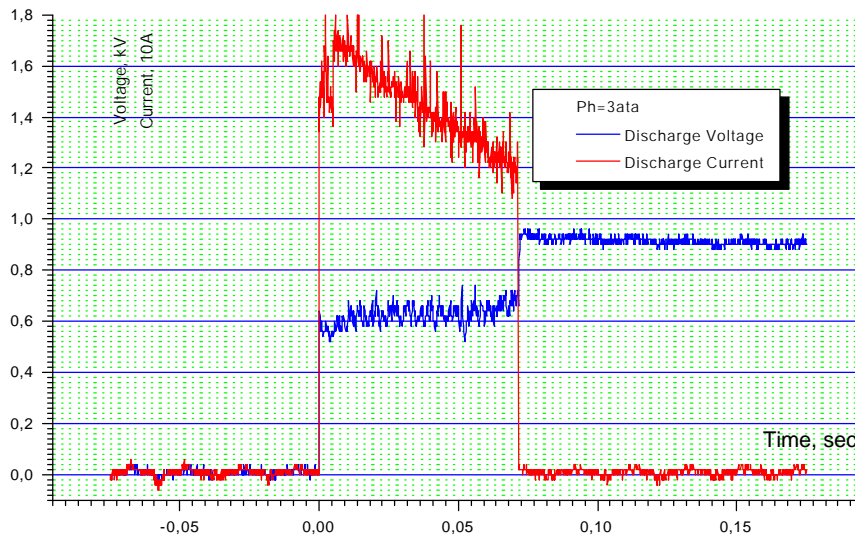
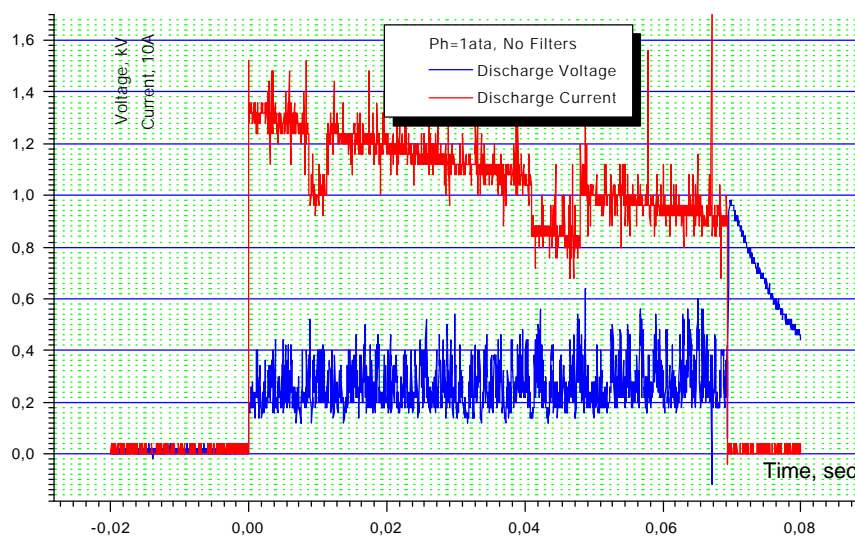


Fig. 4.1.3.1. Time trend of a discharge voltage and current. Standard. Ph=3ata.

Fig. 4.1.3.2. Time trend of a discharge voltage and current. No filters. Ph=1ata.



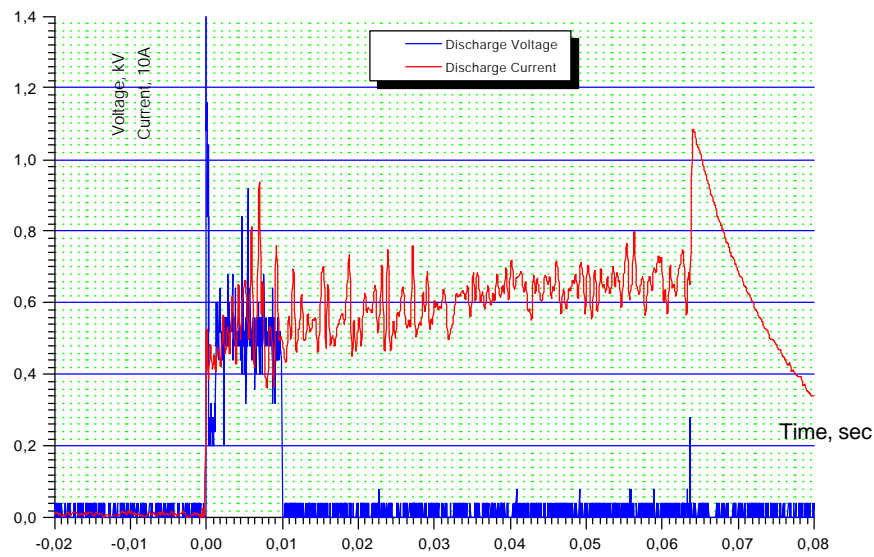


Fig. 4.1.3.3. Time trend of a discharge voltage and current. $Ph=3ata$.
Discharge displacement to a separation zone.

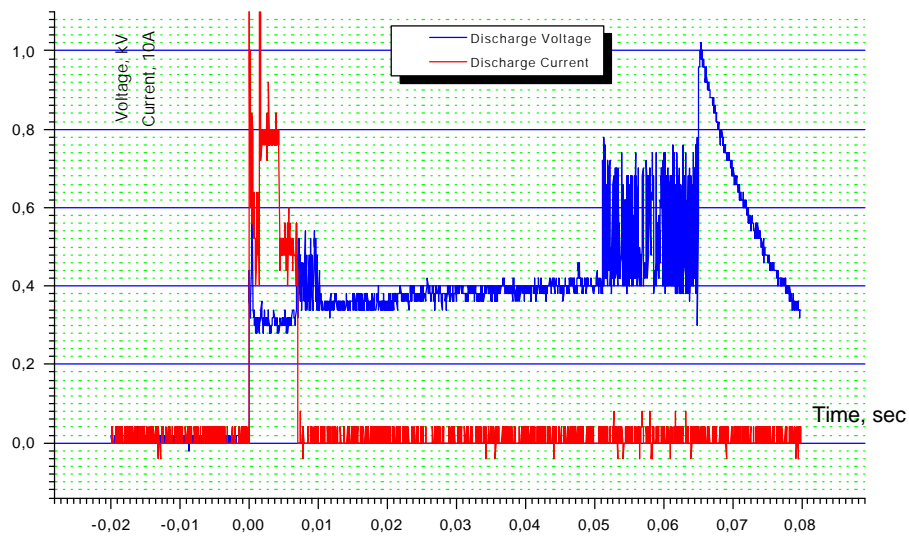


Fig. 4.1.3.4. Time trend of a discharge voltage and current. $Ph=1ata$.
Discharge displacement to a separation zone and instability
due to separation zone disappearance.

Second picture in Fig.4.1.3.2 shows unfiltered oscillogram of a gap voltage. Well seen that the discharge in airflow is unstable.

In some important cases the discharge displaces from the discharge plate to a

separation zone (see section 4.2.1). An appropriate behavior is shown in Fig.4.1.3.3. When a separation zone is disappeared (change of airflow regime), one can see an intensive instability in a discharge voltage in Fig.4.1.3.4.

The dependence of a gap voltage on a static pressure is presented in Fig.4.1.3.5 roughly for a discharge current about 15A.

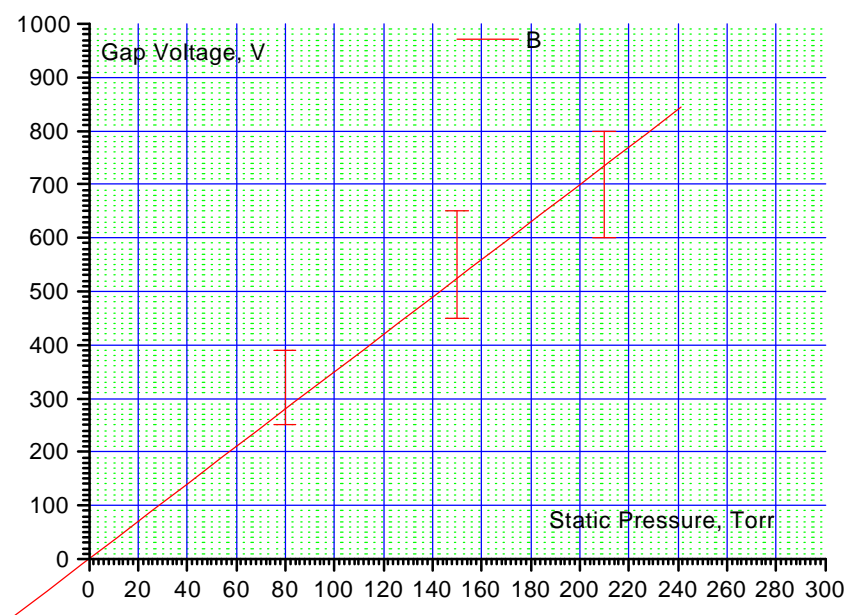


Fig.4.1.3.5. Gap voltage vs Static pressure.

4.1.4. Measurement System and Synchronization.

Measuring system includes following elements for this test.

- Measurements of airflow parameters on a base of “Honeywell” transducers and data acquisition system.
- Measurements of electro-physical parameters of electric discharge: symmetric dividers, current shunt, filters and oscilloscope “Tektronix TDS-210”. It was connected with computer by serial port cable.
- Measurements of pressure distribution in a separation zone on base of electronic commutator ESP-32 and data acquisition system.
- Measurements of a gas temperature on a base of spectroscopic system: quartz fiber optic transmitting line, poly-chromator, CCD-camera, special board and PC computer with an original software.
- Measurements of a light emission on base of a well collimated optical sensor with a photo-multi-amplifier.
- Photo-records.
- Video-tape records.
- Synchronization system.

4.1.4.1. Pressure measurements.

The block-diagram of measurement system is presented in Fig.4.1.4.1. A flow parameters (P_0 and P_{st}) channels, voltage and plasma current references and 16 channels of the pressure distribution were measured. After preconditioning this signals were digitized and stored by a data acquisition system using “National Instruments”[®] data acquisition card (16 bit resolution, 100 kS/s). The system is connected to compact computer “Toshiba Satellite-Pro”. A multiducer ESP-32 (32-channel differential pressure transducer) was used to register a pressure distribution on the model surface. Signal from ESP through the isolated amplifier SC-1121 in SCXI conditioning system goes on DAQ-Card AI-16E-4 and is stored as data files. The original address line driver for ESP with optical isolated outputs was used to form ESP addressing. This signals also was measured to verify process of data flow and for sequential channel separation.

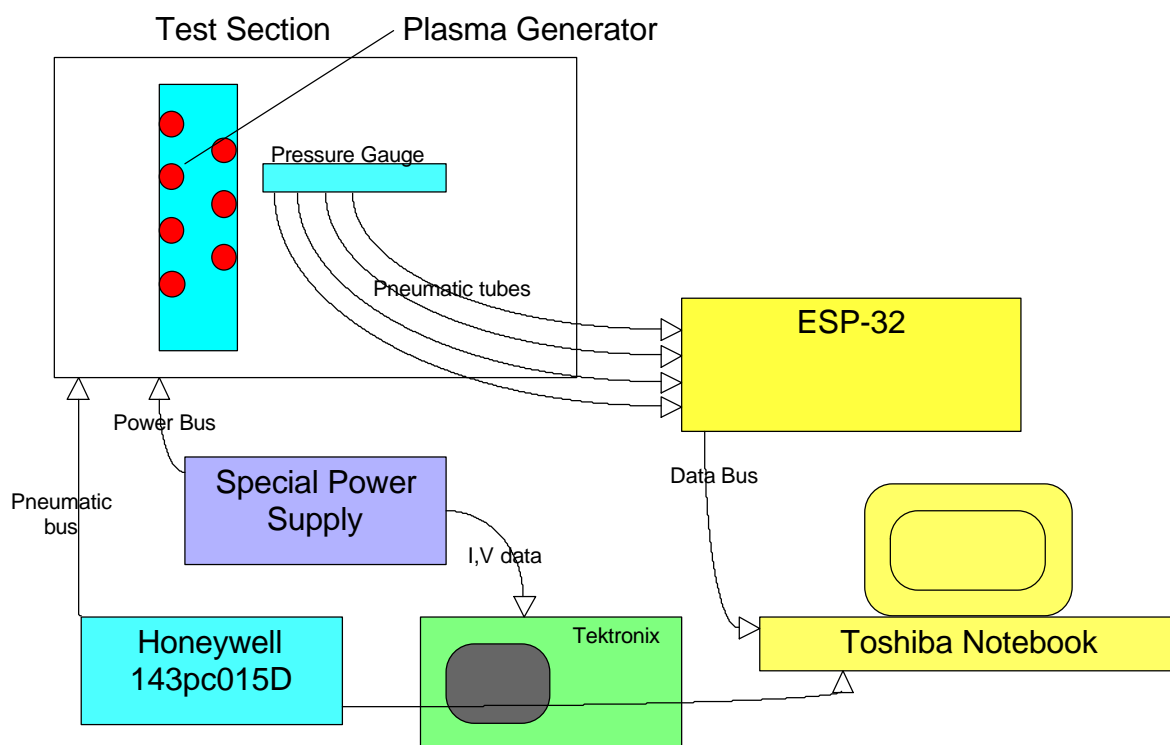


Fig.4.1.4.1. Block-layout of a pressure measurements.

Some measurements were performed in very noisy conditions. Partly this problem was solved by using non-grounded isolated power suppliers.

The main Software was developed on NI LabView™ program language. Data acquisition, sequential representation, treatment and calculation was performed using original programs. The acquired data are viewed, primary filtered (with using build-in digital Median or Butterworth filters), qualified and estimated. On this stage, the interference of electrical noise could be excluded. For the ESP data, additional channels separation with using address signals was performed.

Flow parameters were calculated from data about P_0 , P_{st} and chamber temperature T . For surface pressure distribution we can build a pressure cross-section along line of transducers at any time moment.

4.1.4.2. Spectroscopic measurements.

Spectroscopy of the second positive system of molecular nitrogen and CN molecular spectrum were chosen as a method of gas temperature measurements. The optical spectrums are registered by means of a spectrograph (poly-chromator) MDR-23 connected with a CCD camera. The CCD camera has 3600 sensitive elements with linear location and 0.2mm of height. A theoretical resolution is about 0.1Å. The hardware has a spectral resolution about 0.01nm/pixel. The device spread-function is 0.12-0.4nm in dependence on an input optic slit. To diminish an EM noise the computer and CCD camera have been moved away on a few meters. A plasma radiation is being transported to a spectral system by means of a quartz fiber optic line. The signal from CCD matrix is amplified and recorded by PC as binary or ASCII-file. Schematic layout of spectroscopic measurements is shown in Fig.4.1.4.2.

Layout of Optical
Measurements

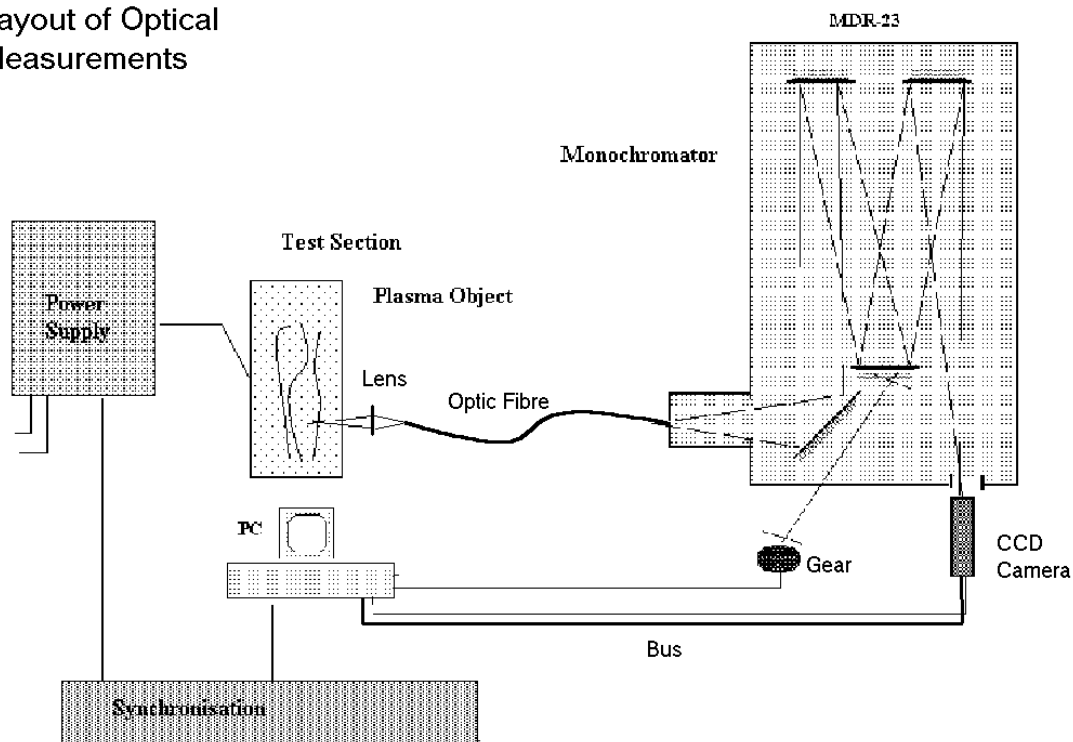


Fig.4.1.4.2. Principal layout of spectroscopic measurements.

It has to be noted that main methods for plasma parameters measurements are contact-less methods, namely, methods based on a spectroscopy. A partially resolved molecular spectrum can be obtained in experiment. For the determination of gas temperature in a discharge the method of optical emission spectrum shape fitting is adopted. The exact full spectrum of different transitions of the second positive nitrogen system, including R-, P- and Q-branches (the last is very weak) is generating under the defined temperature and it is then convoluted with the spread function of the spectral device. The synthetic spectrum obtained in such a manner is then compared with the real one. It is made in a procedure of best fitting of the spectrum contour by variation of the defined temperature. In this case the special attention is paid for the best coincidence of the spectral shape at the lower rotational numbers, where the distribution over the rotational levels is known to establish at a temperature practically equal to that of the gas.

The accuracy of the temperature determination by this procedure can be estimated in 50K at a spread function 0.1nm and in 300K at the temperature in a range of 3000K with a spread function 0.3nm. This method is a modification of a relative intensity method in application to rotational lines of molecular bands. Nevertheless, determination of gas and vibrational temperatures remains one of the most delicate and debatable procedures in gas discharge physics and demands additional investigation in every case under consideration.

Nitrogen and carbon presence in a plasma substance gives observation of CN spectrum the most available due to high intensity. Such kind of spectrum allows getting a rotational temperature of CN molecules on partly resolved structure of rotational-vibrational transitions at different "j". Vibrational temperature could be estimated on relative intensity of unresolved bands at different numbers "v", for example, transitions 0→1, 1→2, 2→3 in violet system with an edge 422nm (A, B and C correspondingly below).

The problem of temperature calculations from a spectral data is not simple. In this work we use a calibration dependencies from literature. In a further work it going to be pointed. Fig.4.1.4.3 presents appropriate charts. Here the intensity of the 0→1 transition (A) is normalized on 1. In temperature range 5000-8000K the accuracy of such a method can be estimated in 1000K.

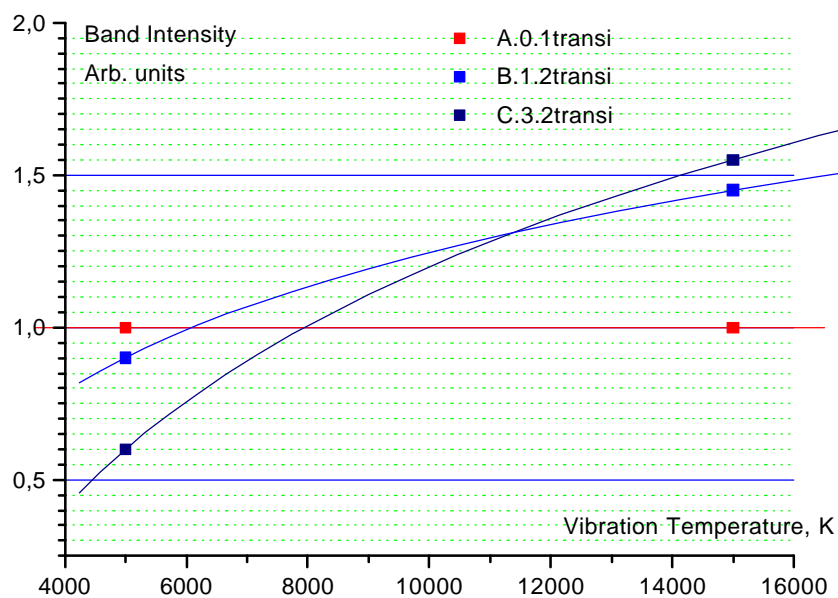


Fig.4.1.4.3. A normalized dependence of CN bands intensity on vibrational temperature.

4.1.4.3. Synchronization.

Two systems for synchronization of PWT-10 operation, discharge operation and measuring devices have been used. First system gives a signal when the main valve opens. It uses a relay contacts, fiber optic line and pulse generator, which applies for needed delays. The fiber optic line together with “Siemens” photo radiators and transducers has been used to avoid an EM noise. Typically, time delay between airflow start and the discharge excitation was 0.05-0.1sec. Discharge duration was about 0.070sec.

Second system has been used for data acquisition system synchronization. It consists of a well-collimated optical sensor (on a base of photo-multi-amplifier), threshold pulse generator and a command pulse generator.

A time consequence of the typical test is shown in Fig.4.1.4.4 schematically.

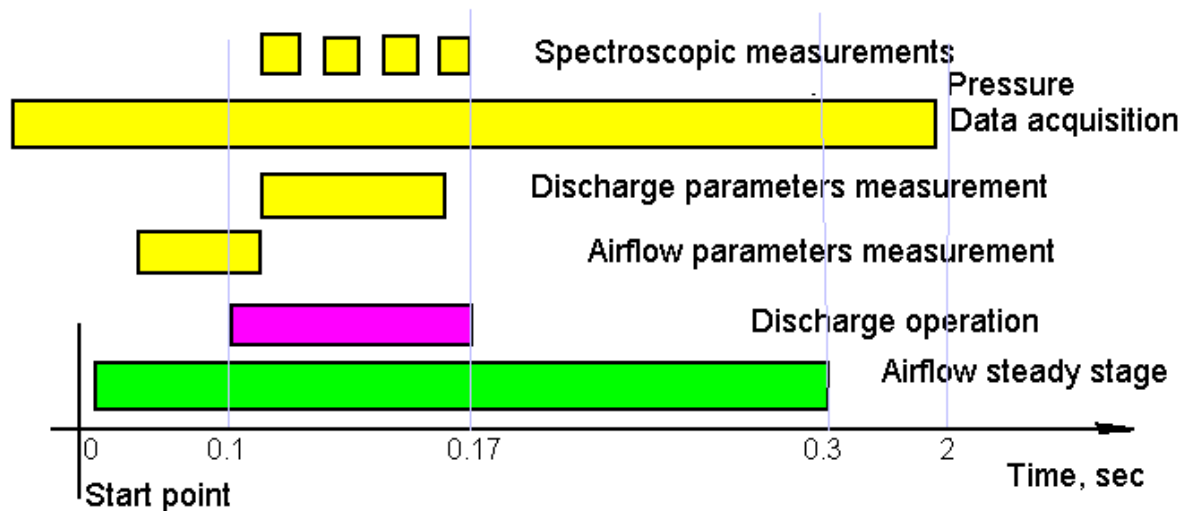


Fig.4.1.4.4. Time diagram of the test.

3.2. Experimental Results.

Nine experimental sessions took place in frames of this Contract: July, 5-7; September, 27-28; October, 02; October, 04-05; October, 25-30; November, 02-03; November, 12-13; December, 18-20 in 2000 year and February, 6-8 in 2001 year. The experimental results are represented in this chapter. The data have been obtained at the following conditions.

- Mach Number of airflow, M_∞ 0.99-0.3;
- Stagnation pressure, P_0 750-780Torr;
- Static pressure, P_{st} 400-700Torr;
- Stagnation temperature, T_0 ambient, 290-305K;
- Static temperature, T_{st} 250-300K;
- Reynolds number on 0.1m $(1\div 3)\times 10^6$;
- Calculated position of transition line fore and on a movable plate;
- Dimension of WT test section 250×300mm;
- Dimension of the model 250×250×45mm;
- Dimension of the movable (tested) plate plain 100×120×10mm,
profiled plate 100×120×18(7%)mm;
- Angle of attack $0\div 1^\circ$;
- Number of electrodes 17 (7 “hot” +10 grounded);
- Ballast resistance in a circuit 10k Ω and 2k Ω per each “hot”
electrode;
- Voltage of Power Supply 5kV + 50kVpulsed;
- Main capacitance in Power Supply 4.8mF;
- Storage Energy 60kJ;
- Plasma pulse duration 2sec;
- Total electric current $1\div 15A$;
- Input power $2\div 18kW$.

Two problems are being considered on the results of the experiments: skin friction reduction by means of surface plasma generation and surface plasma influence on position and conditions of separation zones.

3.2.1. Description of the Runs.

The most important data and results of the WT runs are represented in Table 3.2.1.

Table 3.2.1. WT Runs Description.

Date, No	Mach Number, M_∞	Type of the model	Conditions: P_{st} (Torr), Ballast resistors, Flow over the plate.	Mean power Input, kW	Result
July, 6, 2000 System testing					
No1s	0.98	Plain Plate	$P_{st}=410$ Torr; R=10kOhm; Transonic	~1.5-3kW	Effect on Schlieren Photo.
2s	0.7	Plain Plate	$P_{st}=550$ Torr; R=10kOhm; Subsonic	~1.5-3kW	???
3s	0.92	Plain Plate	$P_{st}=460$ Torr; R=10kOhm; Transonic; Obstacle before discharge area.	~1.5-3kW	Effect on Schlieren Photo.
4s	0.9	Plain Plate	$P_{st}=470$ Torr; R=10kOhm; Transonic; Obstacle before discharge area.	~1.5-3kW	Effect on Schlieren Photo.
5s	0.85	Plain Plate	$P_{st}=490$ Torr; R=10kOhm; Transonic; Obstacle before discharge area.	~1.5-3kW	???
September, 28,2000 Schlieren and Balances Measurements					
No1	0.97	Plain Plate	$P_{st}=425$ Torr; R=10kOhm, Transonic	2-3kW	Noise.
2	0.80	Plain Plate	$P_{st}=510$ Torr; R=10kOhm Transonic	2-3kW	Noise.
3	0.6	Plain Plate	$P_{st}=600$ Torr; R=10kOhm Subsonic	2-3kW	Noise.
4	0.7	Plain Plate	$P_{st}=555$ Torr; R=10kOhm Subsonic	2-3kW	Balances Effect, 0.2N at 2N of the force
5	0.6	Plain Plate	$P_{st}=600$ Torr; R=10kOhm, Subsonic, Artificial obstacle on moving plate	2-3kW	No balances effect
6	0.55	Plain Plate	$P_{st}=625$ Torr; R=10kOhm Subsonic, Artificial obstacle on moving plate	2kW	No balances effect

7	0.4	Plain Plate	$P_{st}=685\text{Torr}$; $R=10\text{k}\Omega$ Subsonic. Obstacle before discharge area.	4-4.5kW	
October, 2, 2000 Schlieren and Balances Measurements					
No01	0.97	Plain Plate	$P_{st}=418\text{Torr}$; $R=10\text{k}\Omega$ Transonic, Artificial obstacle before discharge area.	2-4kW	Visible effect on Schlieren Photos
02	0.55	Plain Plate	$P_{st}=625\text{Torr}$; $R=10\text{k}\Omega$ Subsonic, Artificial obstacle before discharge area.	4-4.5kW	No Discharge
03	0.5	Plain Plate	$P_{st}=645\text{Torr}$; $R=10\text{k}\Omega$ Subsonic	No discharge	No discharge

October, 5, 2000 Schlieren and Balances Measurements					
No11	0.98	Plain Plate	$P_{st}=410\text{Torr}$; $R=10\text{k}\Omega$ Transonic	No discharge	No discharge
12	0.95	Plain Plate	$P_{st}=420\text{Torr}$; $R=10\text{k}\Omega$ Transonic	2-3kW	Effect
13	0.9	Plain Plate	$P_{st}=450\text{Torr}$; $R=2\text{k}\Omega$; Transonic	2-3kW	No discharges
14	0.8	Plain Plate	$P_{st}=510\text{Torr}$; $R=2\text{k}\Omega$ Transonic (small area, unsteady)	3-6kW	Unsteady operation mode, 20% amplitude of vibrations.
15	0.75	Profiled Plate	$P_{st}=530\text{Torr}$; $R=2\text{k}\Omega$; Subsonic	6kW	Balances Effect; Effect in Schlieren photo.
16	0.6	Profiled Plate	$P_{st}=605\text{Torr}$; $R=2\text{k}\Omega$; Subsonic	8kW	Two polar balances effect. Effect in Schlieren Photo.
17	0.56	Profiled Plate	$P_{st}=625\text{Torr}$; $R=2\text{k}\Omega$; Artificial Separation Zone, Subsonic	15kW	Balances Effect.
18	0.45	Profiled Plate	$P_{st}=660\text{Torr}$; $R=2\text{k}\Omega$; Artificial Separation Zone, Subsonic	12kW	Balances Effect of drag reduction; Effect in Schlieren photo.

25-27.10.2000 Schlieren and Balances Measurements			Conditions, Data for usage		
21	1.1	Profile with obstacle	Oscillogram Schlieren photo	?	Drag reduction 15%, Force up to 3N Splitting of main shock
22	1.0	Profile without obstacle			Drag reduction 10%, Force up to 10N
23	1.0	Profile, no obstacle			Drag reduction 7% Force up to 10N
24	1.0	Profile, no obstacle			Drag reduction 5% Force up to 10N
25	1.1	Profile with obstacle	Oscillogram		Drag reduction 20% Force up to 3N
30.10.2000 Measurements at separation processes.					
31	1.0	Plain plate with obstacle			No effect
32	1.0	Plain plate with obstacle			Traction increase 0.5N
33			Discharge fault		

2.11.2000 Measurements at separation processes.					
41	0.95	Plain plate with obstacle	Construction fault		
42	0.9	Plain plate with obstacle	Discharge fault		
43	0.9	Plain plate with obstacle	Vdis=2kV	15kW	Traction 2N, No effect
44	0.7	Plain plate with obstacle	Vdis=3.4kV	15kW	Traction 1N, No effect
45	1.1	Plain plate, no obstacle	Vdis=4kV, Discharge unstable at voltage decrease. Schlieren photo.	8kW	Traction 1N, Effect !!! Slow traction grow.
46	0.7	Plain plate, no obstacle	Breakdown of wires at the end of pulse. Separation!!!		Traction 0.5N, No effect !!!

47		Cavity at plain plate	Construction fault		
48	1.0	Cavity at plain plate	Vdis=0.8kV	8kW	Traction 1N, Effect !!!
49	0.85	Cavity at plain plate	Vdis=2kV Oscillogram, Schlieren photo	15kW	Traction 3N, Effect 0.7N
491	0.4	Cavity at plain plate	Vdis=3.5kV	15kW	Drag 1N, Small effect
492	0.52	Cavity at plain plate	Vdis=4kV Oscillogram, Schlieren Photo	8kW	Drag 2N, Effect 0.5N

13.11.2000 Balance measurements at discharge in Cavity					
61	1.1	Cavity before Plain Plate		~10kW	Fault
62	1.0	Cavity before Plain Plate		~10kW	Fault
63	0.9-0.95	-Cavity before Plain Plate	Oscillogram, Schlieren photos	~10kW	Effect 1N
64	0.7	-Cavity before Plain Plate	Oscillogram	~10kW	Effect in Drag Reduction 0.5N
65			Discharge fault		Fault
19.12.2000 Pressure Distribution Measurements					
71	Mach Number	Plain Plate Discharge in Cavity	Pressure sensors in model splits Luminosity, Balances, Schlieren pictures	~10kW	Model has been destroyed
72	0.7	Plain Plate Discharge in Cavity	File 72.nbk Frames 1,2	~10kW	No balances effect
73	0.95	Plain Plate Discharge in Cavity	File 73.nbk Frames 3,4	~10kW	Balance effect
74	0.95	Plain Plate Discharge in Cavity	File 74.nbk Frames 5,6	~10kW	Balance effect, Turbulence decrease
75	0.7	Plain Plate Discharge in Cavity	File 75.nbk Frames 7,8	~10kW	Fault

76	0.5	Plain Plate Discharge in Cavity	File 76.nbk Frames 9,10	~10kW	Balance effect
77	0.5	Plain Plate Discharge in Cavity	File 77.nbk Frames 11,12	~10kW	Fault
6-8.02.2001 Pressure distribution measurements					
81	0.9	Profiled Plate, Discharge in Cavity	Static pressure along plate, stagnation pressure on plate, Plasma Luminosity.	~8kW	Measurements fault
82	1.1	Profiled Plate, Discharge in Cavity	-‘-	~8kW	Measurements problems
83	1.0	Profiled Plate, Discharge in Cavity	“-	~8kW	Discharge fault
84	0.9	Profiled Plate, Discharge in Cavity	ChA-Pst(4), ChB-Pst(2), Ch1-Pl. Luminosity, Ch2-Po(2)	~8kW	Effect in Pst and Po!!! $\Delta P_o = -16\%$ $\Delta P_{st} = 16\text{Torr}/400\text{Torr}$
85	0.9	Profiled Plate, Discharge in Cavity	Ch2-Po(3)	~8kW	No effect
86	0.9	Profiled Plate, Discharge in Cavity	ChA-Po(2), ChB- Po(1), Ch2-Po(3)	~8kW	Change of turbulence spectra Effect in full pressure
87	0.6	Profiled Plate, Discharge in Cavity	Stagnation pressure on plate, Plasma Luminosity.	~8kW	Small Effect
88	1.0	Profiled Plate, Discharge in Cavity		~8kW	Effect!!!
89	0.9	Profiled Plate, Discharge in Cavity		~8kW	Effect in full pressure point1
891	0.9	Profiled Plate, Discharge in Cavity		~8kW	EM noise
892	0.8	Profiled Plate, Discharge in Cavity		~8kW	Small effect
893	0.5	Profiled Plate, Discharge in Cavity		~8kW	No effect
894	0.4	Profiled Plate, Discharge in Cavity		~8kW	Fault of measurements
895	0.4	Profiled Plate, Discharge in Cavity		~8kW	Small effect

3.2.2. Balances Measurements.

Skin friction reduction. Several competitive mechanisms can be realized at surface plasma generation near the plain plate: BL heating, surface heating, generation of artificial separation zones, change of a local shock position at transonic mode, stabilization of airflow disturbances and i.e. Sometimes it is difficult to separate different processes. All experimental evidences can be divided in accordance with three main mechanisms:

- Skin friction reduction by means of surface plasma. No change in a wave structure of airflow. Separation processes don't define a total drag. Subsonic and transonic modes at plane plate can be included to this point.
- Wave structure change at profiled model.
- Change of position, volume and parameters of a separation area.

In a two last cases the effect of a total drag reduction might be related to a pressure redistribution near the model surface.

Subsonic and transonic runs. Plain plate. The balances effect exists definitely but sometimes is unstable. In can be referred to unstable position of a main shock above the plate (see 3.2.3). The balance record of the run 12 (see table 3.2.1) is presented in Fig.3.2.2.1. Seen that a plasma effect occurs not just after switching on (sharp pike is referred to a EM noise at the relay operation). A signal trend is not a constant due to change of airflow parameters and high sensitivity of a main shock to them.

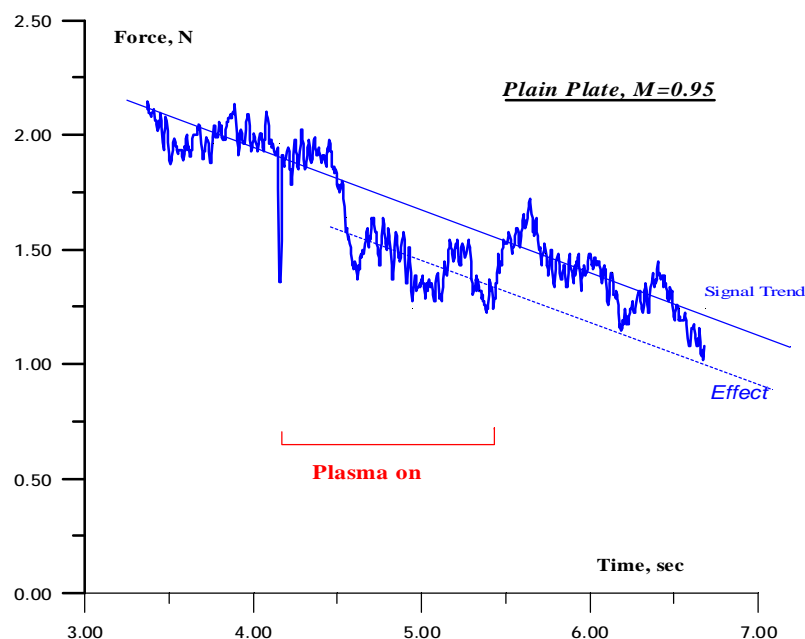


Fig.3.2.2.1. Balance record of Run No12. Transonic mode.

Seen that the value of a friction reduction is about 0.2N or about 10% of a friction force.

Next chart in Fig.3.2.2.2 shows a balance record for the run No 45.

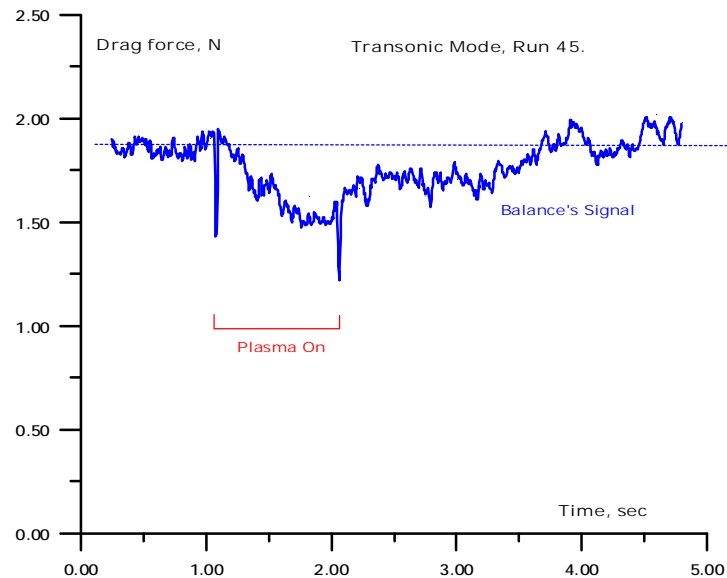


Fig.3.2.2.2. Graph of a balance measurement.

Well seen that the balance signal has a shape which is typical for a thermal processes. It can be suggested that a surface heating plays an important role in this case. The value of a friction drag reduction was 15-20% of initial level. An input power was about 8kW, i.e. 3 times more than for previous case. At the same time a main gasdynamic structure doesn't change practically. A main direct shock is displaced upstream slightly. So the effect can be related to a skin friction reduction. Note, that the local flow disturbances are suppressed by plasma (see 3.2.3.).

The next picture in Fig.3.2.2.3 presents the balance record for run 49. Plasma luminosity is shown for a time reference. Power input in this case was more than in previous cases because of special cavity for discharge excitation. A thermal type of a chart's curve can be noted again.

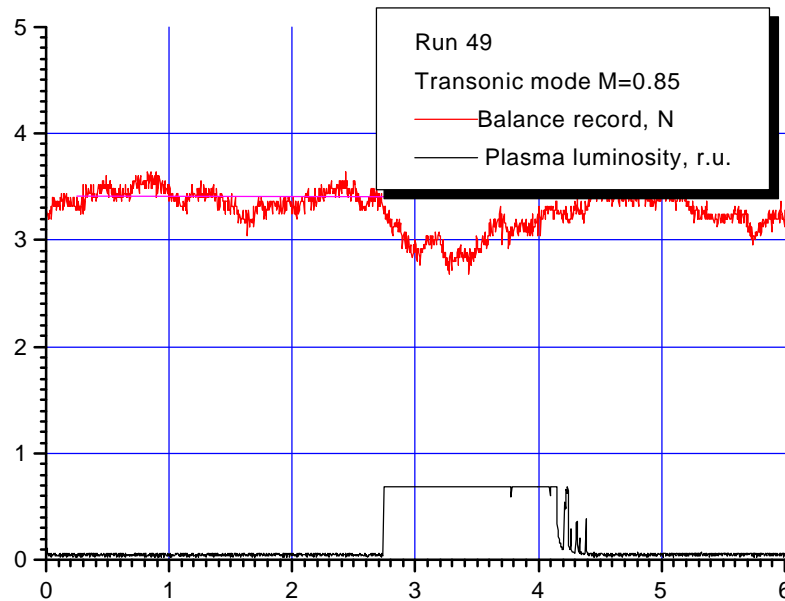


Fig.3.2.2.3. Graph of a balance measurement.

The balance record of the run 4 is presented in Fig3.2.2.4. This record was made by light-beam oscillograph. Here is a fragment. A force signal polarity is negative. A signal trend is not a constant due to change of airflow parameters.

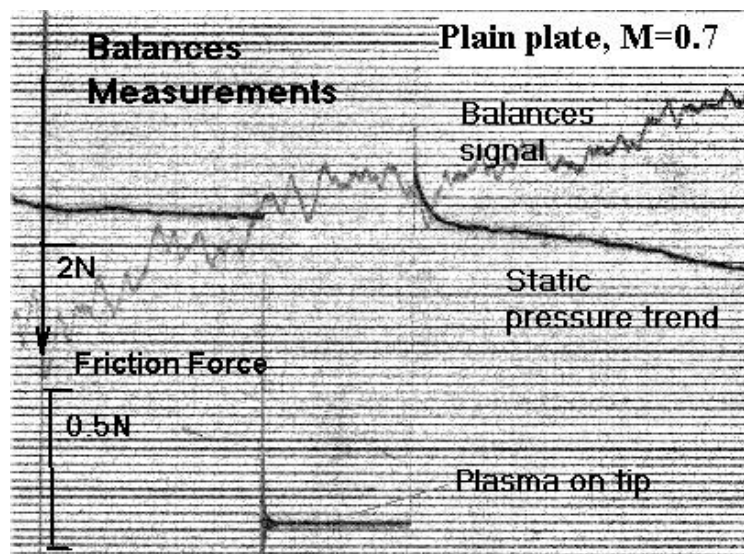


Fig. 3.2.2.4. Balance record of Run No4. Subsonic mode.

Seen that the value of a friction reduction is 0.1-0.2N or less than 10% of friction force at about 2kW of a power release.

It is clear that a more power input leads to a more effect in a friction drag reduction. Nevertheless, seems that the effect might be saturated due to a fast mixing of plasma with a cold gas and some principal physical limitation. The experimental results are summarized below.

Effect of a shock position change. Some cases at transonic mode demonstrate a much more plasma influence in respect of plane plate at subsonic airflow. As a sample the run 63 can be described. Fig.3.2.2.5 shows the balance record. A significant change of shocks position and amplitude took place (see 3.2.3 for this run).

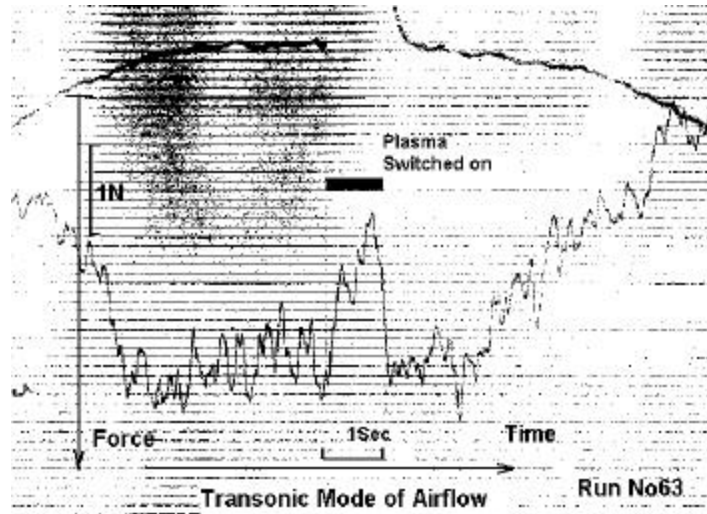


Fig.3.2.2.5. Graph of a balance measurement.

Effect on a Profiled Model. A profiled model has been tested at the same conditions. It was a cylindrical chord at 7% of thickness (i.e. close to profile NASA-0014). The surface plasma excitation upstream of profiled model leads to an obvious effect of drag reduction at subsonic and transonic operation modes as well as with and without artificial obstacle for a separation initiation.

At this case the drag reduction occurs due to two reasons: skin friction decrease and pressure redistribution on the profile surface. The main mechanism of the profile (shape) drag reduction is a displacement of the line of a separation zone reattachment downstream due to plasma influence on gas parameters inside of the separation zone. Fig.3.2.2.6 shows samples of balance measurements at transonic airflow. The first case appropriates a free stream; the second one has been recorded at artificial separation zone generation (see above 3.1.).

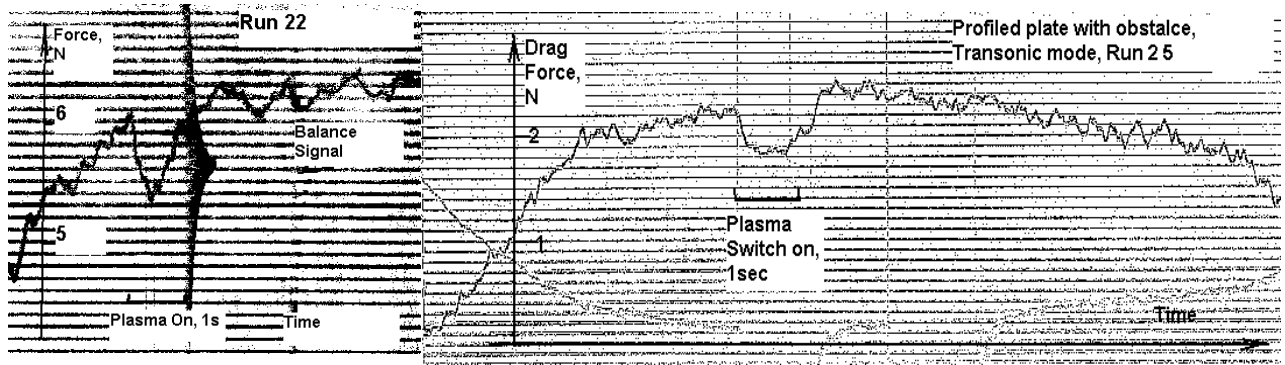


Fig.3.2.2.6. Balance records of plasma influence on a profiled model drag at transonic airflow $M=0.95$. Run22- no artificial separation, Run 25- at the obstacle before the discharge area.

Should be noted that at different value of the drag force the effects are closed each other. So, the mechanism of the interaction is the same. Moreover, subsonic streamlining shows the similar result. There were several runs at these conditions. The balance effect definitely exists. Sometimes a two-polar plasma effect can be obtained. The balance record of the run 15 is presented in Fig.3.2.2.7. This record was made by light-beam oscillograph. Here is a fragment. A force signal polarity is positive. The value of friction drag reduction was about 2N or about 40% of an initial level of the force.

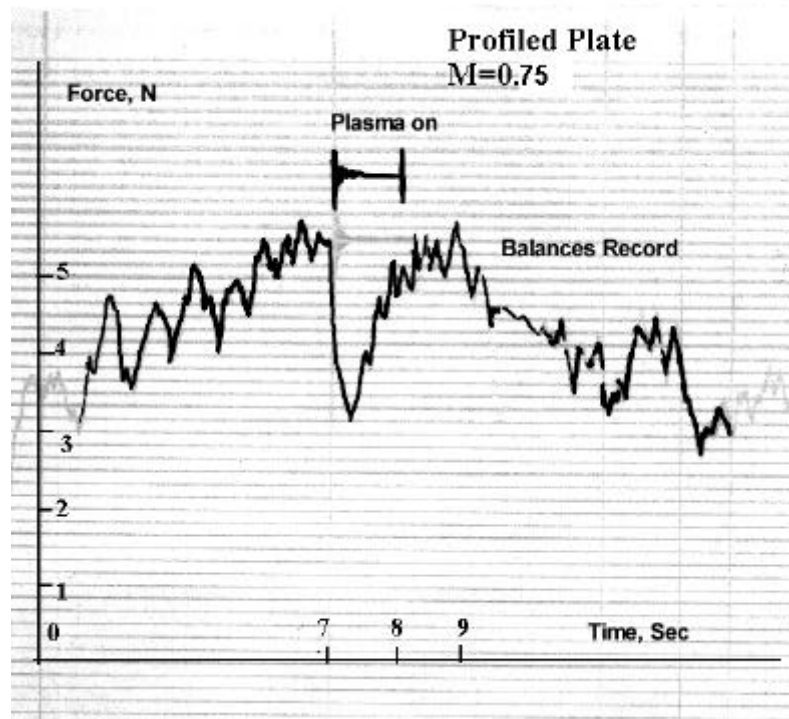


Fig. 4.2.3. Balance record of Run No15. Subsonic mode.

The balance record of the run 17 is presented in Fig.3.2.2.8. It is differed by an artificial obstacle presence. A signal trend is not a constant due to change of airflow parameters. Well seen that value of a tangential force is decreasing significantly. It happens due to plasma influence. A signal curve has a specific shape with relaxation fronts. It is a circumstantial evidence of a thermal nature of the effect in this case.

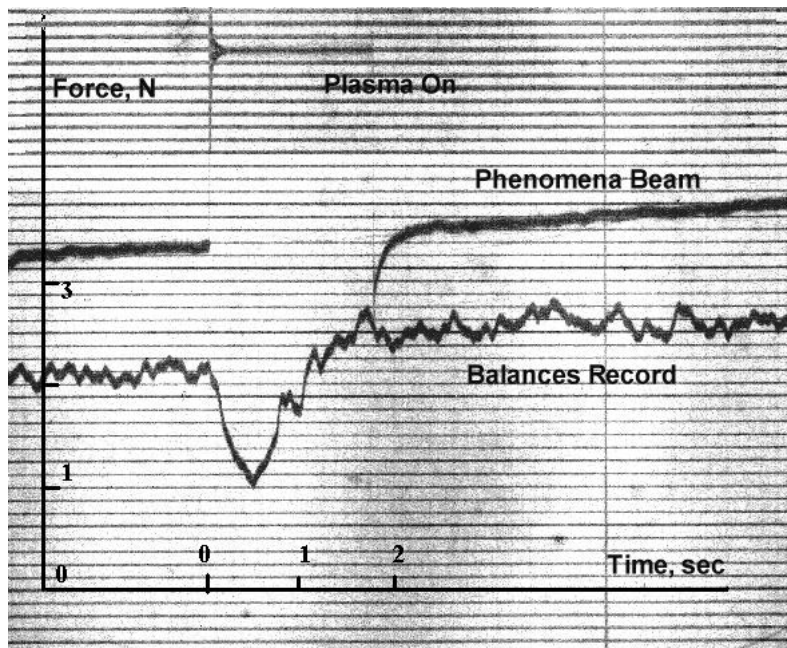


Fig. 3.2.2.8. Balance record of Run No17. Profiled plate. Subsonic mode. Artificial obstacle.

The time of plasma switching on was about 2sec and the electric power input was large because of discharge location in a separation zone. Large current leads to fast discharging of a capacitance. So the voltage in power supply is drop. As a result the plasma was stable only the first 0.5sec. An appropriate signal behavior one can see in the balance record. The value of friction drag reduction was about 1N or about 50% of an initial level of the force.

The most interesting case of a tangential force behavior is shown in Fig.3.2.9. It has been obtained at subsonic airflow, profiled plate, and artificial obstacle before the model. There large change of the volume of separation zone is observed. The process leads to late separation area reattachment on the model surface. An appropriate Schlieren photo and processing are shown in the next section.

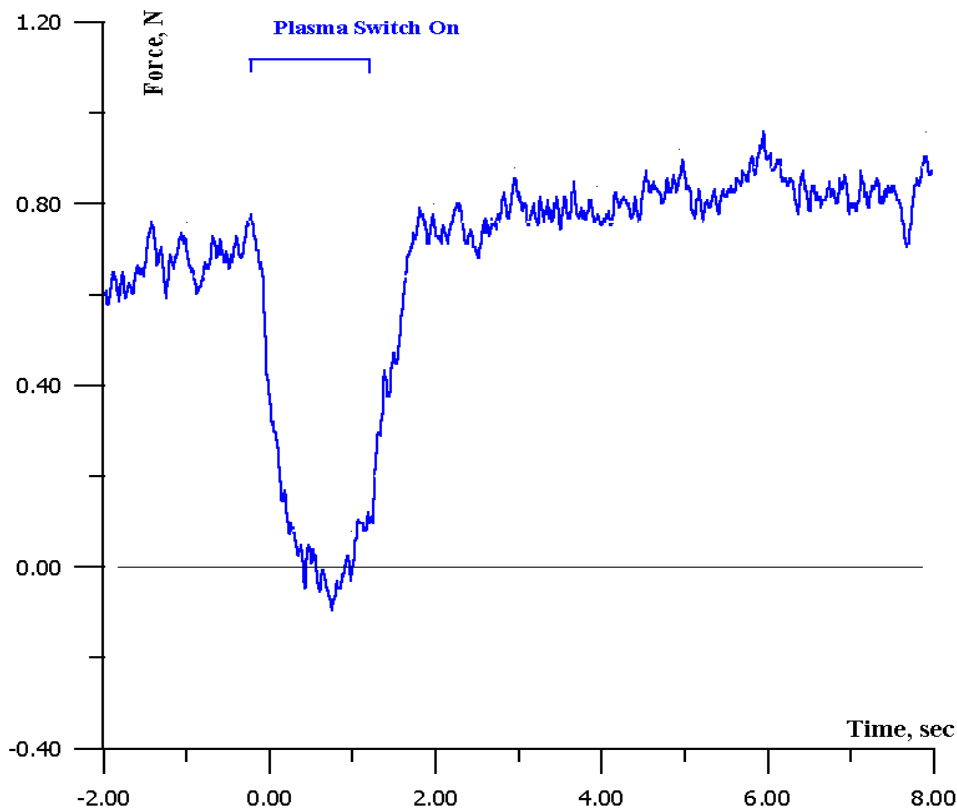


Fig. 3.2.2.9. Balance record of Run No18. Profiled plate.

Subsonic mode. Artificial obstacle.

The value of a tangential force is decreasing dramatically. It occurs due to plasma influence. In this case the input power to the discharge was a little bit less than in previous run (the pressure was larger). The value of friction drag reduction was about 100% of an initial level of the force. Such behavior is not contradicted to gasdynamic laws. Very probably that in this case a separation zone is swelled up and the pressure in a fore part of the profiled model can be less than in a base part.

Resulting graph is presented in Fig.3.2.2.10. Seen that a red point, which can be related to a skin friction effect lie closed to a linear fit.

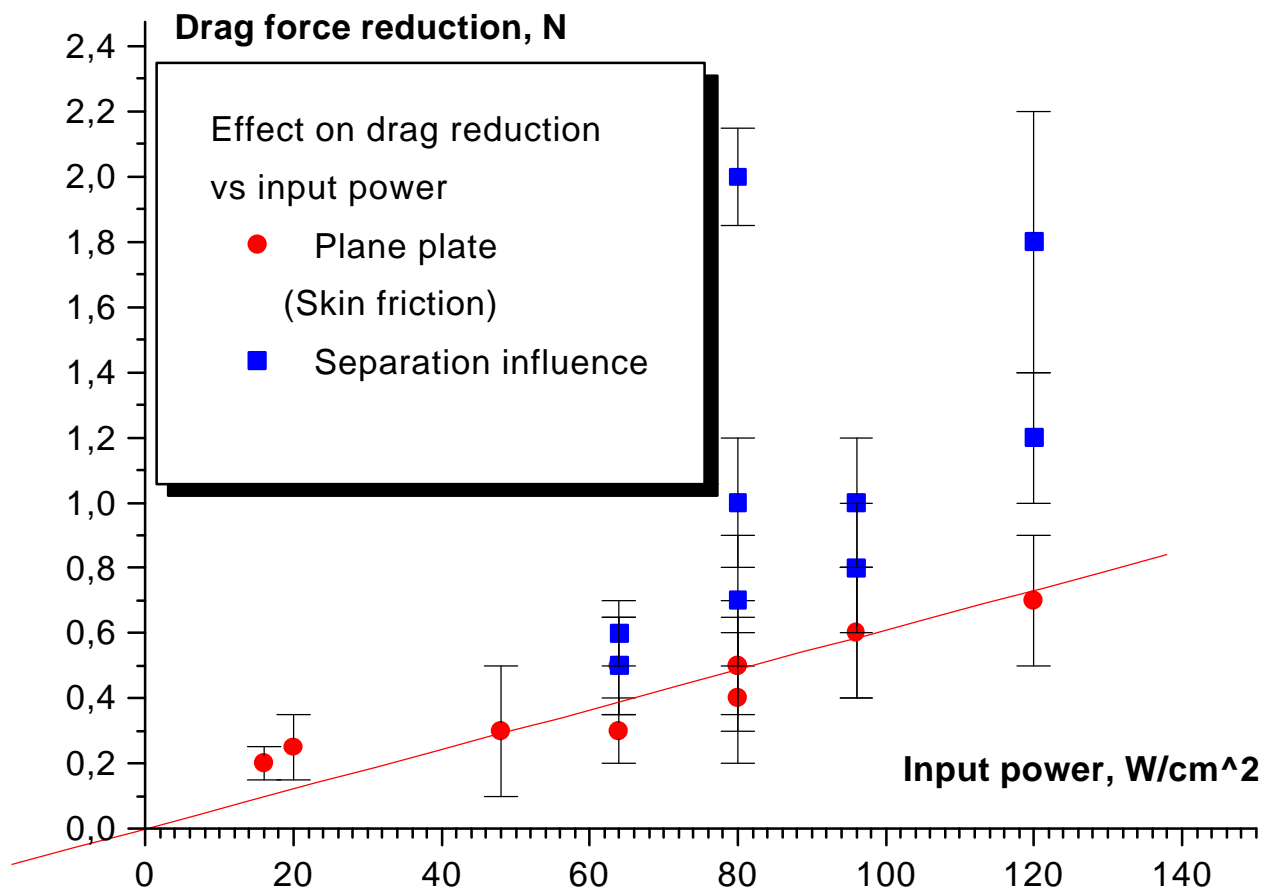


Fig.3.2.2.10. Effect of plate drag reduction vs input power to surface discharge.

3.2.3. Visualization of the Interaction.

The visualization was provided by means of videotape camera and by Schlieren device. Here only the most interested runs are shown. Numbers of runs correspond to numbers in Table 3.2.1. Exposure was about 2ms.

Schlieren photos very often do not give a clear picture of change of a density distribution. Some methods of the picture's processing allow us to extract needed details. Modern powerful graphic editors give possibility to do it relatively easy. We are using methods of a gradiental analysis GA and a nonlinear gradiental analysis NGA (psychedelic). Image-to-digital conversion procedure has been carried out by Boris Timofeev.

Plasma excitation near the model surface leads to a gas density redistribution and a generation of weak separation areas at subsonic airflow. Figure 3.2.3.1 shows a Schlieren photo of a model at subsonic airflow without plasma and with plasma generation accordingly.

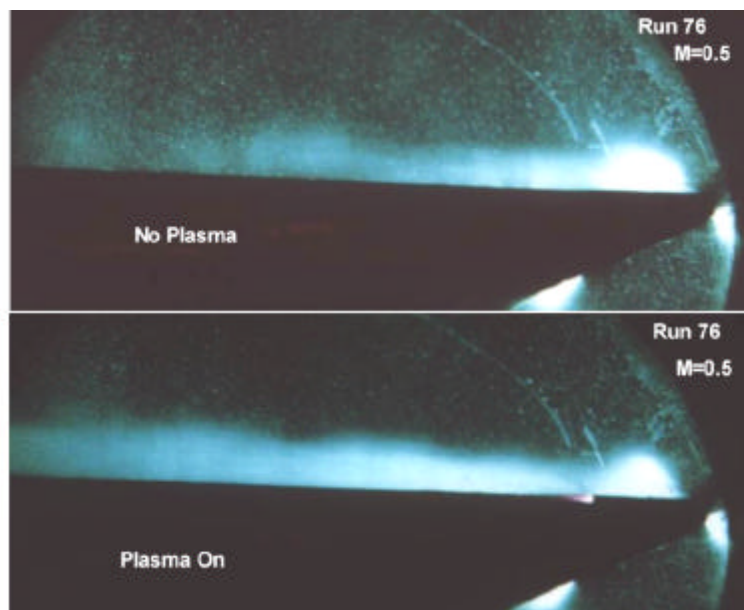


Fig.3.2.3.1. Schlieren photo of the interaction. Run 76. Subsonic airflow. Discharge in cavity.

Well seen that the discharge produces a low-density layer near the surface. Consequence of this could be in decrease of tangential strength. Besides a longitudinal gradient of density is less. Figure 3.2.3.2 presents a graph of intensity in a Schlieren photo along line, which is parallel to the surface and locates in 2 and 5mm from it. Seen, that new image contains one rarefaction wave in area upstream cavity instead of two weak waves without plasma.

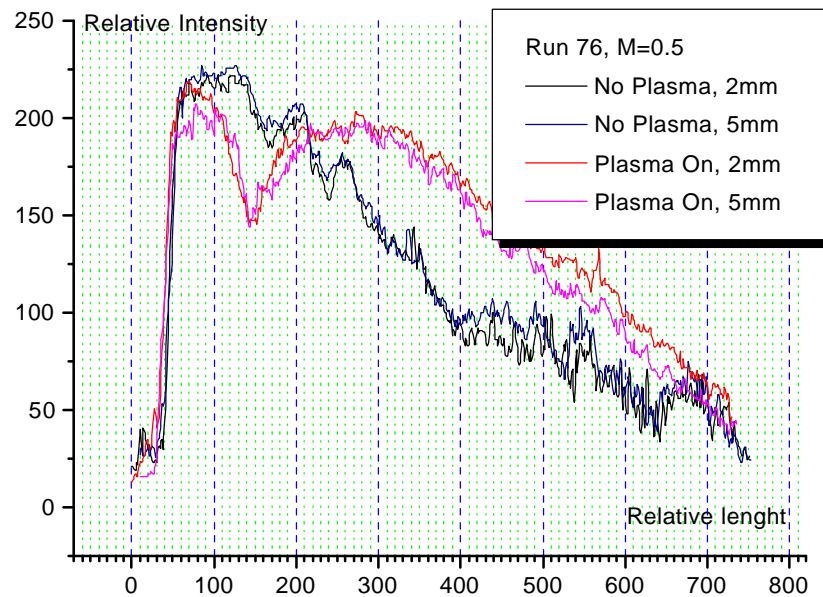


Fig.3.2.3.2. Image intensity along a line above the model surface.

A more complex picture can be observed at transonic mode of airflow. The appropriate Schlieren photos are shown in Fig.3.2.3.3. A direct shock wave in a “lambda”-configuration replaced upstream as well as a secondary shock.

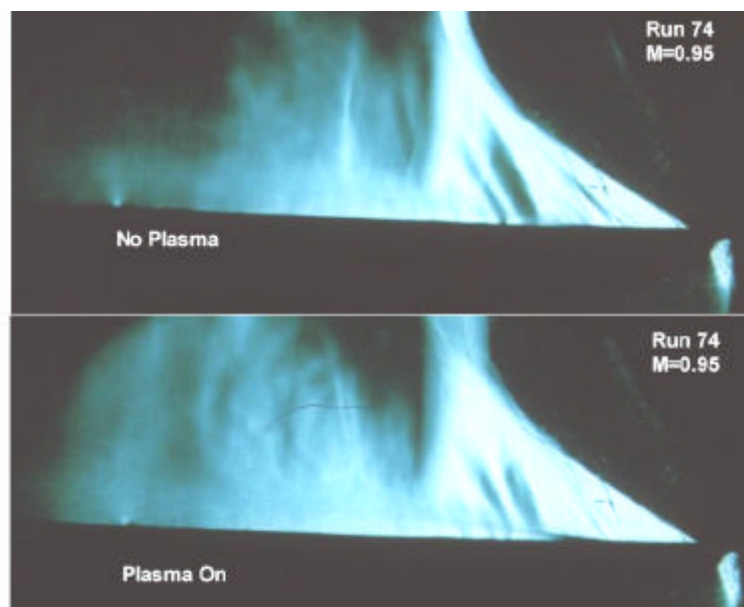


Fig.3.2.3.3. Schlieren photo of the interaction. Run 74. Transonic airflow. Discharge in cavity.

Figure 3.2.3.4 presents graphs of intensity in a Schlieren photo along lines, which are parallel to the surface and locates in 2 and 5mm from it.

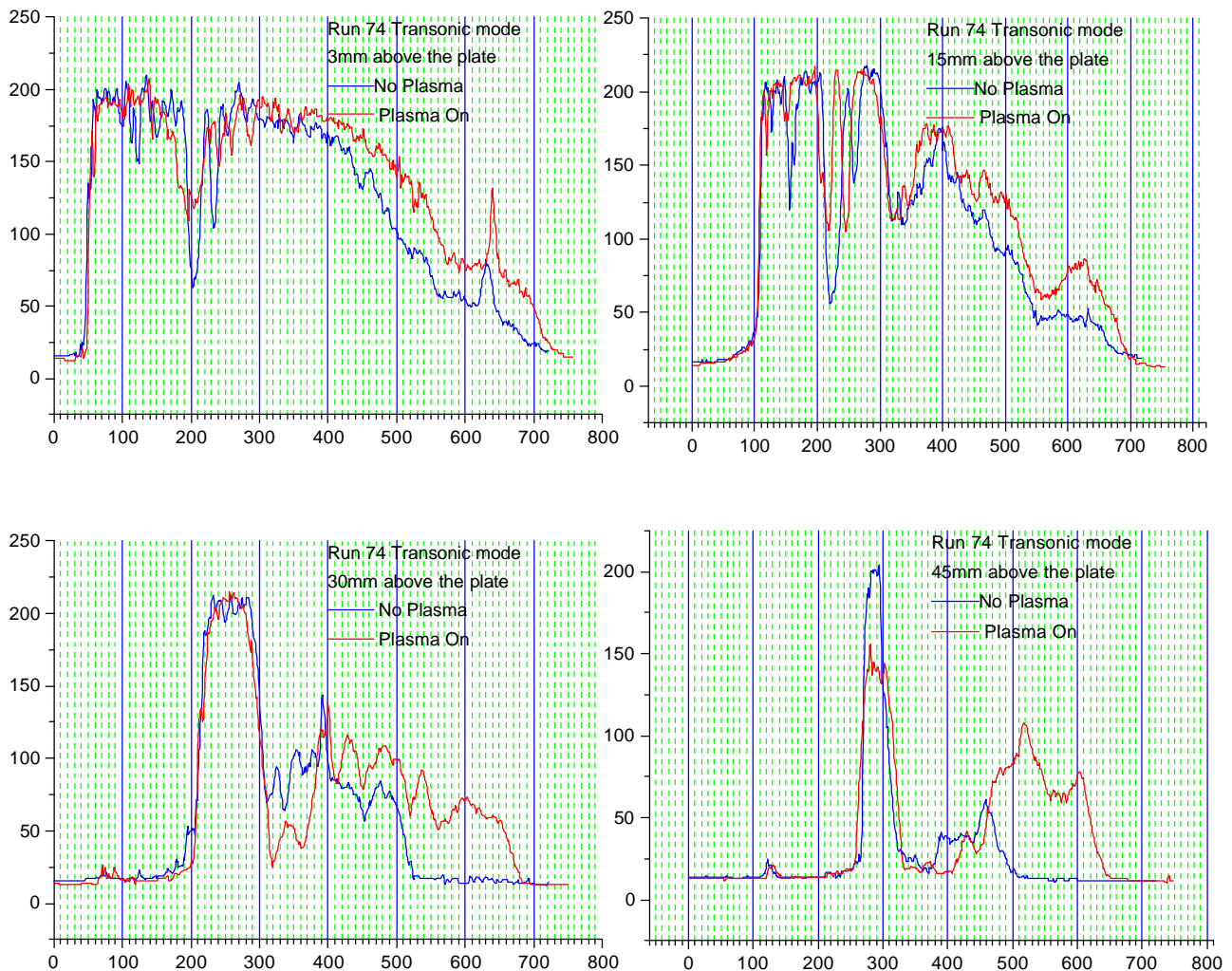


Fig.3.2.3.4. Image intensity along a line above the model surface. Transonic mode.

Seen that a picture of a flow structure change significantly. Gradients of density occurs less at plasma influence. Some disturbances transform to seria of low gradiental non-homogeneities.

The discharge generation on surface of a plain plate leads to generation of artificial local separation zone at subsonic airflow (or the discharge plasma is located in an existing separation zone). This separation zone distributes forward airflow. As the result, the heated gas doesn't interact with namely a BL, but with a main airflow. From the other side the energy input to the plasma is low due to low gap voltage and large electrodes heating. The thermal sensors give a low surface temperature for a test plate. So, a friction drag reduction can be weak. If the separation zone reconnects to a surface, the effect of a friction drag reduction is visible. The images in Fig.3.2.3.5 show such a case. Image processing allows us to recognize the details of interaction. Should be notes that the plasma distributes forward the

airflow from the electrode area.

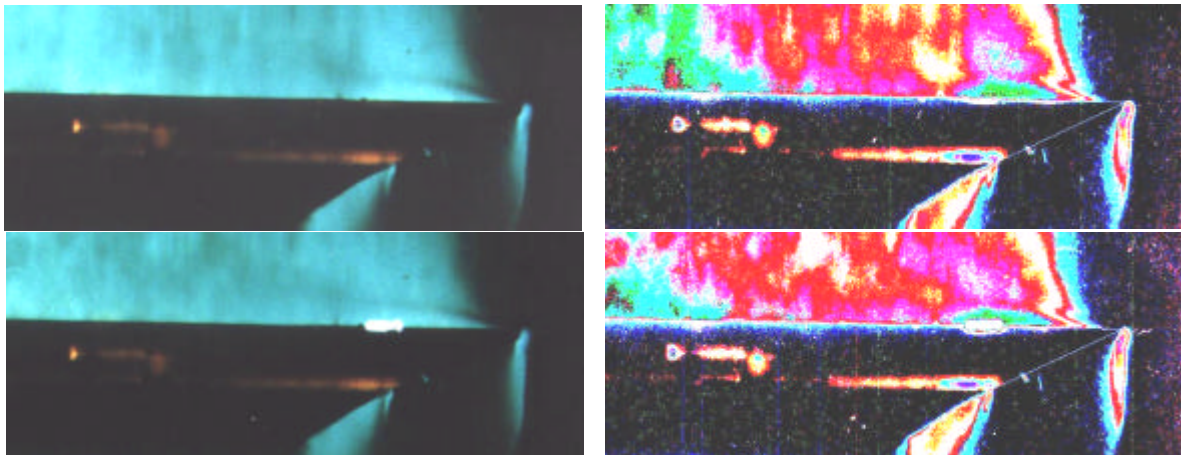


Fig.3.2.3.5. Schlieren and processed Schlieren images of a surface plasma generation at subsonic airflow $M=0.7$. The airflow direction is from right side. Top images is related to “no plasma” operation, base images –to “plasma on” case.

The drag reduction in this case was less than 0.2N from 2N of a drag force. Such an influence can be explained by some displacement of a laminar-turbulent transition line downstream. Well seen that a strong turbulence in a main flow take place later at plasma generation. A stabilizing plasma effect occurs typically when plasma is generated near the area of the BL reconnection.

At critical Mach number near $M \leq 1$ a typical structure of a transonic flow is settled. Over the plate the “lambda” shock configuration is formed. Between a first inclined shock and a direct shock supersonic airflow with $M > 1$ is realized. The position of a direct shock and volume of supersonic zone are depended on Mach number of an external airflow. When the discharge area locates inside of supersonic part of a transonic flow, the effect can be much more. In this case the energy input to the plasma is increased and the active interaction of the plasma with a BL takes place. The sample of such a behavior is presented in Fig.3.2.3.6.

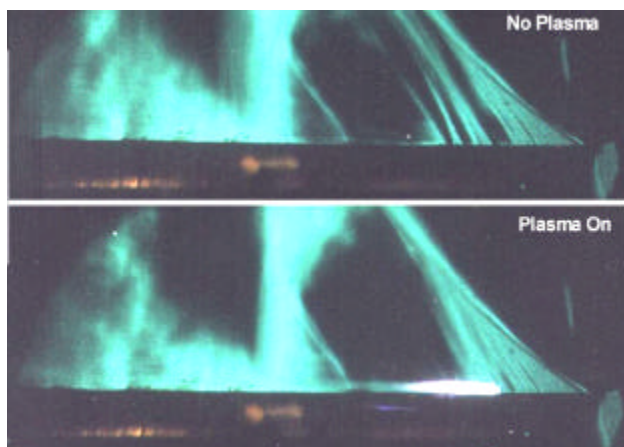


Fig.3.2.3.6. Schlieren images of plasma interaction with a plain plate at transonic mode $M=0.95$.

Separation Zone Effect. As has been talk above the optimal place for a surface discharge generation is a separation zone. From the other side the λ -structure at transonic airflow can be stabilized by small artificial obstacle. The Schlieren photos of such a case are presented in Fig.3.2.3.7.

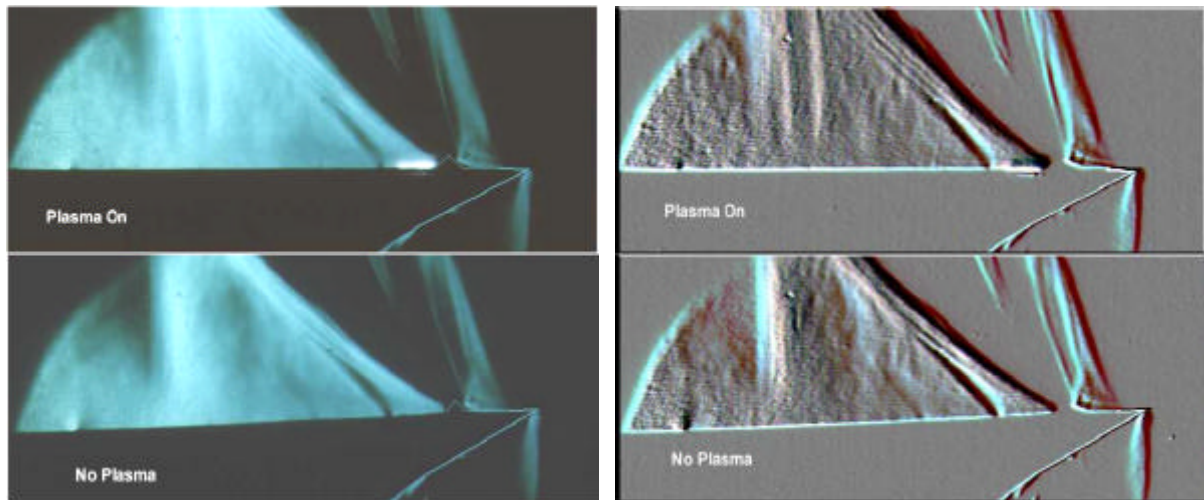


Fig.3.2.3.7. Schlieren and processed Schlieren images of a surface plasma generation at transonic airflow $M=0.95$. An artificial obstacle is installed on the surface. The airflow direction is from right side.

At this case the visible splitting of a main shock takes place. Actually, we see two shocks: first (“old”) shock is from a part of model, which is without plasma generator; second shock is from a test plate. Thus the plasma influents on whole supersonic zone by decreasing of effective Mach number inside of it. This process is reflected in displacement of a main direct shock upstream. The effective power deposition in this case is much more due to increase of power input and more time of a heated gas presence inside of an interaction area. As the result the intensity of a direct shock near the surface drops.

A similar result and change of wave structure of airflow has been obtained when a special cavity on the surface has been applied for the discharge stabilization. Appropriate data is presented in Figs.3.2.3.8 for the run No63 (see previous section).

Following consequences in a plasma excitation process can be observed. The separation zone in a cavity is increase and penetrates upstream. It leads to suppression of local supersonic disturbances just near (upstream) the cavity. The angle of a λ -shock is increase (i.e. the effective Mach number is decrease). The direct shock is displacement to an external airflow. Behind of the main shock the sequential weak shocks and waves of rarefaction are

generated. The rarefaction zone behind of a test plate becomes slighter. The sum of these changes gives a significant effect in a drag force up to 40%.

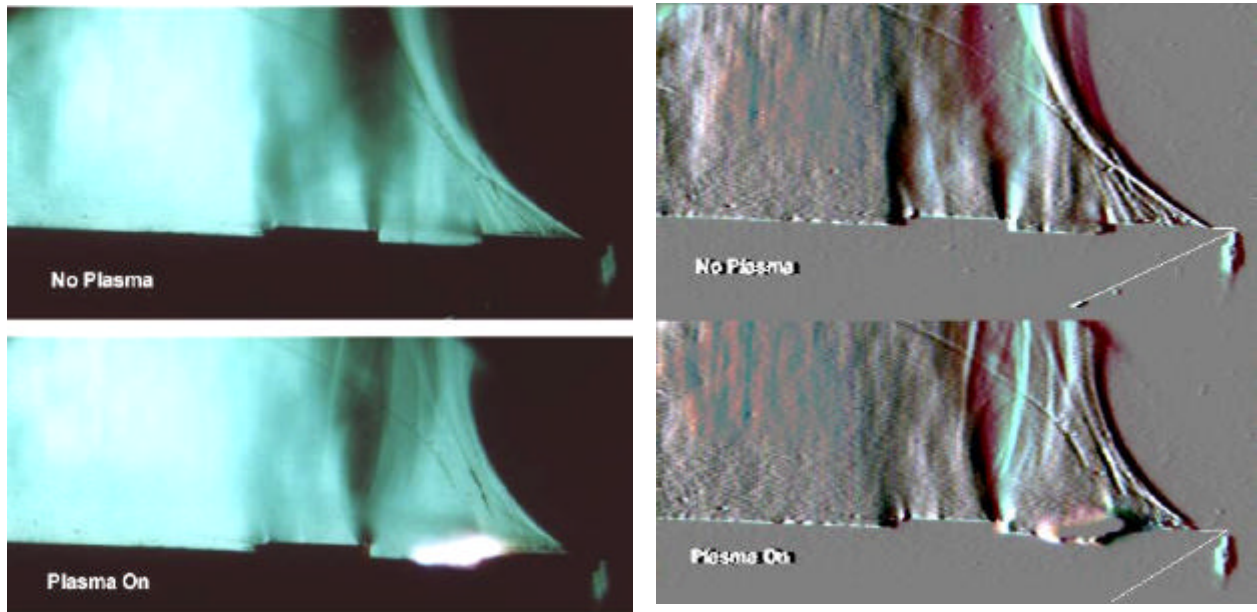
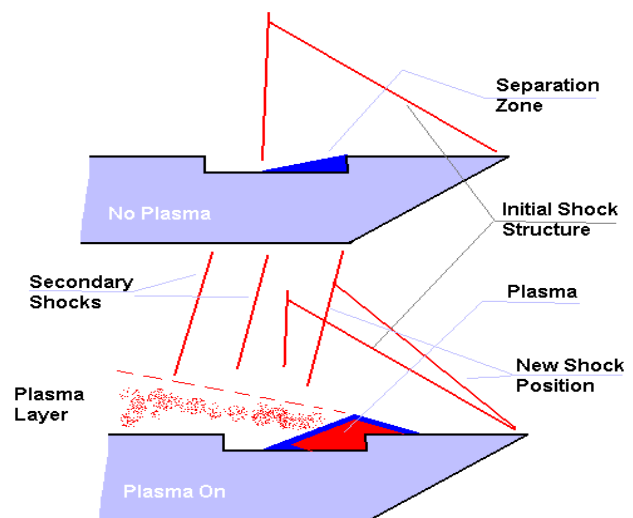


Fig.3.2.3.8. Run 63. Schlieren and processed Schlieren images of a surface plasma generation at transonic airflow $M=0.9$. An artificial cavity is made. The airflow direction is from right side. Reconstruction of the Schlieren picture.



Following processed Schlieren photos in Fig.3.2.3.9 are presented for subsonic operation mode. Drag reduction was about 1.5N from 5N of initial force. Well seen that the line of separation zone reattachment is displaced downstream. A specific input of each a mechanism to a drag reduction can be defined by measurements of pressure distribution.

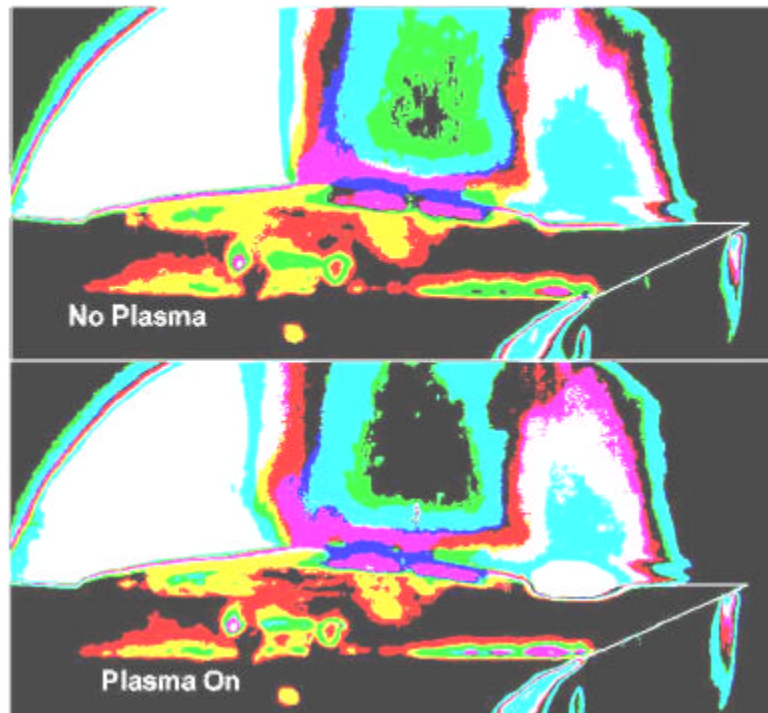


Fig.3.2.3.9. Processed Schlieren images of a surface plasma generation at subsonic airflow $M=0.75$. The airflow direction is from right side.

The most spectacular result has been obtained at subsonic airflow and an artificial obstacle application for a stabilization of discharge plasma. The following Figure 3.2.3.10 shows processed Schlieren photos. The balance record was shown in Fig.3.2.2.9.

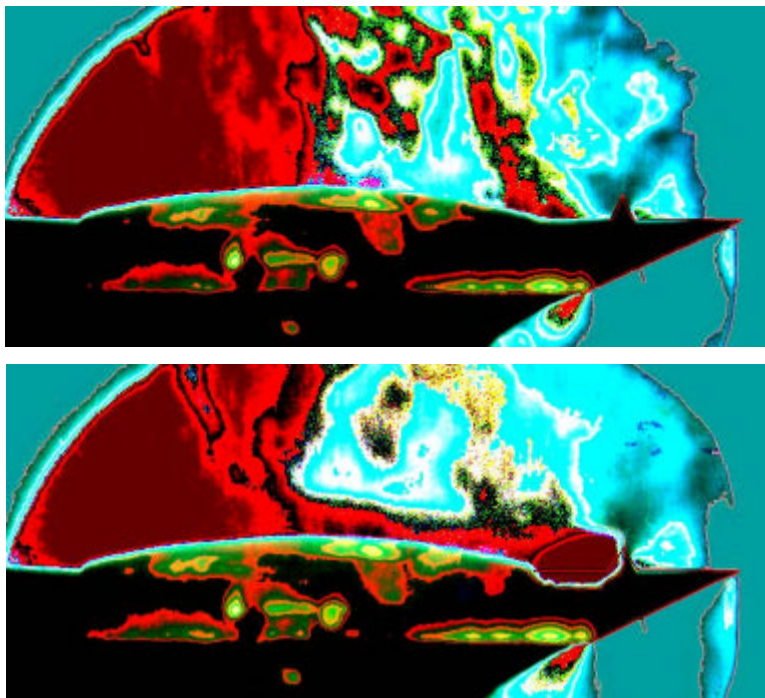


Fig.3.2.3.10. Processed Schlieren photos of a profiled plate at subsonic airflow $M=0.45$ without plasma and at plasma generation.

Well seen that this case gives no reattachment of a separated flow. The formally obtained drag force is close to zero. Obviously, the result shows that the real forces are counterbalanced.

3.2.4. Measurements of Pressure Redistribution.

Measurements of pressure distribution along the profiled model have been made by means of conventional method of a surface pipes' drainage. Scheme of pipes arrangement on a profiled model is presented in Fig.3.2.4.1. At the first test several pressure sensors have been used separately.

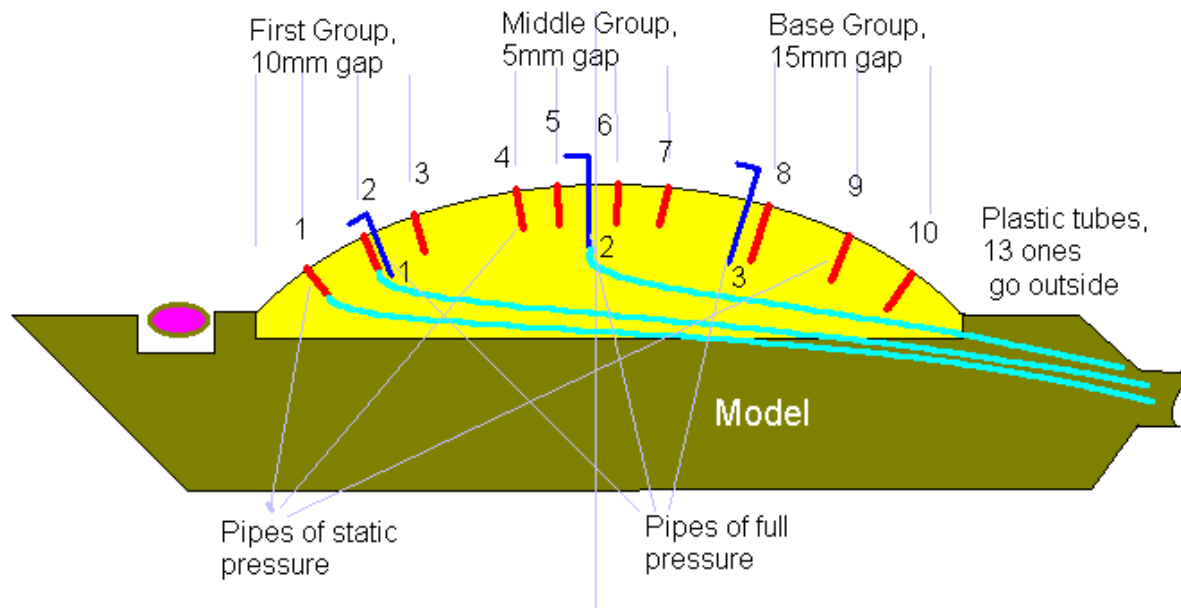


Fig.3.2.4.1. Pipes spacing at the model.

There were ten pipes for a static pressure measurements and three pipes for a full pressure estimation near the surface. Full pressure pipes are spaced in 1mm, 1.5mm and 2mm over the surface correspondingly. Sensor Po(1) is located in 20mm from fore edge, sensor Po(2) in a middle cross-section and sensor Po(3) in a 30mm downstream from Po(2). They were installed in a different position along airflow direction to avoid a “shadow” effect.

As a rule, a change of a static pressure due to plasma influence is not so large for this test configuration. Note, that an artificial obstacle is absent in this configuration. So the influence of the first separation zone is not significant. At the same time a change of position of a main shock can lead to static pressure redistribution at transonic mode of streamlining.

In the most cases static pressure is decrease slightly, especially, near a fore edge of the model. When the position of a main shock is changed, the second group of pipes demonstrates unstable behavior of static pressure. Such a sample is shown in Fig.3.2.4.2 for transonic mode of airflow with Mach number about $M=0.9$ (see also previous section of the Report).

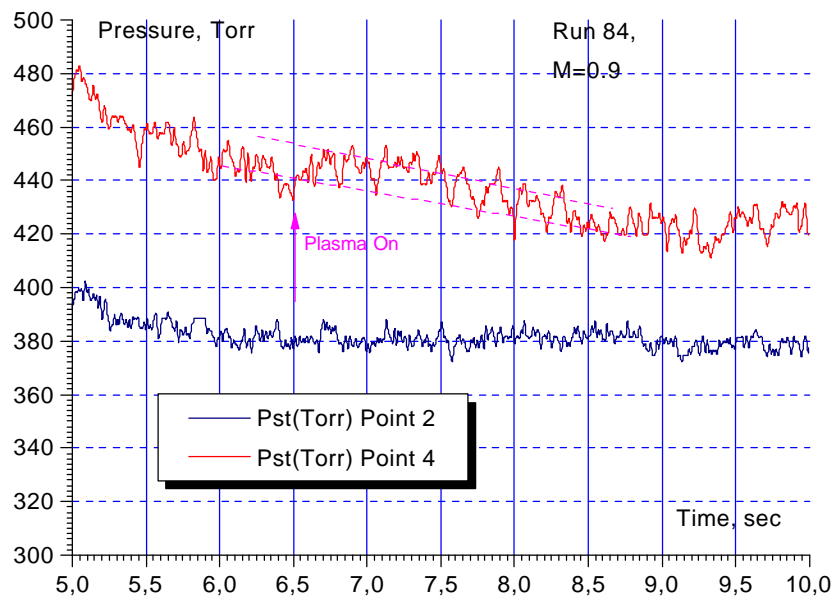


Fig.3.2.4.2. Static pressure record at transonic mode.

The first and the second groups of pressure sensors.

At the same time a total pressure near the surface is decreased under the plasma influence, as a rule. A sample of a typical total pressure behavior at plasma generation is shown in Fig.3.2.4.3&4.

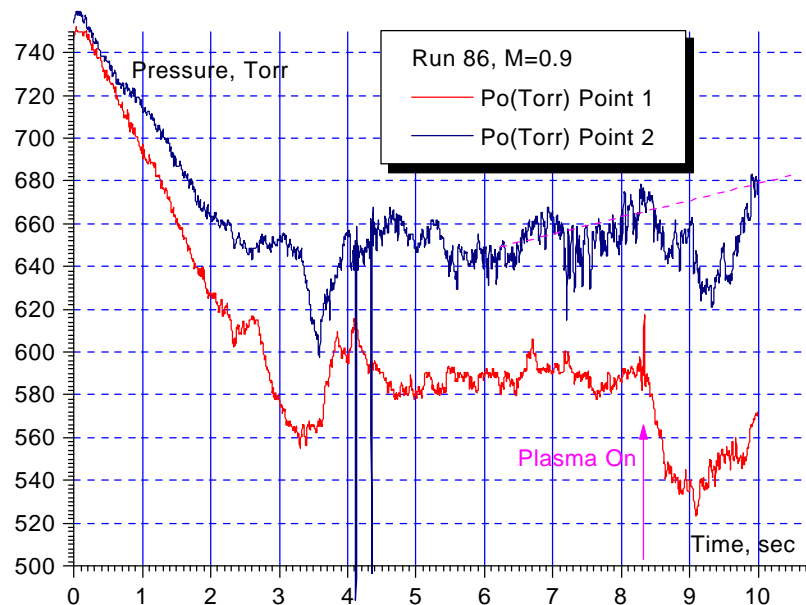


Fig.3.2.4.3. Total pressure record at transonic mode.

The first and the second points of measurements.

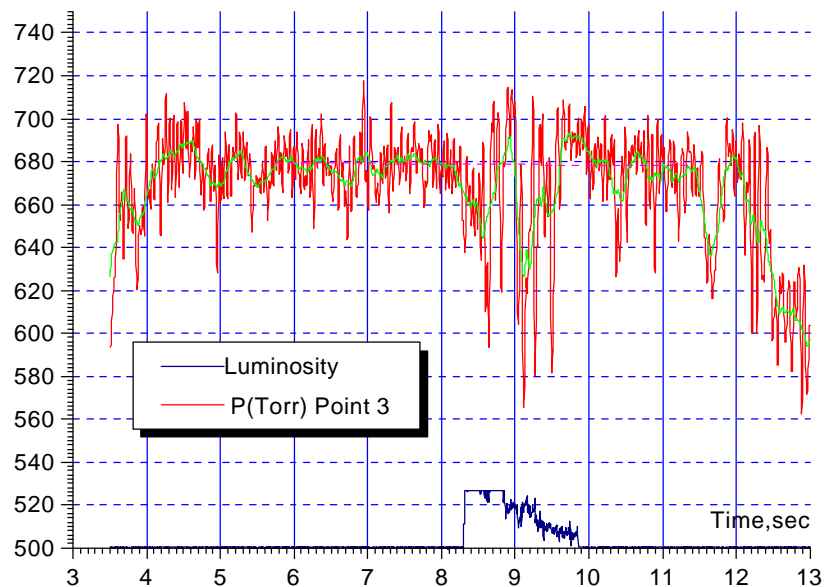


Fig.3.2.4.4. Static pressure record at transonic mode.

The third pressure sensor and plasma luminosity.

Well seen that the nearest sensor shows the largest decrease of a total pressure. Such a decrease is exceeded a value of 10% of amplitude. The third sensor demonstrates unstable effect at plasma generation, probably, due to unstable position of a shock wave.

Thus, a total pressure changes much larger than a static pressure in this aerodynamic configuration. It means, that tangential strength is decrease near the surface and a friction drag might be less.

Note, that the effect of a total pressure decrease is not so significant at subsonic mode of airflow.

3.2.5. Plasma Influence on Turbulence.

Suppression of flow disturbances has been observed at surface plasma excitation in transonic and subsonic modes of airflow both. Such an effect becomes apparent in Schlieren photos, balances measurements and, in a less degree, in pressure measurements.

Note, that two contradictory effects take place: generation of disturbances by plasma (especially at pulse-repetitive mode of discharge) and suppression of airflow disturbances by plasma layers. There are a lot of evidences when plasma adds own disturbances to airflow downstream. Here the samples of turbulence suppression are done.

Figures 3.2.3.5 and 3.2.3.6 shows that the turbulence downstream of a model is suppressed (it is visible in processed photos). The same result for subsonic airflow is presented in Fig.3.2.5.1.

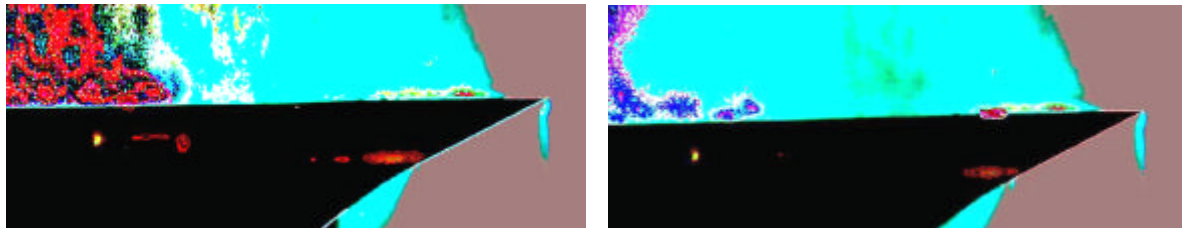


Fig.3.2.5.1. Processed Schlieren Photos. Subsonic airflow $M=0.6$.

Left picture- no plasma; right picture- plasma on.

Processing of the images allows us to recognize some details. Namely, here is well visible that a strong turbulence is started later downstream, if surface plasma is excited. Another sample is related to transonic mode of airflow. Fig.3.2.5.2 presents an appropriate processed Schlieren photos. Seen, how a direct shock provokes the turbulence. In a case with plasma

generation the turbulence is weaker, probably, due to a less amplitude of the shock near the surface.

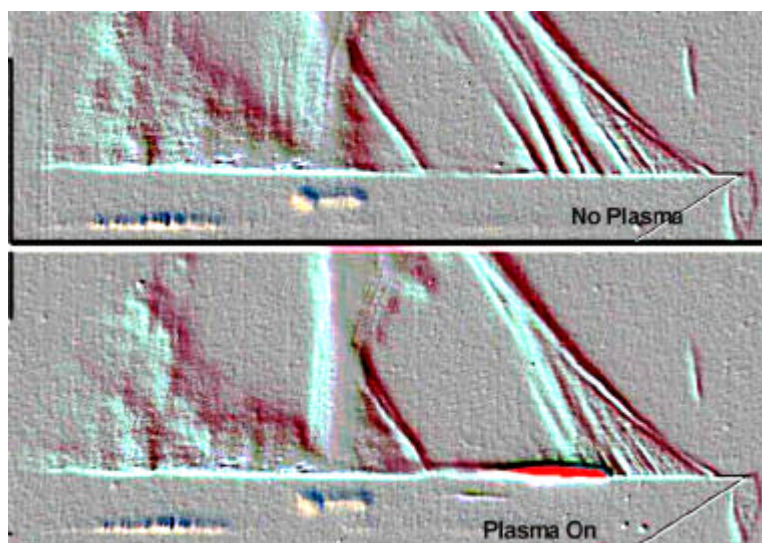


Fig.3.2.5.2. Processed Schlieren Photos. Transonic airflow.

The next picture in Fig.3.2.5.3 shows a balance record, where the amplitude of a tangential force vibration is less during the time of plasma generation. It doesn't mean that at any cases we can see the same picture.

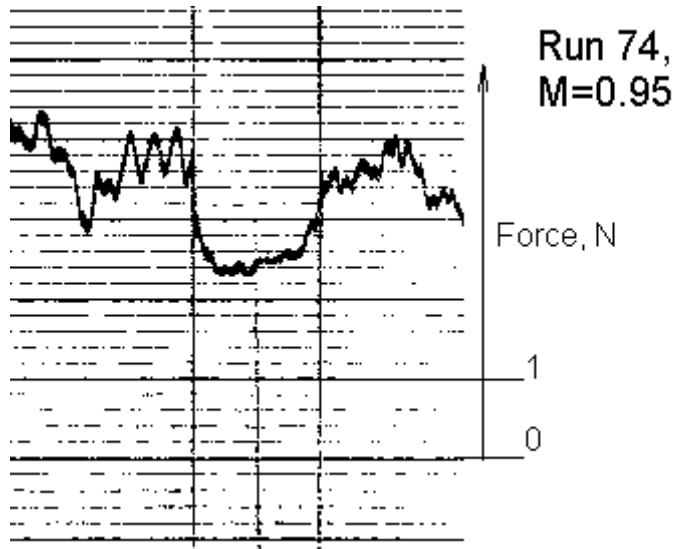


Fig.3.2.5.3. Balance's record at transonic mode. Vibration decrease.

Charts in Fig.3.2.5.4 shows Fourier spectrum of a total pressure without plasma generation and at plasma generation. Seen that plasma add some disturbances at relatively high frequencies. At the same time one can see that a weak suppression of a flow disturbance at relatively low frequency take place.

The results of this section require an additional verification.

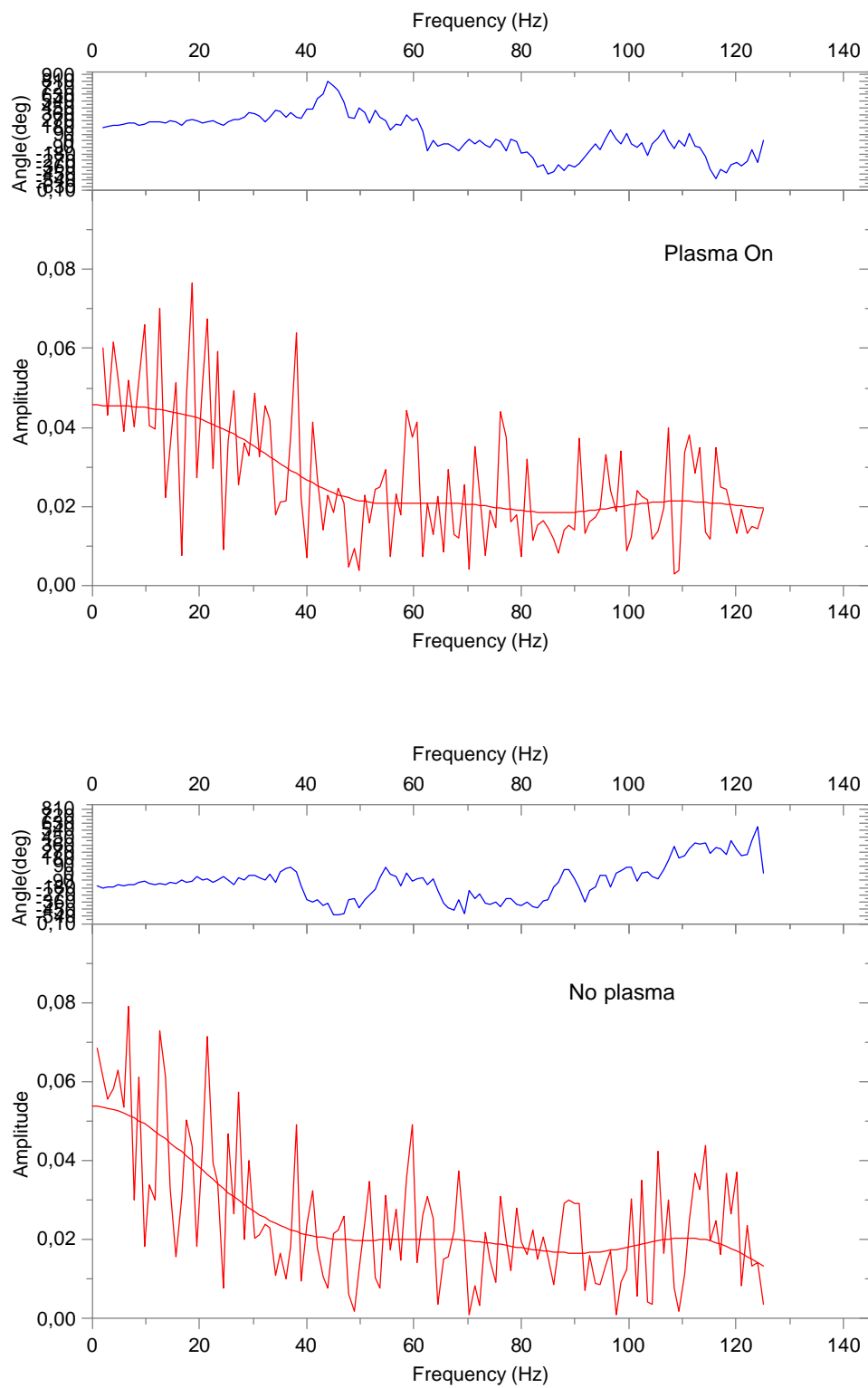


Fig.3.2.5.4. Fourier spectrum of a total pressure signal at plasma presence and without it.

3.3. Mathematical Simulation.

The numerical analysis of experiments has been performed on a basis of plane viscous flow model at presence in the stream near wall a local heat supply region. Discharge on the model was simulated of this heat source. The thermally equilibrium chemically frozen model of heated air was used in these calculations. The turbulent flow is described by the Favre-averaged Navier-Stokes equations with additional source term in the energy equation. The Boussinesq approximation for the Reynolds stress tensor and algebraic Baldwin-Lomax turbulence model for calculation of turbulent transport coefficients is used. The laminar flow equations (Navier-Stokes equations) are obtained by neglecting the turbulent contributions. It is supposed that heat source term in co-ordinate system (s,n) , where s is distance along plate from its begin and n distance along normal from plate to point with co-ordinate (s,n) is written in the following form:

$$q_h = C_q F(s) G(n)$$

where functions $F(s)$ and $G(s)$ are given by

$$F(s) = \begin{cases} 1 & \text{for } s_{hb} \leq s \leq s_{he} \\ 0 & \text{for other cases} \end{cases} ; G(n) = \begin{cases} 1 & \text{for } 0 \leq n \leq n_{he} \\ 0 & \text{for other cases} \end{cases}$$

The value of C_q is defined from conditions

$$\int_{S_c} q_h ds = P_d$$

where S_c is computation domain, P_d - input power in heat per unit length. The viscosity is calculated using a power law variation with temperature, $\mu = a_\mu T^{0.683}$, molecular Prandtl number is $Pr = 0.7$ and turbulent Prandtl number is $Pr_t = 0.9$. It is supposed that on a body surface for velocity the no-slip condition $\vec{u} = 0$ and for temperature heat-isolated condition $q_w = 0$ are fulfilled, where q_w is heat flux to the wall.

The steady solution was found with help of time-marching technique using for numerical integrating of unsteady Navier-Stokes equations an implicit monotone difference scheme second order of accuracy, constructed with finite-volume approach. The inviscid fluxes through the interfaces of cells are calculated using exact Riemann problem solution defined by interfacial values of parameters in the adjoining cells. For determination these

values it was used the non-oscillating one-dimensional reconstruction of primitive variables: pressure p , temperature T and vector velocities \vec{u} inside cells along appropriate coordinate direction. Viscous fluxes through the "interior" sides of cells were determined on the space centered difference formulas and through the sides lying on the body surface using one-sided three-dot difference approximations. On every time step the flowfield parameters were defined due Gauss-Seidel line relaxation numerical technique.

The calculations were performed for laminar and turbulent models of flow at Mach number $M_\infty = 0.6$ and 1.0 , total pressure $p_0 = 1$ atm, total temperature $T_0 = 300$ K, $P_d = 0$ and 270 W/cm, $s_{hb} = 2.5$ cm, $s_{he} = 3.5$ cm, $n_{he} = 0.1$ cm. The grid 150×150 adapted to flow peculiarity was employed. The grid cells were condensed near plate surface, so that in a laminar sublayer region not less than 10 grid points are placed.

Fig. 3.3.1 shows the distributions along plate a Reynolds number Re_q calculated through momentum thickness θ for conditions at outer edge of the laminar boundary layer (for $P_d = 0$). The value $Re_q = 300$ often is used as criterion of laminar –to-turbulent transitions. As the Fig.3.3.1 indicates transition (without heat supply) begins at $s \approx 2$ cm for both Mach number if this criterion use.

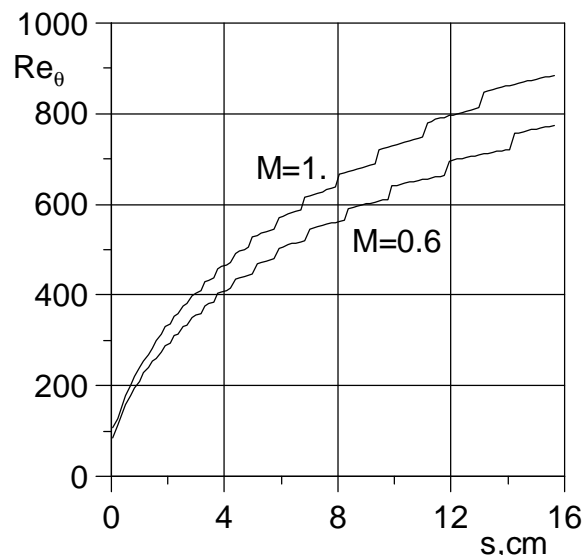


Fig. 3.3.1. Distributions of Reynolds number, calculated through momentum thickness

In table 3.3.1 it is listed values of total skin-friction coefficients C_f of moving part of plate (test plate) that was placed from $x = 4$ cm to $x = 16$ cm. The value of C_f is defined by expression

$$C_f = \int_{s_1}^{s_2} t_w ds / 0.5 \rho_\infty V_\infty^2 (s_2 - s_1),$$

where t_w is skin-friction.

Table 3.3.1 Skin-friction coefficients of test plate

$C_f \cdot 10^3$	M	Pd, W/cm	Flow regime
0.662	0.6	0	laminar
0.449	0.6	375	laminar
3.17	0.6	0	turbulent
2.00	0.6	375	turbulent
0.563	1.0	0	laminar
0.420	1.0	375	laminar
2.90	1.0	0	turbulent
1.98	1.0	375	turbulent

This table indicates that the heat supply leads to decreasing of skin-friction both for laminar and turbulent flow. The peak of drag reduction for laminar flow is 0.68 and for turbulent flow it is 0.63.

On Fig.3.3.2-3.3.4 it is compared the distributions of wall temperature, pressure and local skin-friction coefficient along plate surface obtained in considered variants of calculations for $M_\infty = 0.6$. Similar data for $M_\infty = 1.0$ are presented in Fig. 3.3.5-3.3.7. Here and on all other figures by light symbols are designated results corresponding to $P_d = 0$, but by dark symbols correspond to results for $P_d = 375$ W/cm. The square symbols correspond to laminar flow, by round symbols are presented data for turbulent flow regime.

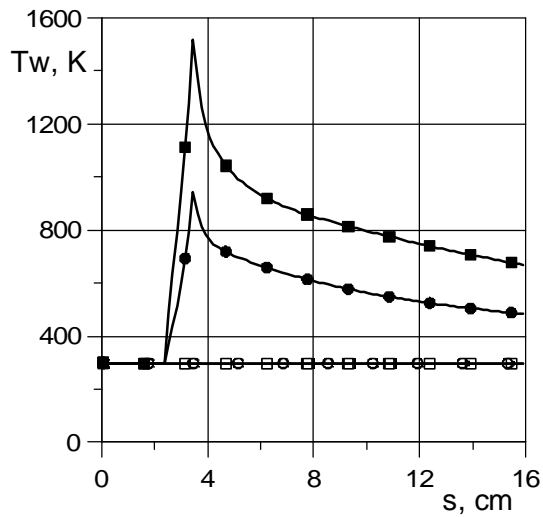


Fig.3.3.2. Wall temperature. $M_\infty = 0.6$.

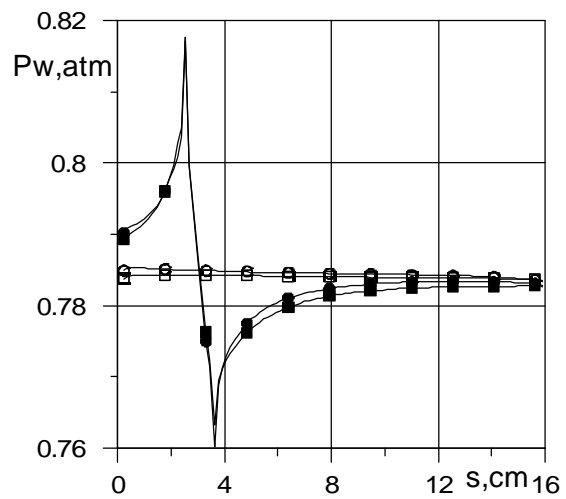


Fig.3.3.3. Wall pressure. $M_\infty = 0.6$

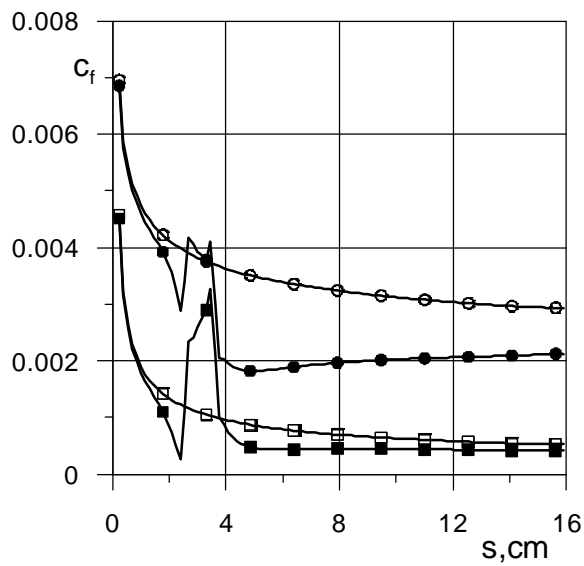


Fig.3.3.4. Skin friction coefficient. $M_\infty = 0.6$

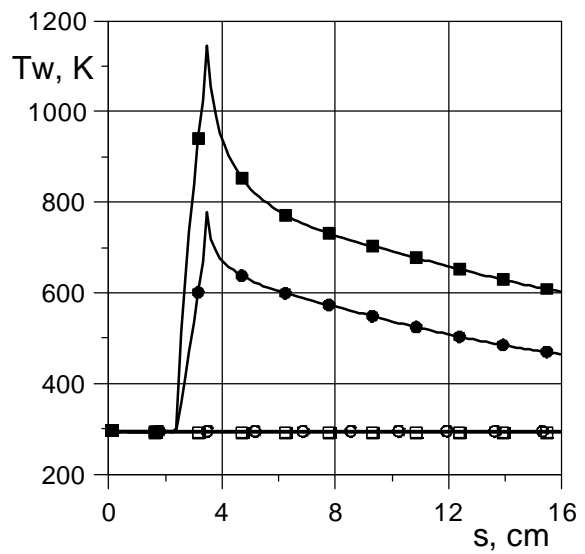


Fig.3.3.5. Wall-temperature $M_\infty = 1$.

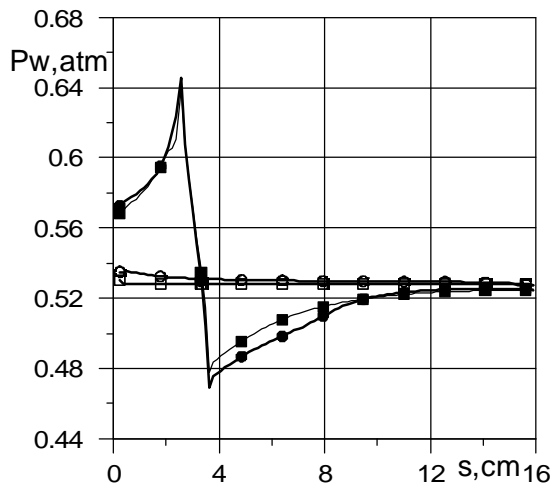


Fig.3.3.6. Wall pressure distribution.

$$M_{\infty} = 1.$$

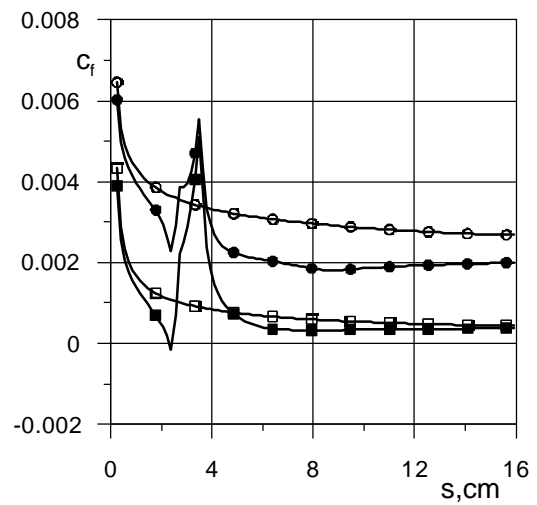


Fig.3.3.7. Skin-friction coefficient.

$$M_{\infty} = 1.$$

In Fig. 3.3.8-3.3.11 the distributions of the longitudinal component of velocity vector divided on free stream velocity, u / u_{∞} and gas temperature, T, K along normal to plate surface at $s = 3.6 \text{ cm}$ (in the end of heating region) and at $s = 10 \text{ cm}$ (in the moving plate center) are presented.

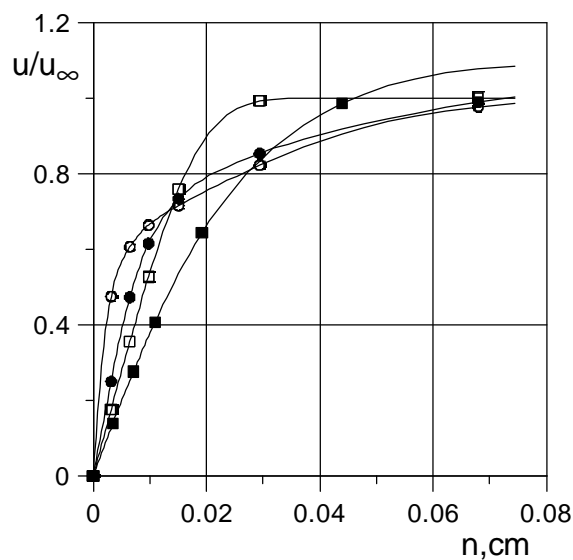


Fig.3.3.8. Velocity distributions.

$$M_{\infty} = 0.6, \quad s = 3.6 \text{ cm}$$

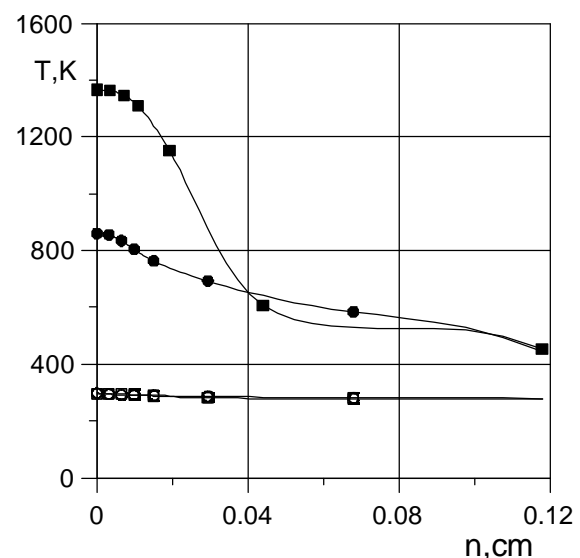


Fig.3.3.9. Temperature distributions

$$M_{\infty} = 0.6, \quad s = 3.6 \text{ cm}$$

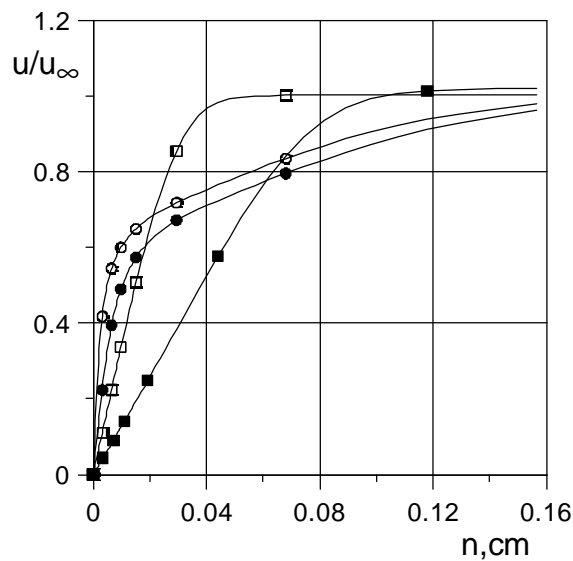


Fig. 3.3.10. Velocity distributions.

$M_{\infty} = 0.6$, $s = 10$. cm

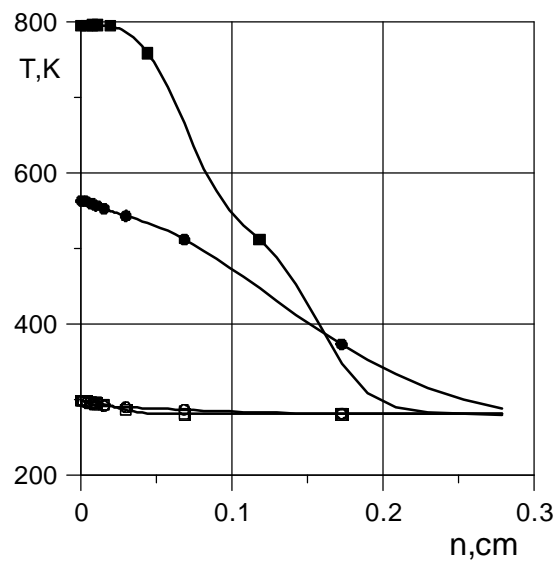


Fig.3.3.11. Temperature distributions

$M_{\infty} = 0.6$, $s = 10$. cm

This data were obtained for $M_{\infty} = 0.6$. Similar results for $M_{\infty} = 1$. is displayed in Fig. 3.3.12-3.3.15.

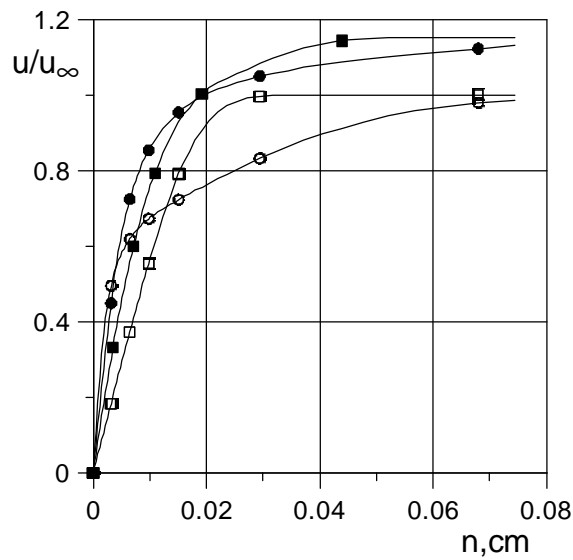


Fig.3.3.12. Velocity distributions

$M_{\infty} = 1.0$, $s = 3.6$ cm

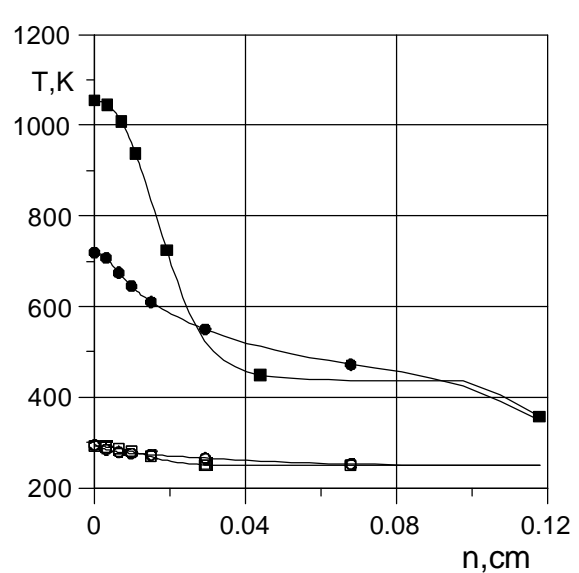


Fig.3.3.13. Temperature distributions

$M_{\infty} = 1.0$, $s = 3.6$ cm

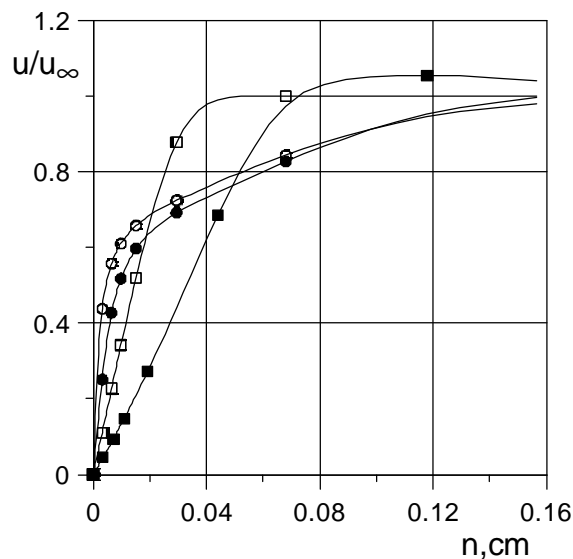


Fig.3.3.14. Velocity distributions

$M_{\infty} = 1.0$, $s = 10$ cm

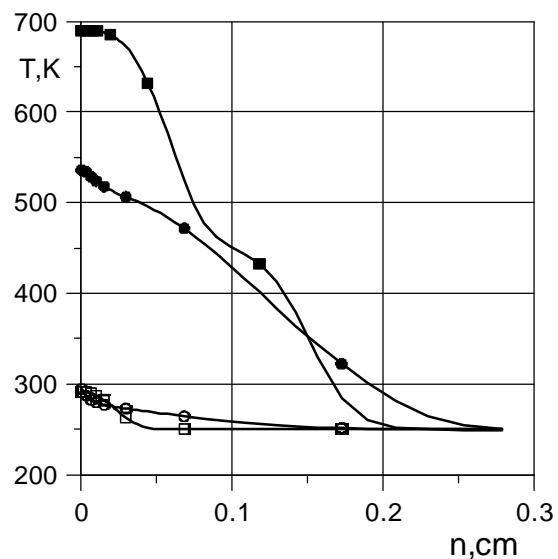


Fig.3.3.15. Temperature distribution

$M_{\infty} = 1.0$, $s = 10$ cm

The results of simulation are closed to the experimental data qualitatively. At subsonic operation mode calculated velocity profiles have less normal gradients near the surface when the plasma is generated. It leads to decrease of a tangential stress along the plate. At the transonic operation mode the same behavior takes place excluding the area just near (downstream) the line of a heat deposition. In such a place a tangential force can increase locally due to more full velocity profile. From the other side such a velocity profile is more stable in respect of a separation process.

So, the intermediate conclusion is that simulation in frames of turbulent boundary layer gives a good agreement with an experimental data qualitatively. A quantitatively agreement can be achieved by adjusting of condition and initial data. A more comprehensive simulations in a such way are required.

3.4. Interim Conclusion.

The experimental work and simulations show a large potential of plasma applications for a friction reduction and a separation zone modification near surfaces under the high-speed airflow. The skin friction of a plain plate is decrease at surface discharge plasma influence if the effect of another mechanisms, like separation zone generation, is negligible. The plasma generation in a separation zones leads to a redistribution of loads (pressure) near these zones and downstream. The purposeful plasma influence on parameters of BL near bodies of complex shape can lead not only to friction drag decrease but also change a wave component of a whole drag.

The discharge plasma is much stable if it is excited in a separation zone. The efficiency of plasma effect is higher when the plasma generator locates in natural or artificial separation zones, like at obstacles or cavities. Moreover, fact of plasma presence in such an area gives the effect in increasing of its volume and change the position. The plasma generation near the body surface can lead to separation processes, especially, at subsonic airflow.

Change a position of local shocks is observed at transonic mode of airflow as well as decrease of amplitude of flow disturbances due to effect of surface discharge plasma generation. Local flow disturbances as well as shocks and rarefaction areas can be suppressed under surface plasma influence.

4.2. Experimental Data.

4.2.1. Two Modes of Plasma Spacing.

As has been considered above, two different modes of the discharge location have been found. They differ by the direction of an electric current. Under the first, standard, mode the current flows from positive (hot) electrodes to grounded electrodes, which are located on an insulating plane plate. At the second mode electric current changes the direction and flow to a grounded metallic wall of the test section. At that the current flows through a separation zone.

Process of the first mode transformation to the second one started from one electrode current displacement. After this all other electrodes connected through a separation zone immediately. If a separation zone is disappeared due to flow weakening, the discharge can transform back to the first mode.

Figures 4.2.1.1 and 4.2.1.2 show the photos of multi-electrode surface discharge in two different modes. Near the photos on the right side the graphs of plasma luminosity are presented. They were done for two cross-sections: just downstream of the electrodes and in a separation zone. Well seen that plasma luminosity in a separation zone is quite homogeneous.

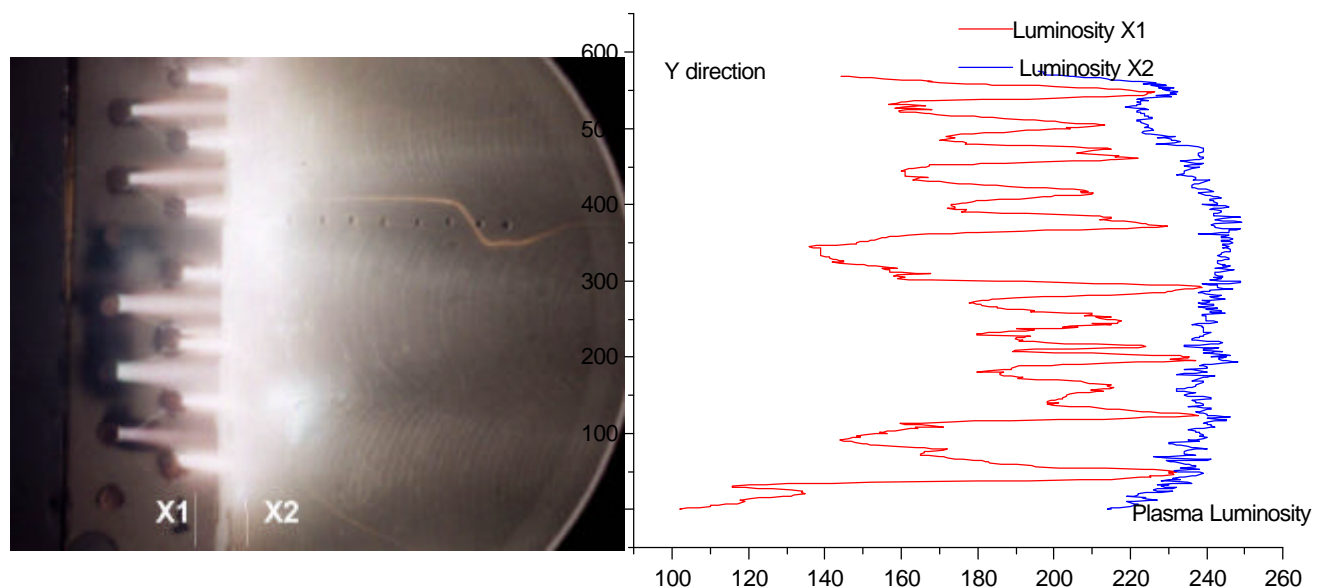


Fig.4.2.1. Photo of a multi-electrode discharge. The first mode: current flows through grounded electrodes. Right side: plasma luminosity distribution in two cross-sections.

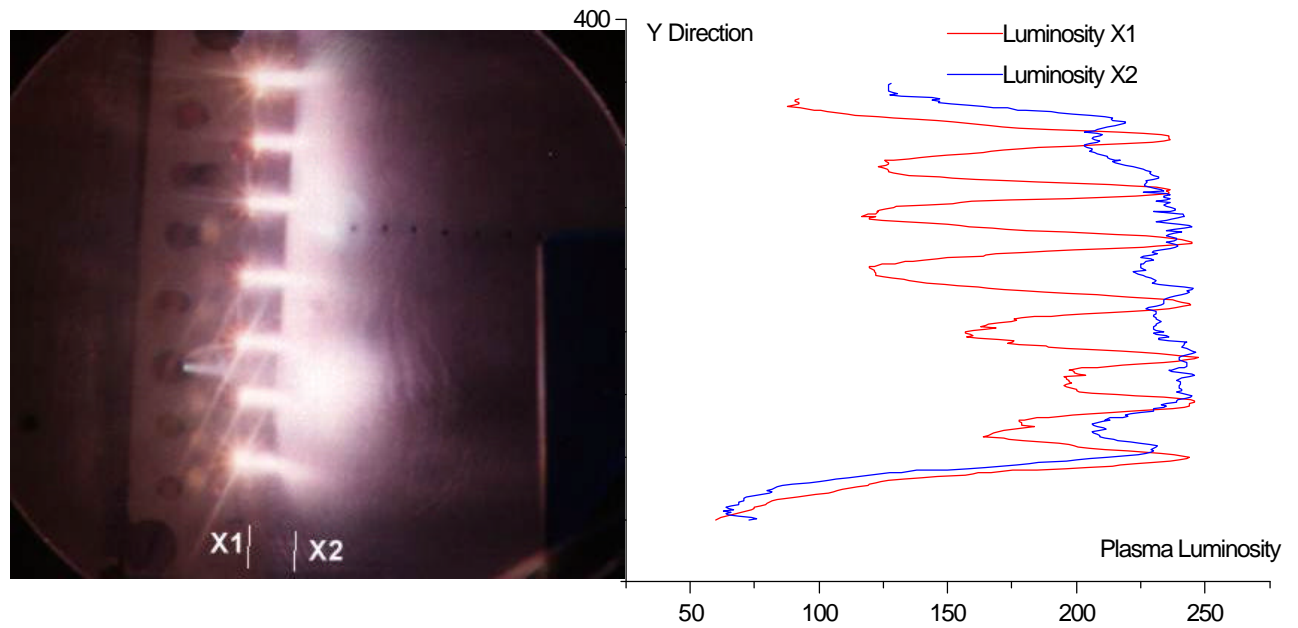


Fig.4.2.1.2. Photo of a multi-electrode discharge. Second mode: current flows through separation zone on a wall of TS. Right side: plasma luminosity distribution in two cross-sections.

To recognize how the current connect to a wall a photo-record at the angle 45° has been done. Fragments of such a photo together with the processed images are presented in Fig.4.2.1.3 for a standard mode and in Fig.4.2.1.4 for the case when current flows through a separation zone. The result is well seen.

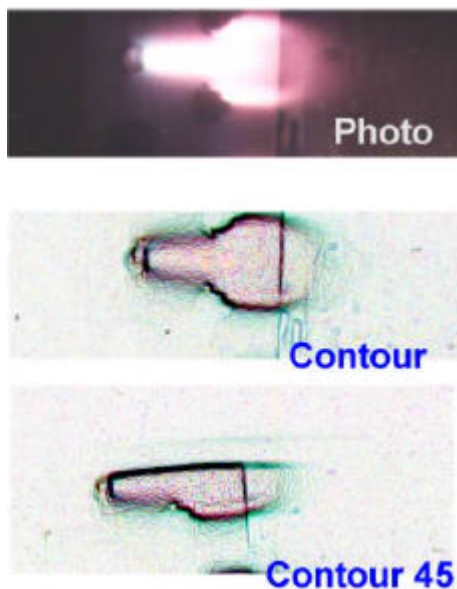


Fig.4.2.1.3. Electrode discharge.

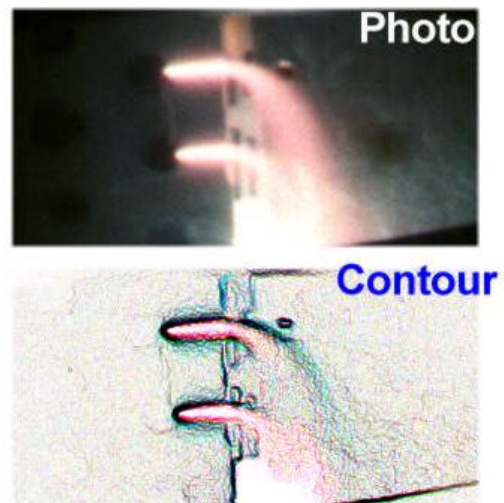


Fig.4.2.1.4. Discharge on the wall.

4.2.2. Discharge Influence on Pressure Distribution.

Plasma excitation near and inside of a separation zone effects on a static pressure distribution in this zone. Nine pressure pipes were installed on a back wall of a test section with a gap 5mm each from other downstream. Additional pipes are installed upstream discharge area and in a separation zone in 8mm from a wall step.

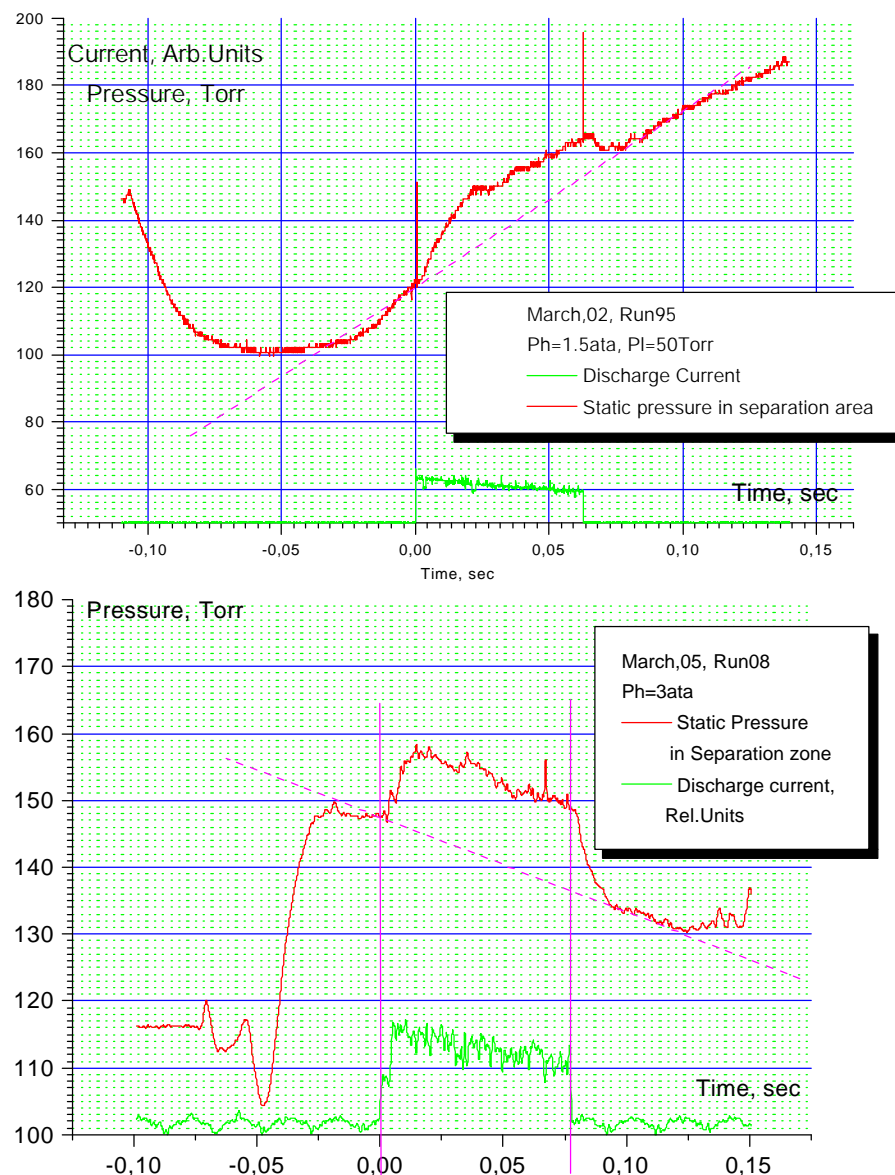


Fig.4.2.2.1. Pressure behavior in a separation zone at plasma excitation, Ph=1.5bar.

Fig.4.2.2.2. Pressure behavior in a separation zone at plasma excitation, Ph=3bar.

Data from the last point are presented in Figs.4.2.2.1 and 4.2.2.2. The charts include also graphs of discharge current to synchronize a time period of discharge switching on. At observation of them it can be considered, that at different conditions the result for this point is the same: plasma excitation leads to increase of a static pressure near wall step approximately on 10%. Generally, this statement is correct for the standard and the second mode of the discharge spacing both.

Fig.4.2.2.3.

Ph=1bar

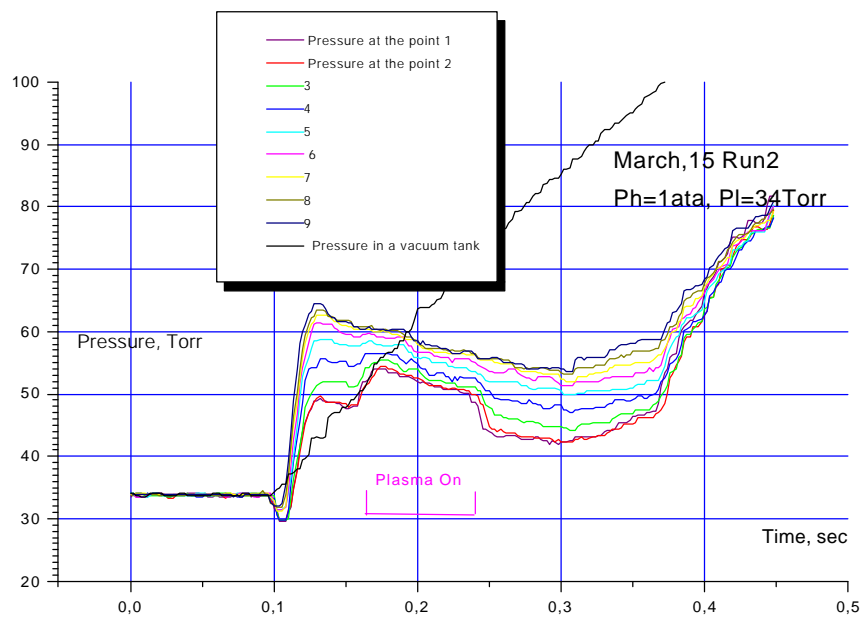
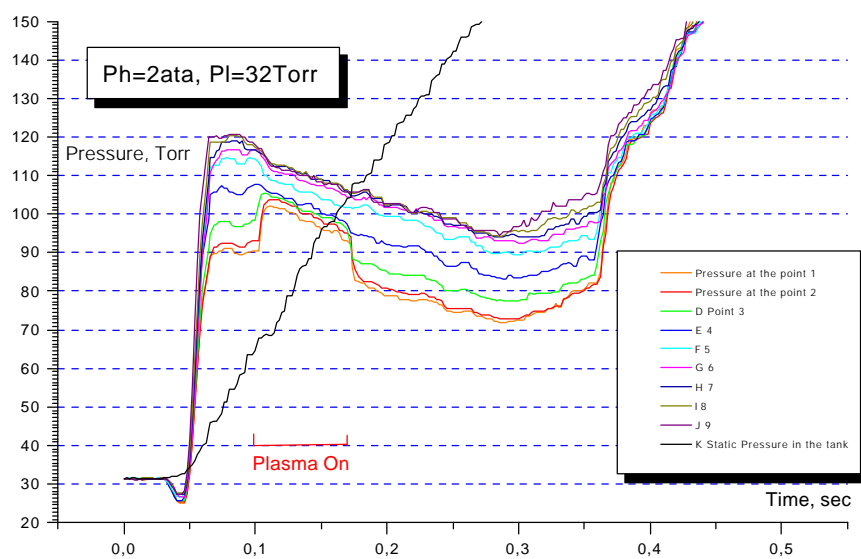


Fig.4.2.2.4.

Ph=2ata.



Results of pressure redistribution measurements are presented in Figures 4.2.2.3-4.2.2.6. Standard behavior of pressure in different points in a separation zone is shown at different initial conditions. It can be considered that the pressure distribution in a separation zone is change significantly. The pressure gradient occurs much less than in the case without plasma.

Fig.4.2.2.5.

Ph=3bar

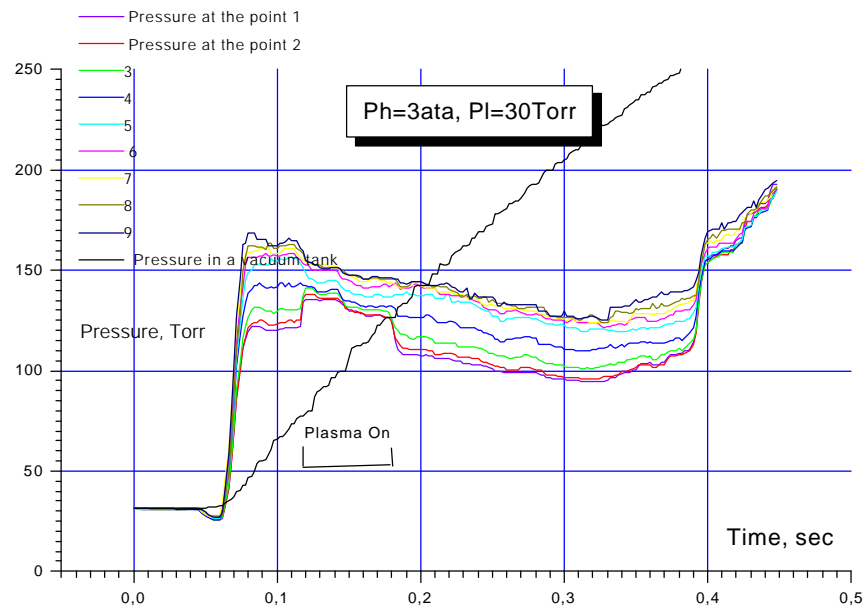
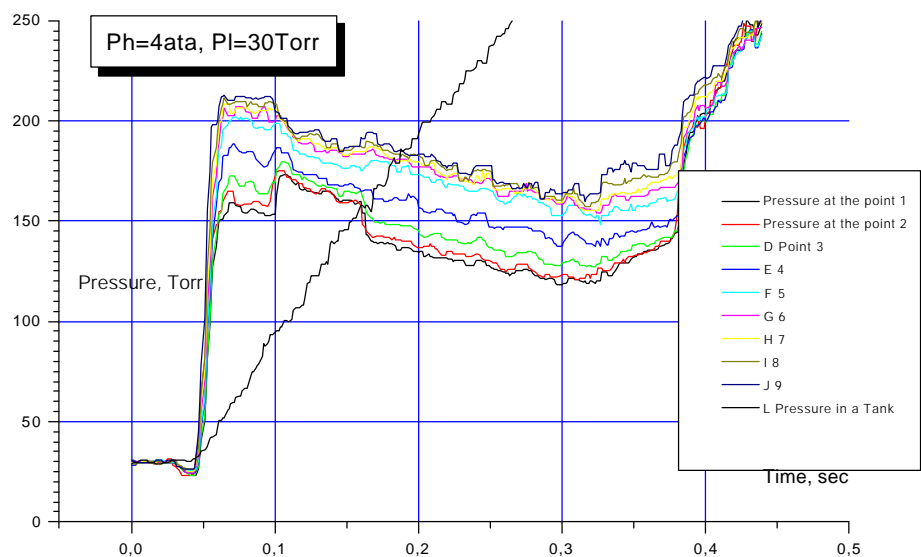


Fig.4.2.2.6.

Ph=4bar



Pressure distribution and along a separation zone is presented in Fig.4.2.2.7 as well as its evolution due to plasma influence.

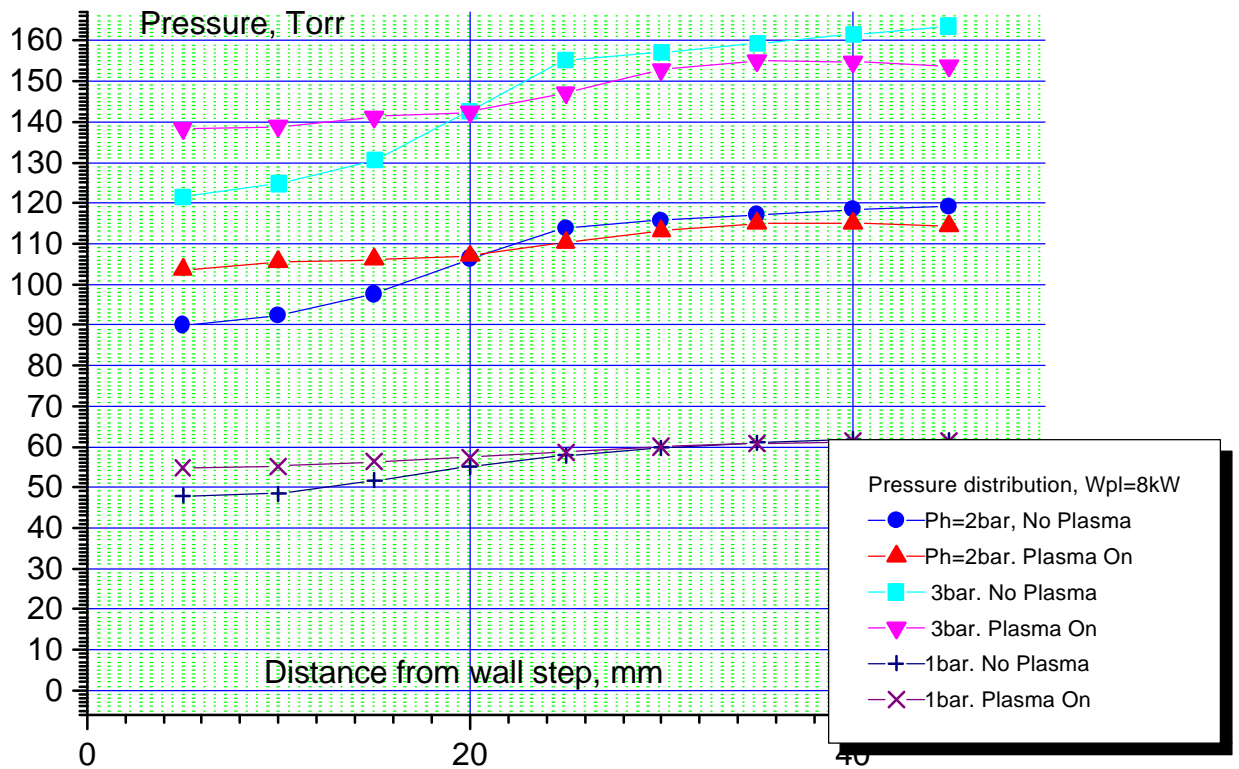


Fig.4.2.2.7. Pressure redistribution in a separation zone due to plasma effect.

It might be considered that a significant change of a pressure distribution inside of a separation area takes place. Such an effect can lead to increasing of gas exchange between a separation zone and a main flow.

4.2.3. Temperature in a Separation Zone.

Rotation (translation) temperature. Rotation temperature has been measured by molecular spectroscopy of the second positive band of nitrogen. An input lens of a quartz fiber line has a sharp focus. So, we could obtain the spectra from any defined point of observation. Three following basic conditions of the spectra getting have been chosen.

- Area between electrodes on a plane plate.
- Area in a separation area in 5mm downstream.
- Area on an electrode plate when an artificial separating obstacle has been installed in 5mm upstream of electrode plate.

Thus, we can review three different situations: plasma generation in a free stream, plasma in separation zone at upstream generation and plasma generation in a small artificial separation zone. The typical non-processed N2 spectra (0-2 transition) are shown in Fig.4.2.3.1. Conditions are clear from comments.

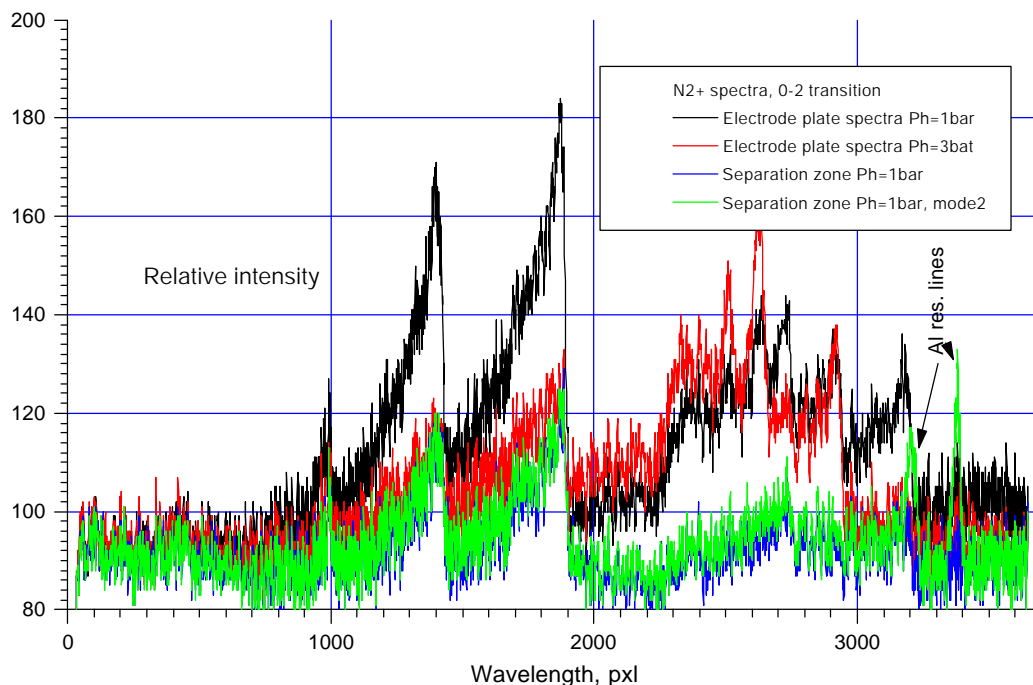


Fig.4.2.3.1. Typical unresolved spectra N2+.
Centerline appropriate wavelength 380nm.

The spectra from a separation area are more pure. At some important cases a resonance lines of Aluminum are observed. It says about an erosion of a back wall of a test section.

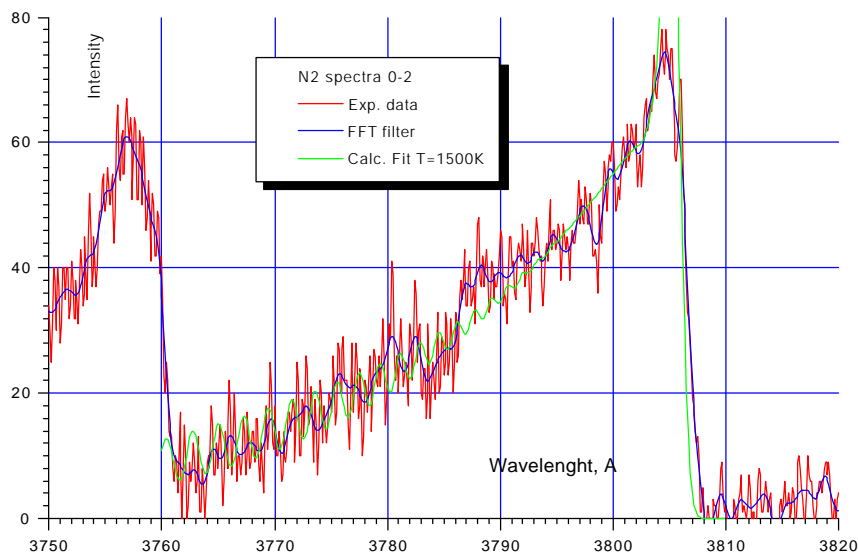


Fig.4.2.3.2. Processed spectra from electrode plate.

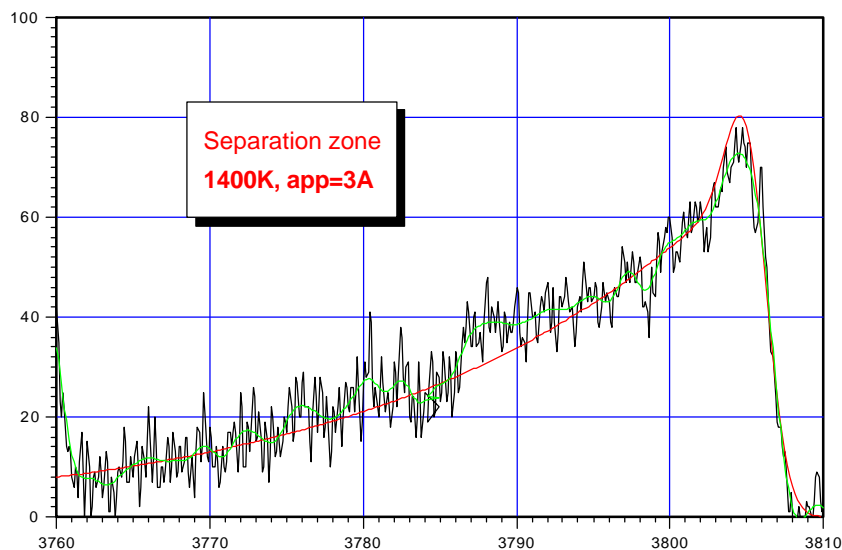


Fig.4.2.3.3. Processed spectra from standard separation zone.

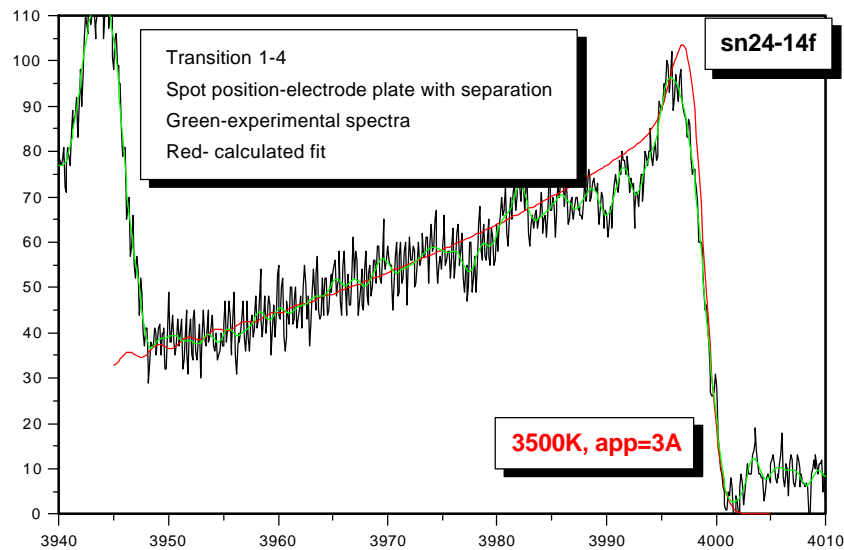


Fig.4.2.3.4. Processed spectra from plasma in artificial separation area.

Samples of spectra processing are presented in Fig.4.2.3.2÷4.2.3.4 for the three cases. Summarizing the experimental data we can conclude the following values of a rotation temperature:

- Electrode plate in a free stream $T_r=1600\pm 200\text{K.}$
- Standard separation zone, modes 1&2 $T_r=1400\pm 200\text{K.}$
- Discharge in an artificial separation area $T_r=3300\pm 500\text{K.}$

Vibration temperature. Vibration temperature of gas has been measured in a standard separation zone downstream a wall step when the discharge current flows through it on a back wall. Such a data, probably, is the most important for applications. As was described above, the measurements were made by means of CN molecular bands analysis. A small addition of a C-contained impurity is enough to see such a spectra.

Samples of two different bands spectra are presented in Fig.4.2.3.5 (band with edge 388,3nm) and in Fig.4.2.3.6 (band with edge 421,6nm).

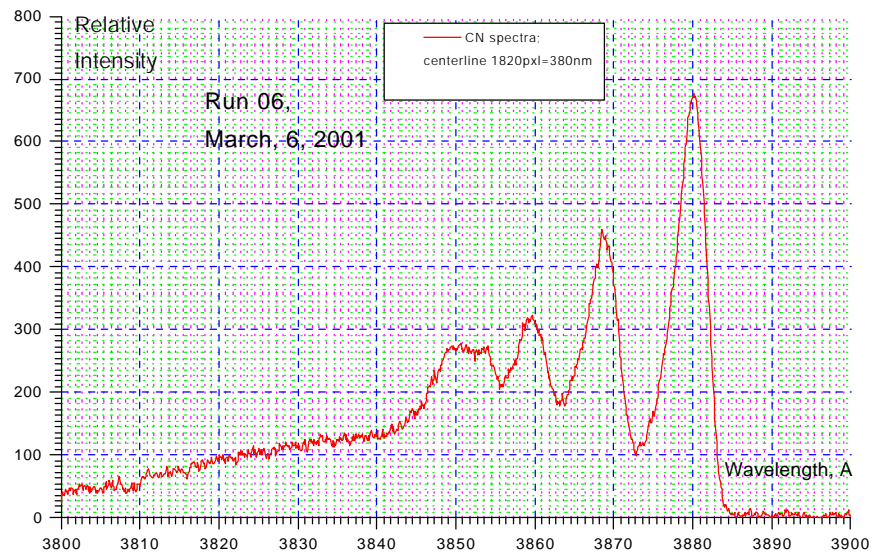


Fig.4.2.3.5. Vibration-rotational band of CN spectra (388,3 band).

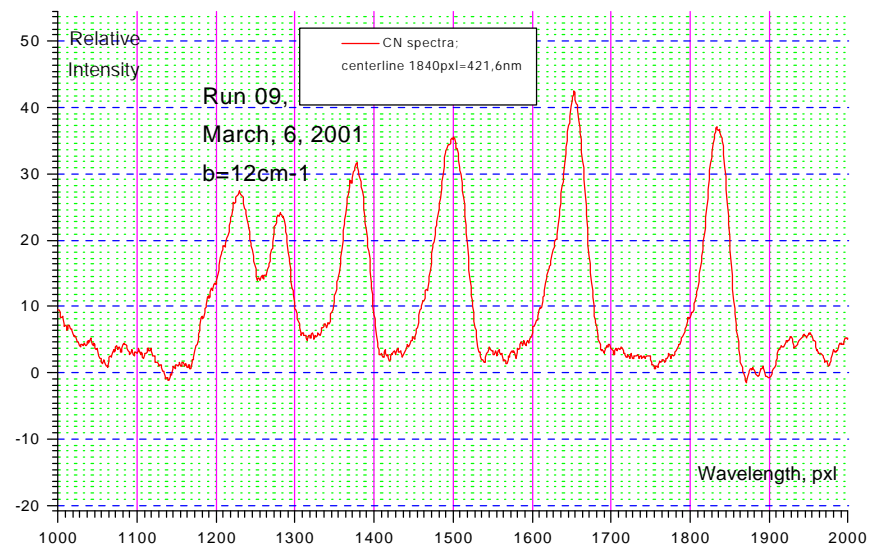


Fig.4.2.3.6. Vibration-rotational band of CN spectra (421,6 band).

Analysis of CN spectra allows us to getting a typical value of a vibration temperature of plasma inside of a separation zone $T_v=6000 \pm 1000K$. At some cases the temperature was less than this value- up to 4000K. Thus, a vibration temperature, at least, 3 times more than a rotation (translation) temperature.

4.2.4. Discharge Influence on Turbulence.

Measurements of a gas turbulence in a separation zone at a plasma presence have been done by means of high frequency response pressure sensor “Kulite”™. The sensor has an own characteristic frequency up to 500kHz. Also a short tube adds a some limitation. So, an actual frequency response might be about 10kHz.

Sample of a sensor signal is presented in Fig.4.2.4.1. Seen that it reflect the most of disturbances.

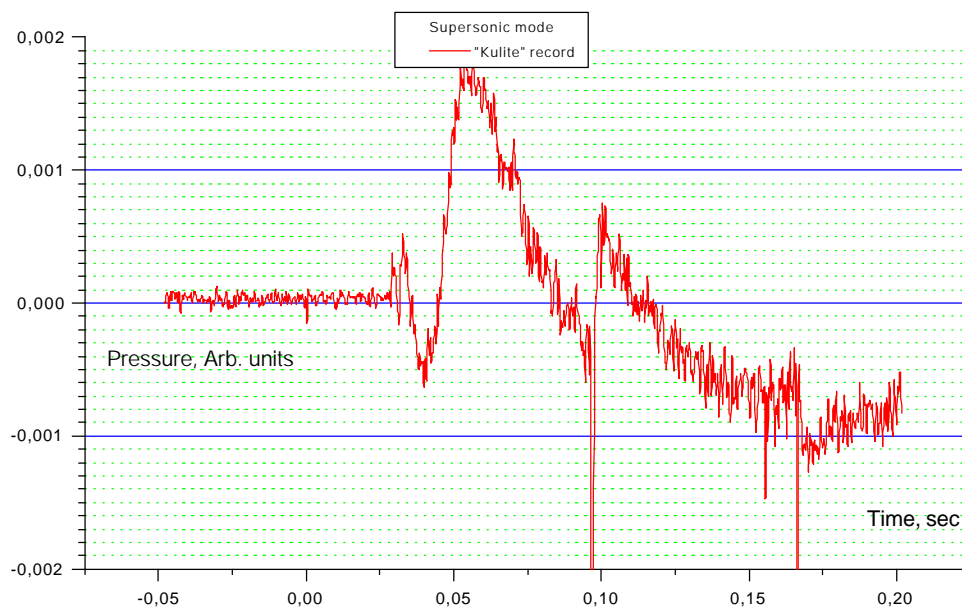


Fig.4.2.4.1. High frequency sensor response.

Fourier transformation of the signal has been done. The results are shown in Fig.4.2.4.2 for record without plasma and in Fig.4.2.4.3 at plasma excitation. The following consideration can be done.

- Plasma increases high frequency disturbances slightly.
- Relatively low frequency turbulence (up to 500Hz) decreases of amplitude.

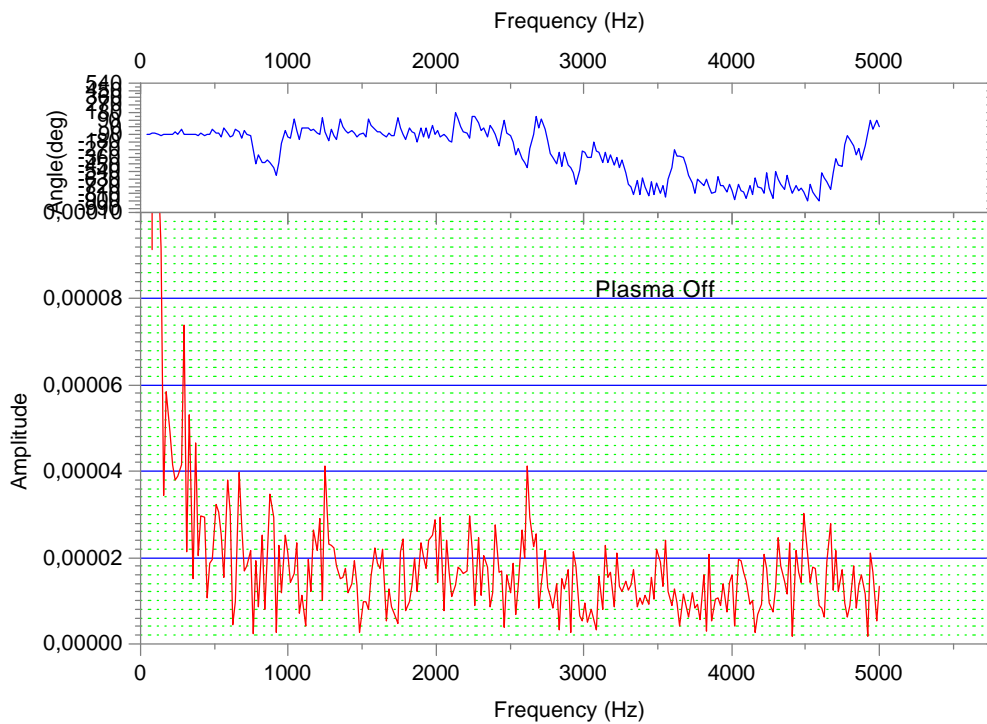


Fig.4.2.4.2. Fourier spectrum of a pressure signal in a separation zone.

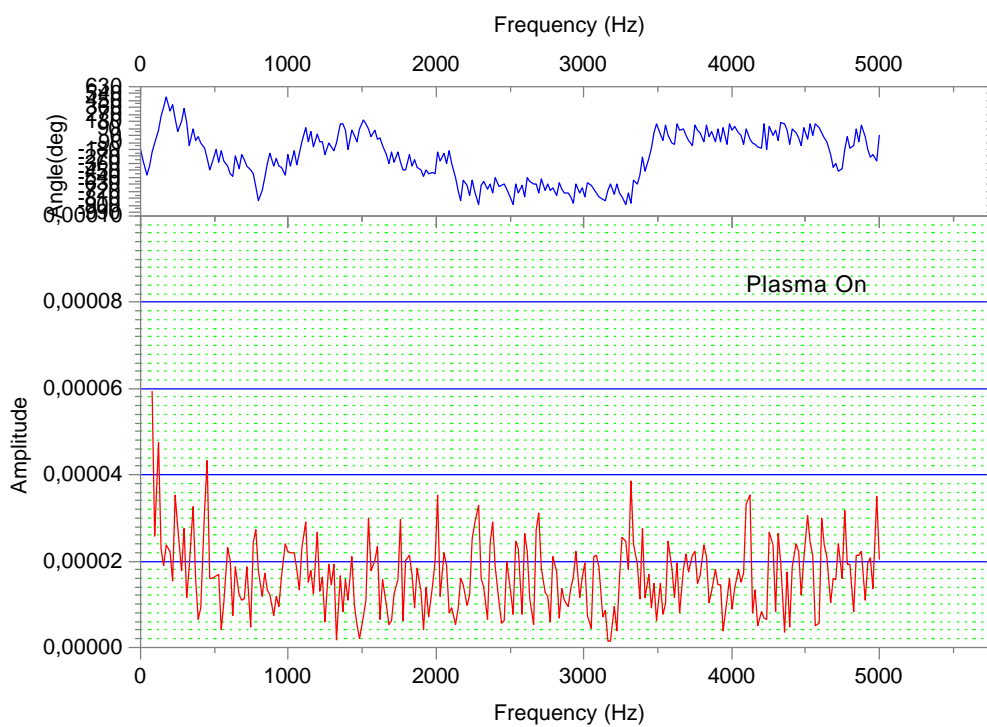


Fig.4.2.4.3. Fourier spectrum of a pressure signal at plasma generation.

4.3. Mathematical Simulation.

Introduction. It is well known that if there is a gas flow in the channel with the step expansion profile the vortex is formed down stream off the step. The goal of this work is to numerically investigate the influence of the energy release on the vortex characteristics (form, pressure and temperature distribution). The energy release is takes place in the vortex region and is caused by Ohm's dissipation due to gas discharge.

Mathematical model. The system of equations describing investigated flow is the system of Euler's equations with the heat source in the energy equation:

$$\frac{\partial \mathbf{r}}{\partial t} + \frac{\partial}{\partial x}(\mathbf{r}u) + \frac{\partial}{\partial y}(\mathbf{r}v) = 0, \quad (1)$$

$$\frac{\partial}{\partial t}(\mathbf{r}u) + \frac{\partial}{\partial x}(\mathbf{r}uu) + \frac{\partial}{\partial y}(\mathbf{r}uv) = -\frac{\partial p}{\partial x}, \quad (2)$$

$$\frac{\partial}{\partial t}(\mathbf{r}v) + \frac{\partial}{\partial x}(\mathbf{r}uv) + \frac{\partial}{\partial y}(\mathbf{r}vv) = -\frac{\partial p}{\partial y}, \quad (3)$$

$$\frac{\partial}{\partial t}(\mathbf{r}(e + \frac{u^2 + v^2}{2})) + \frac{\partial}{\partial x}(\mathbf{r}u(e + \frac{u^2 + v^2}{2})) + \frac{\partial}{\partial y}(\mathbf{r}v(e + \frac{u^2 + v^2}{2})) = -\frac{\partial}{\partial x}(up) - \frac{\partial}{\partial y}(vp) + \alpha Q, \quad (4)$$

where \mathbf{r} , u , v , p , e – density, longitudinal and transversal component of velocity, static pressure and specific internal energy respectively. It is supposed that volume source Q in the right part of the energy equation (4) are caused by heat release in the gas discharge. Coefficient α modulates the intensity of the heat release. System (1)-(4) are closed by the equation of state of ideal gas:

$$e = \frac{1}{g-1} \frac{p}{\mathbf{r}}, \quad \text{where } g\text{- specific heat ratio is equal to } 1.4. \quad (5)$$

Scheme of the flow and boundary conditions. Scheme of the flow is represented in Fig.4.3.1.

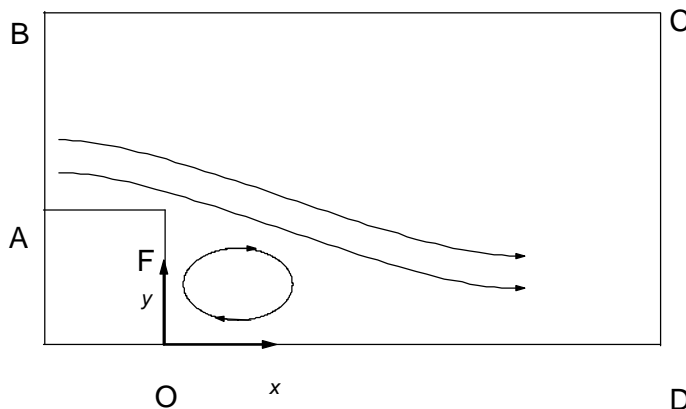


Fig.4.3.1. Scheme of the flow.

The computational region ABCDOF has following dimensions: AB=0.02 m, BC=0.203 m, OF=0.015 m. The beginning of coordinate system is placed in the point O. The “supersonic” boundary condition - $u_1=367$ m/s, $v_1=0$, $p_1=32.99$ kPa, $\rho_1=0.494$ kg/m³, $M=1.2$, $T=233$ K, $p^0=10^5$ Pa is placed on the AB. The “not passing” conditions - $U_n=0$ are placed on AF, OF, BC, OD. The “soft” boundary condition - $\partial/\partial n=0$ are placed on CD.

The distribution of source Q in equation (4) has been taken as follows:

$$Q = \frac{W}{Lc} \left\{ \sin \left(\frac{2p}{L} y - \frac{p}{2} \right) + 1 \right\} \exp \left(-\frac{x}{c} \right) \quad x \geq 0, y \leq L, \quad (6)$$

$$Q=0 \quad x < 0 \text{ or } y > L$$

where $W=50$ W/m, $L=OF$, $c=3 \cdot 10^{-3}$ m. Corresponding profiles of $Q(x,y)$ distribution are presented in Fig.4.3.2.

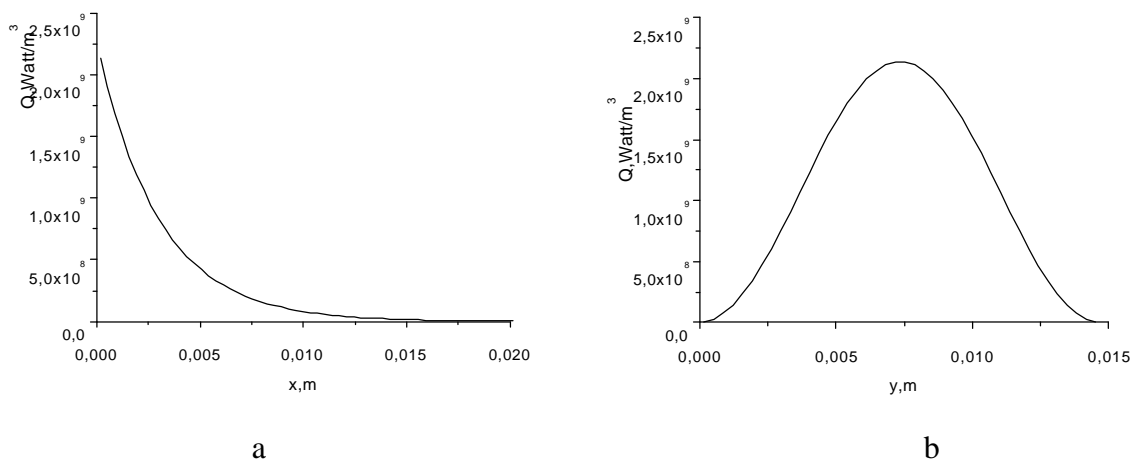


Fig.4.3.2. Distribution of Q : a- $Q(x, 7.5 \cdot 10^{-3} \text{ m})$, b- $Q(3.5 \cdot 10^{-4} \text{ m}, y)$

The series of numerical calculations with coefficient α equal to 0,1,2,5 has been made in this work.

Numerical solutions. Streamlines and pressure contours for $\alpha=0,1,2,5$ are presented at Fig.4.3.3-Fig.4.3.6 respectively.

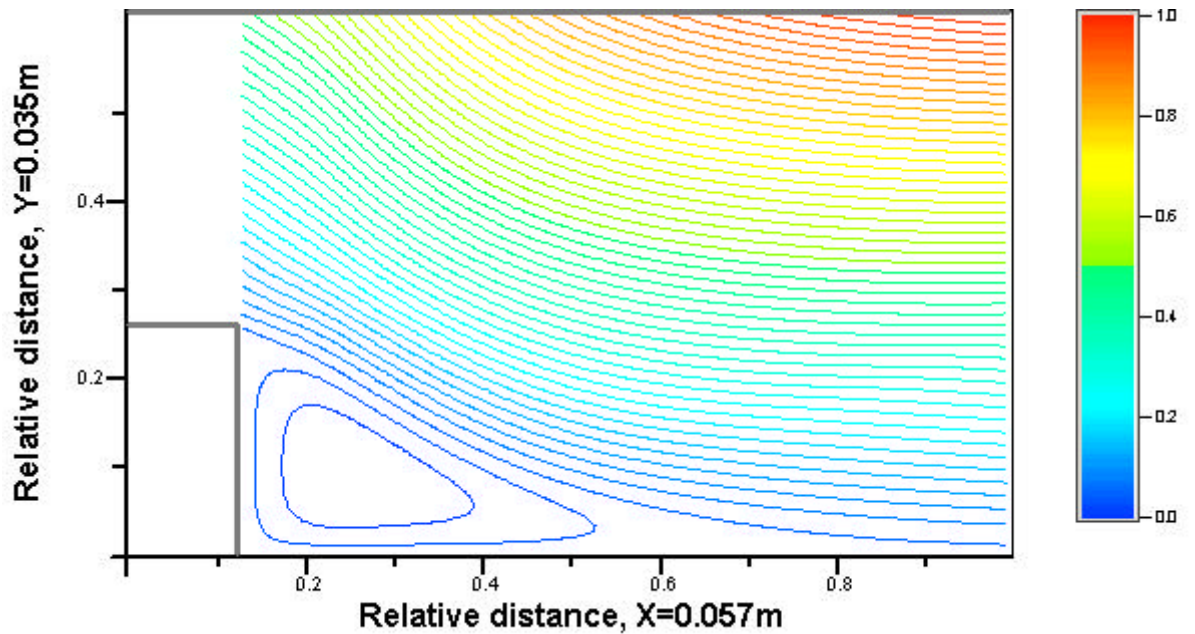


Fig.4.3.3a. Flow streamlines, $W=0$. Step = 0.345, 50 contours.

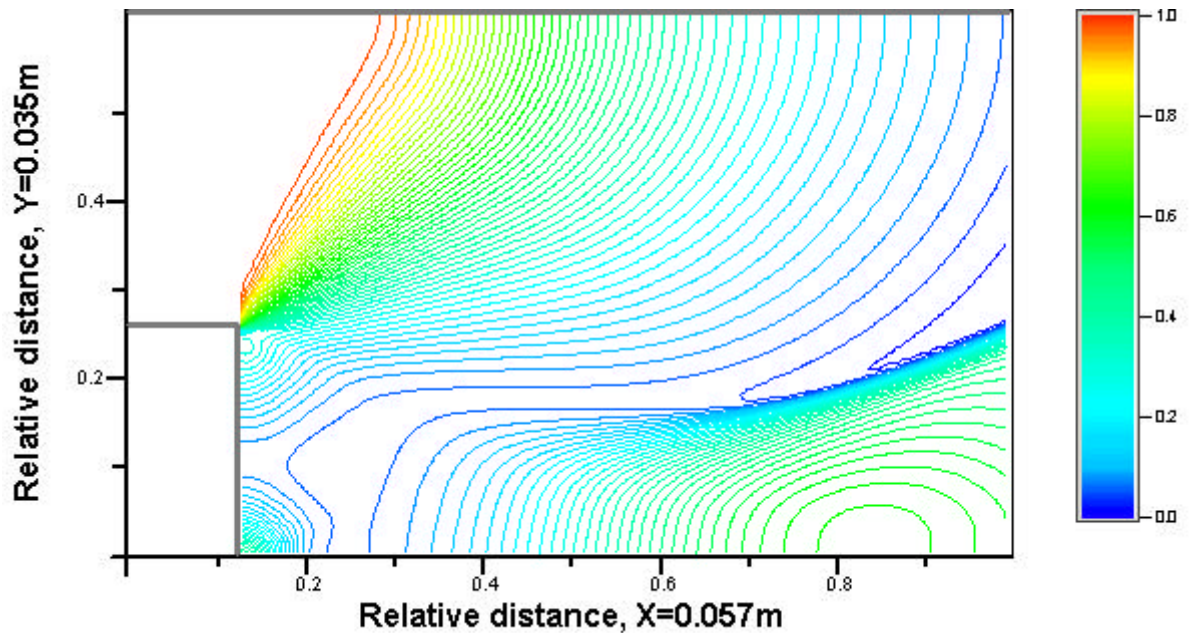


Fig.4.3.3b Pressure contours, $W=0$. $P_{min}=46.75$ Torr, $P_{max}=250.7$ Torr, 50 contours.

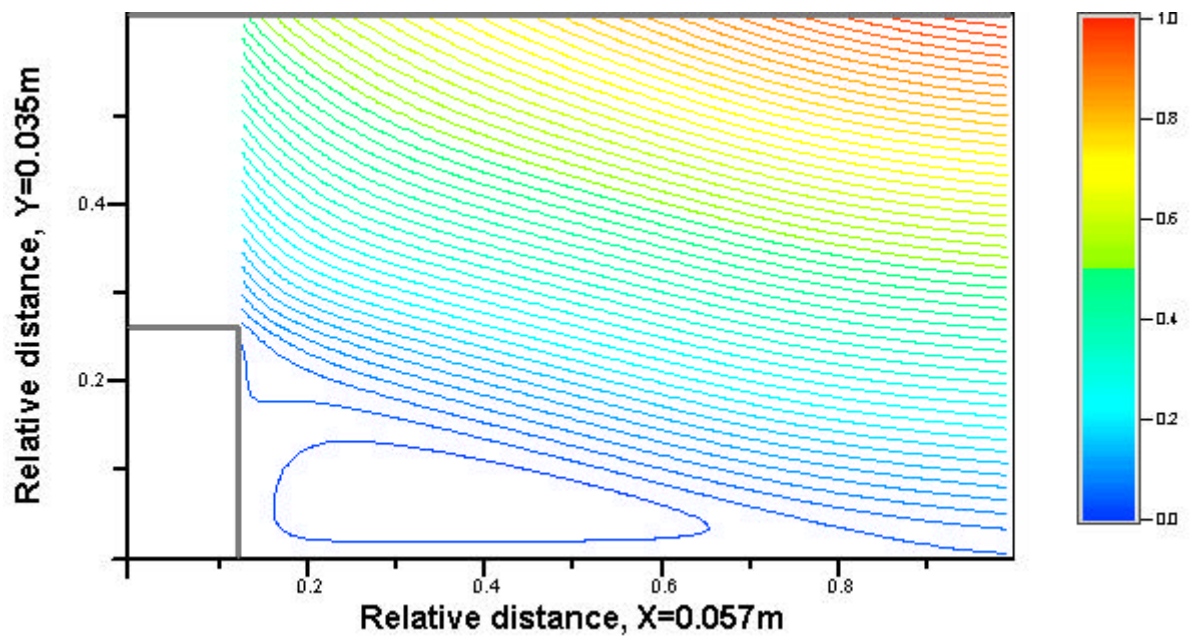


Fig.4.3.4a. Flow streamlines, $W=50$ kW/m. Step = 0.340, 50 contours.

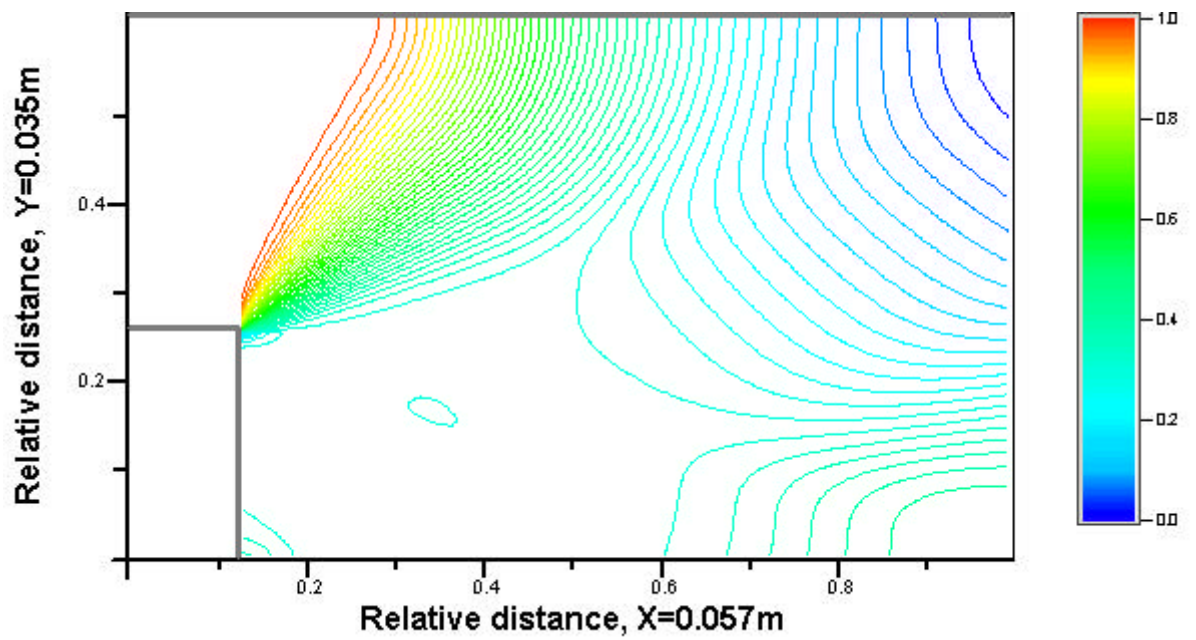


Fig.4.3.4b. Pressure contours, $W=50$ kW/m. $P_{min}=63.1$ Torr, $P_{max}=250.7$ Torr, 50 contours.

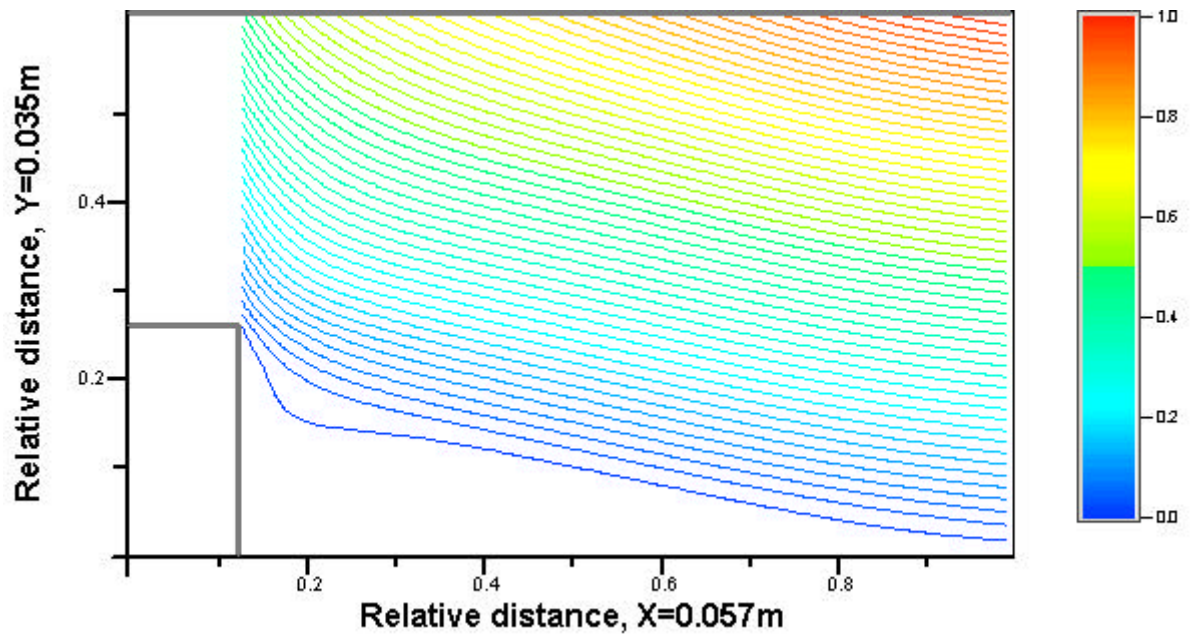


Fig.4.3.5a. Flow streamlines, $W=100$ kW/m. Step = 0.326, 50 contours.

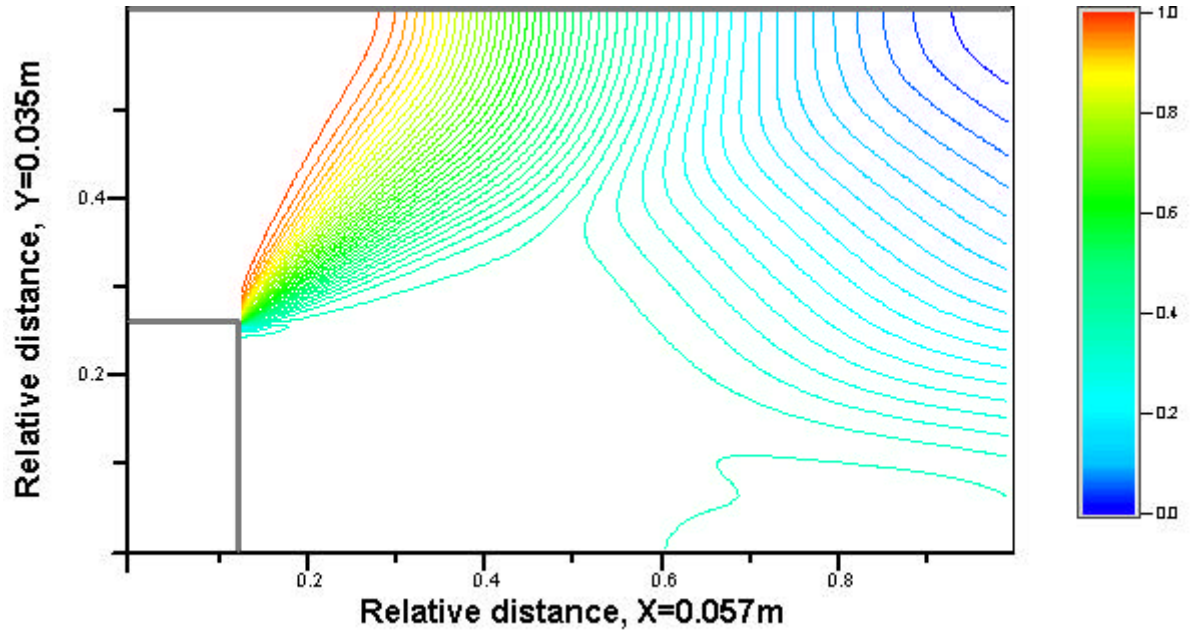


Fig.4.3.5b Pressure contours, $W=100$ kW/m. $P_{min}=71.45$ Torr, $P_{max}=250.7$ Torr, 50 contours.

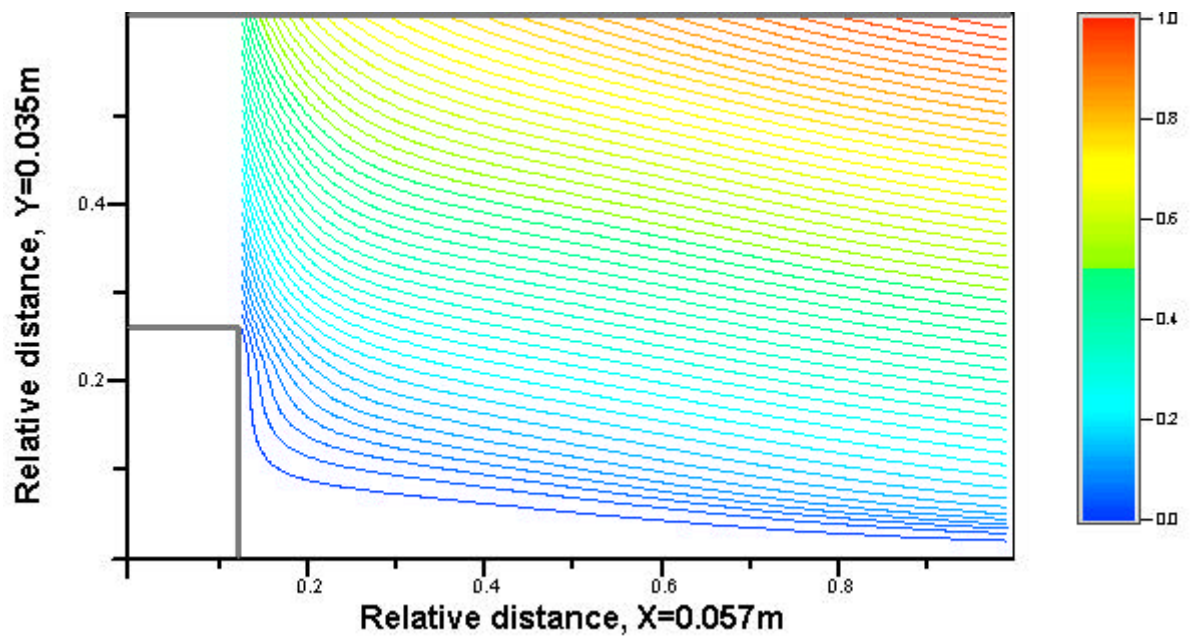


Fig.4.3.6a. Flow streamlines, $W=250\text{ kW/m}$. Step = 0.347, 50 contours.

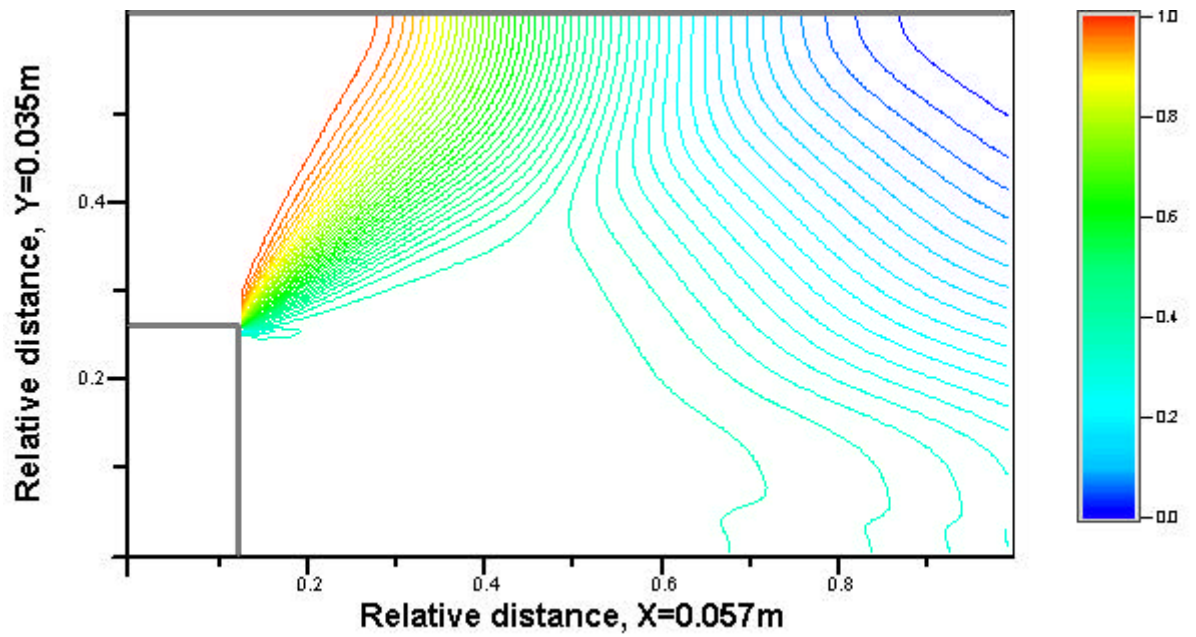


Fig.4.3.6b. Pressure contours, $W=250\text{ kW/m}$. $P_{\min}=89.71\text{ Torr}$, $P_{\max}=250.7\text{ Torr}$, 50 contours.

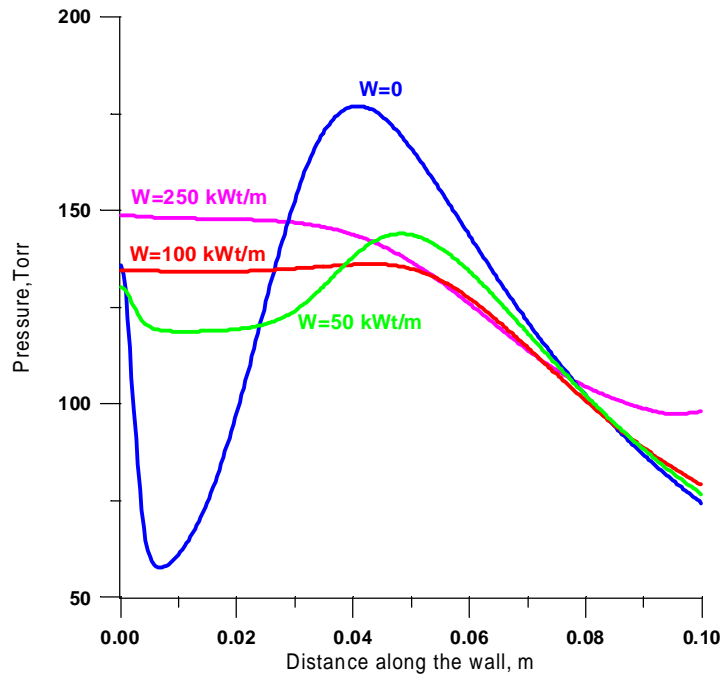


Fig.4.3.7. The distribution of pressure along the wall for different power values.

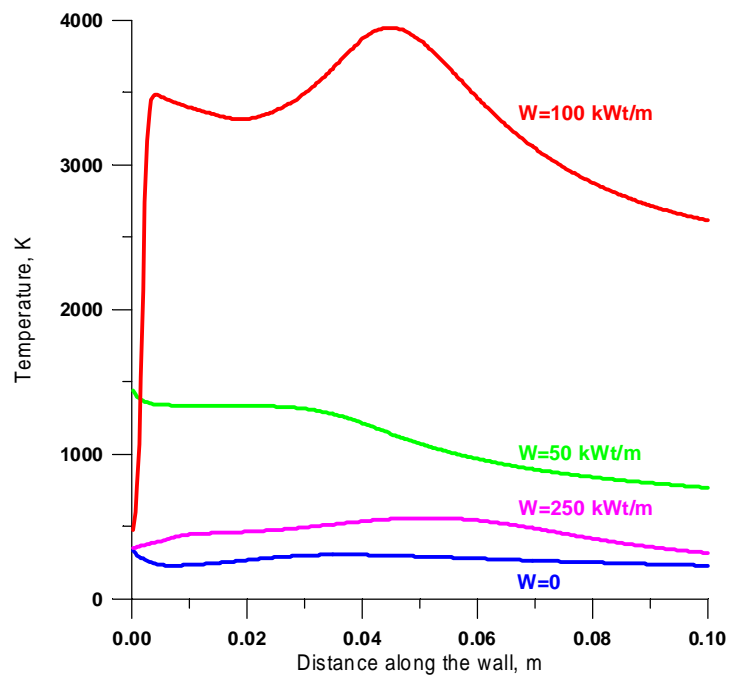


Fig.4.3.8. The distribution of temperature along the wall for different power values.

Comments. The important results have been obtained under the mathematical simulations. They can be formulated as the following:

- Energy release changes a shape and volume of a separated zone. Increase of input power leads finally to a separated zone disappearance i.e. to separation-less streamlining of a wall step.
- Moderate energy release effects in a change of pressure redistribution inside of the zone. Pressure gradients are reduced. It means that the vorticity is decreased. This result appropriates to the experimental measurements not only qualitatively, but also quantitatively.
- The increase of level of energy release leads to increase of the temperature in a separated zone. Exceeding of the power over some level effects in transform the airflow to separation-less mode and fall of temperature consequently. Temperature value at 50kW/m of the energy release corresponds to experimental data.

The numerical modeling showed that a heat deposition to the vortex region near the wall step of the channel gives decreasing of vortex intensity. If the heat release is sufficiently high the gas flows over the step practically without vortex structure. In that case the releasing heat energy pass away by convective gas flow.

4.4. Interim Conclusion.

Following statements can be made in respect of plasma influence on parameters of a fixed separation zone downstream a wall step.

- Two modes of discharge spacing are described: current between the “hot” and grounded electrodes and current from “hot” electrodes to back wall of a test section.
- Plasma excitation in a separation zone region effects on a pressure distribution inside of it. Pressure near the step occurs large and a peripheral pressure is decreased. So, the longitudinal pressure gradient in a separation zone is decrease significantly.
- Translational temperature in a separation zone can achieve the value 1500K. At the same conditions a vibrational temperature can be in a range of 5000K.
- A turbulence spectrum in a separation zone is changed due to plasma effect. Amplitude of low frequency disturbances is decrease. At the same time the amplitude of disturbances at $F > 500\text{Hz}$ is increased.
- A mathematical simulations show qualitatively closed results as at the experiment. Pressure and temperature behavior in a separated zone are described in accordance with experimental data. Moreover, the simulation predicts the effect of flow transformation to separation-less mode at 5 times higher energy release.